

MEASURING AND MODELING THE EFFECTS OF SEA LEVEL RISE  
ON NEAR-COASTAL RIVERINE REGIONS: A GEOSPATIAL  
COMPARISON OF THE SHATT AL-ARAB RIVER IN SOUTHERN IRAQ  
WITH THE MISSISSIPPI RIVER DELTA IN SOUTHERN LOUISIANA,  
USA.

By

Ameen Awad Kadhim

A DISSERTATION

Submitted to  
Michigan State University  
in partial fulfillment of the requirements  
for the degree of

Geography - Doctor of Philosophy

2018

## ABSTRACT

### MEASURING AND MODELING THE EFFECTS OF SEA LEVEL RISE ON NEAR-COASTAL RIVERINE REGIONS: A GEOSPATIAL COMPARISON OF THE SHATT AL-ARAB RIVER IN SOUTHERN IRAQ WITH THE MISSISSIPPI RIVER DELTA IN SOUTHERN LOUISIANA, USA.

By

Ameen Awad Kadhim

There is a growing debate among scientists on how sea level rise (SLR) will impact coastal environments, particularly in countries where economic activities are sustained along these coasts. An important factor in this debate is how best to characterize coastal environmental impacts over time. This study investigates the measurement and modeling of SLR and effects on near-coastal riverine regions. The study uses a variety of data sources, including satellite imagery from 1975 to 2017, digital elevation data and previous studies. This research is focusing on two of these important regions: southern Iraq along the Shatt Al-Arab River (SAR) and the southern United States in Louisiana along the Mississippi River Delta (MRD). These sites are important for both their extensive low-lying land and for their significant coastal economic activities. The dissertation consists of six chapters. Chapter one introduces the topic. Chapter two compares and contrasts both regions and evaluates escalating SLR risk.

Chapter three develops a coupled human and natural system (CHANS) perspective for SARR to reveal multiple sources of environmental degradation in this region. I use the CHANS perspective to identify the problems, and which ones (human or natural systems) are especially responsible for environmental degradation in SARR. I use several measures of ecological, economic, and social systems to outline the problems identified through the CHANS framework. I modeled and analyzed the regions land cover between 1975

and 2017 to understand how the environment has been affected, and found that climate change is responsible for what happened in this region based on other factors.

Chapter four constructs and applies an error propagation model to elevation data in the Mississippi River Delta region (MRDR). This modeling both reduces and accounts for the effects of digital elevation model (DEM) error on a bathtub inundation model used to predict the SLR risk in the region. Digital elevation data is essential to estimate coastal vulnerability to flooding due to sea level rise. Shuttle Radar Topography Mission (SRTM) 1 Arc-Second Global is considered the best free global digital elevation data available. In this study, I conduct an error assessment and develop statistical error modeling for SRTM to improve the quality of elevation data in these at-risk regions.

Chapter five applies MRDR-based model from chapter four to enhance the SRTM 1 Arc-Second Global DEM data in SARR. As such, it is the first study to account for data uncertainty in the evaluation of SLR risk in this sensitive region. This study transfers an error propagation model from MRDR to the Shatt al-Arab river region to understand the impact of DEM error on an inundation model in this sensitive region. The error propagation model involves three stages. First, a multiple regression model, parameterized from MRDR, is used to generate an expected DEM error surface for SARR. Second, residuals from this model are simulated for SARR: these are mean-zero and spatially autocorrelated with a Gaussian covariance model matching that observed in MRDR by convolution filtering of random noise. More than 50 realizations of error were simulated to make sure a stable result was realized. These realizations were subtracted from the adjusted SRTM to produce DEM realizations capturing potential variation. Third, the DEM realizations are each used in bathtub modeling to estimate flooding area in the region with 1 m of sea level rise.

To My Mom...

I dedicate this work to my mom, who passed away in June 2013. It was early days of my Ph.D. program. My mom was everything in my life. She supported me to pursue the Ph.D. degree and supported me at every moment during the program, and my life. I feel that she is happy and proud of me as the dream, that she shares with me, becomes true.

## ACKNOWLEDGMENTS

This dissertation would not have been possible without the support of my advisor Dr. Ashton Shortridge and the financial support of the Higher Committee For Education Development in Iraq (HCED-Iraq), the Department of Geography, Environment, and Spatial Sciences and college of science at Michigan State University. I am especially indebted to my advisor Dr. Ashton Shortridge who is supporting my PhD program goals and how he is working actively to provide me with the academy knowledge with the time to pursue those goals. I am very grateful to my family and my committee (Dr. Lifeng Luo, Dr. Jianguo Qi, and Dr. Hayder Radha, Dr. Warren W Wood) and the large group of people to whom I owe a lot of gratitude especially my friends (Wahab Al-Barakat, Khaldoun Al-Yasiri, Falah AL-Lahaybey and Brad Peter). I would like to thank the Center for Global Change and Earth Observations (CGCEO) at MSU for their hospitality. Thanks for my big family, the geography department at MSU.

## TABLE OF CONTENTS

LIST OF TABLES . . . . .	ix
LIST OF FIGURES . . . . .	x
KEY TO ABBREVIATIONS . . . . .	xiii
<b>Chapter 1 Introduction . . . . .</b>	<b>1</b>
1.1 Background . . . . .	2
1.1.1 Shatt Al-Arab River . . . . .	5
1.1.2 Mississippi River Delta . . . . .	8
1.2 Study Goals . . . . .	9
1.3 Study Objectives . . . . .	10
<b>Chapter 2 A Comparison Between Shatt Al-Arab River Region in Southern Iraq with Mississippi River Region in Southern Louisiana, USA. . .</b>	<b>13</b>
2.1 Introduction . . . . .	13
2.2 The Geographical Characteristics . . . . .	17
2.2.1 Topography Characteristics . . . . .	18
2.2.1.1 Topographic Characteristics of Shatt Al-Arab River Region	19
2.2.1.2 Topographic Characteristics of Mississippi River Delta Re-	
gion . . . . .	19
2.2.2 Geology Characteristics . . . . .	21
2.2.2.1 Mississippi River Delta Geology and Ecology . . . . .	22
2.2.2.2 Shatt Al-Arab Geology and Ecology . . . . .	23
2.2.3 Hydrology Characteristics . . . . .	24
2.2.3.1 Mississippi River Flow . . . . .	24
2.2.3.2 Shatt Al-Arab River Flow . . . . .	25
2.2.4 Climate Characteristics . . . . .	26
2.2.5 Human Activity . . . . .	28
2.3 Conclusion . . . . .	28
<b>Chapter 3 Causes and Consequences of Environmental Degradation Along Shatt Al–Arab River: A Coupled Human and Natural System Per-</b>	<b>31</b>
<b>spective . . . . .</b>	<b>31</b>
3.1 Introduction . . . . .	31
3.2 Data and Methods . . . . .	33
3.2.1 Study Area . . . . .	33
3.2.2 Coupled Human and Natural System . . . . .	34
3.2.2.1 Human Impacts . . . . .	35
3.2.2.2 Environmental Impacts . . . . .	37
3.2.3 Methodology . . . . .	37

3.3	Results . . . . .	39
3.4	Discussion . . . . .	41
3.4.1	Human Impacts . . . . .	42
3.4.1.1	War and Government Policy . . . . .	42
3.4.1.2	Upstream Water Demand . . . . .	44
3.4.1.3	Hydroengineering in SARR . . . . .	45
3.4.1.4	Pollution and Degradation . . . . .	46
3.4.2	Environmental Impacts . . . . .	46
3.4.2.1	Meteorological Factors Associated With Drought . . . . .	47
3.4.2.2	Sea Level Rise . . . . .	47
3.4.2.3	Groundwater Salinity . . . . .	48
3.4.3	Conclusions . . . . .	49
<b>Chapter 4</b>	<b>Flooded With Error: Handling Uncertainty in SRTM For The Assessment of Sea Level Rise in Mississippi River Delta . . . . .</b>	<b>51</b>
4.1	Introduction . . . . .	51
4.2	Data and Methods . . . . .	54
4.2.1	Study Area . . . . .	54
4.2.2	Data . . . . .	55
4.2.2.1	National Elevation Dataset (NED) . . . . .	55
4.2.2.2	SRTM 1 Arc-Second Global Coverage ( 30 meters) . . . . .	56
4.2.2.3	Vegetation Data . . . . .	56
4.2.3	Methodology . . . . .	57
4.2.3.1	Regression Kriging . . . . .	58
4.2.3.2	Inundation Modeling . . . . .	59
4.2.4	Results . . . . .	60
4.2.4.1	Parameter Estimation For SRTM 1 Error Regression Model . . . . .	60
4.2.4.2	Regression and Variogram Results . . . . .	62
4.2.4.3	Inundation Modeling . . . . .	63
4.2.5	Discussion . . . . .	63
4.2.6	Conclusion . . . . .	66
<b>Chapter 5</b>	<b>Accounting for DEM Error in Sea Level Rise Assessment for Shatt Al-Arab River Region . . . . .</b>	<b>69</b>
5.1	Introduction . . . . .	69
5.2	Data and Methods . . . . .	72
5.2.1	Study Area . . . . .	72
5.2.2	SRTM 1 Arc-Second Global Coverage ( 30 meters) . . . . .	74
5.2.3	Vegetation Data . . . . .	74
5.2.4	Methods . . . . .	75
5.2.4.1	Monte Carlo Error Propagation . . . . .	75
5.2.4.2	Unconditional Simulation with Convolution Filtering . . . . .	76
5.2.4.3	Inundation Modeling . . . . .	77
5.3	Results . . . . .	79
5.3.1	Regression Kriging-Based Error Modeling . . . . .	79

5.3.2	Realizations . . . . .	80
5.3.3	Inundation Modeling . . . . .	81
5.4	Limitations . . . . .	85
5.5	Conclusion . . . . .	86
<b>Chapter 6</b>	<b>Conclusion . . . . .</b>	<b>87</b>
6.1	Methods . . . . .	89
6.1.1	Coupled human and natural systems (CHANS) . . . . .	89
6.1.2	The inundation model (bathtub modeling) and error propagation . .	90
6.2	Dissertation Objectives . . . . .	91
6.3	Future Research . . . . .	95

## LIST OF TABLES

Table 2.1: Comparison of the study regions. . . . .	18
Table 3.1: Satellite sensors utilized for the study used three sensors to cover the time (1975, 1985, 1995, 2005 and 2017). . . . .	38
Table 4.1: Regression coefficients of SRTM error model with NED and VCF. . . . .	63
Table 5.1: Regression coefficients for regression model variables . . . . .	81

## LIST OF FIGURES

Figure 1.1:	Modeling the effects of sea level rise on near-coastal riverine regions based on SRTM 30 m data preprocessing for the research work. . . . .	6
Figure 1.2:	Linking dissertation objectives. . . . .	12
Figure 2.1:	The natural system which causes the sea level to change, adopted from Brandimarte et al. (2015). . . . .	15
Figure 2.2:	The change of the mean temperature and the carbon dioxide in the atmosphere for the global in the past and future, adopted from (Clark et al. (2016)).	16
Figure 2.3:	Total sea level change since 1993 based on TOPEX/Poseidon. . . . .	17
Figure 2.4:	Both SARR and MRDR have high rising sea levels, adopted from (Williams (2009)). . . . .	19
Figure 2.5:	Shatt Al-Arab river region in southeastern Iraq. . . . .	20
Figure 2.6:	Mississippi River Delta region in Louisiana, USA. . . . .	21
Figure 2.7:	World climate regions according to Koppen-Geiger classification, adopted from (Peel et al. (2007)). . . . .	27
Figure 2.8:	Projects by Louisiana's Coastal Protection and Restoration Authority since 2007, adopted from (Louisiana (2012)). . . . .	29
Figure 3.1:	Total study area of Shatt Al-Arab river region. . . . .	35
Figure 3.2:	Total conceptualization of coupled human and natural systems (CHANS) in Shatt Al-Arab river region. . . . .	36
Figure 3.3:	Temporal variations of NDVI (A-1975, B-1985, C-1995, D-2005 and E-2017 NDVI greenness density plot) for the Shatt Al-Arab river region. . . . .	39
Figure 3.4:	Regressing trends of temperature, precipitation, humidity, and sea levels for the periods (1975, 1985, 1995, 2005, and 2017) associated with the NDVI trends.	41
Figure 3.5:	Comparative between 1975 and 2017 NDVI in Shatt Al Arab Region (a,b)which shows the difference in the density of vegetation distribution between up and down the junction of Karun river in Iraq and Iran with Shatt Al Arab river. . .	42

Figure 3.6:	Increase in salinity (ppm) in Shatt Al-Arab river from 1980 to 2012. . . . .	49
Figure 4.1:	(a) study area (Mississippi River Delta region in Louisiana state); (b) NED 1/3 arc-second (approximately 10 meters); (c) VCF Landsat 5 TM Collection 1 products 30 m and (d) SRTM 1 Arc-Second Global coverage ( 30 meters). . . .	55
Figure 4.2:	Error modeling and bathtub modeling for Mississippi River Delta Region. . .	58
Figure 4.3:	SRTM error: (a) Regression original SRTM error and raw SRTM error versus: (b) VCF; (c) SRTM elevation; (d) SRTM slope. . . . .	62
Figure 4.4:	Error assessment for variogram model: (a) Regression model performance; (b) histogram of validation error of the regression model; (c) variogram and model of regression model residuals over short distances; (d) variogram and model of regression model residuals over long distances; (e) map of model-predicted SRTM elevation errors and (f) histograms of predicted SRTM errors). . . . .	64
Figure 4.5:	Inundation models (predicting the spatial extent of a 1m sea level rise in the MRD region: (a) initial SRTM and (b) adjusted SRTM DEM after the error modeling. . . . .	65
Figure 4.6:	Inundation model predicting the spatial extent of a 1m sea level rise in the MRDR: (a) NED 10m DEM and (b) adjusted SRTM DEM. . . . .	66
Figure 4.7:	Marsh classes in Mississippi river delta region: a. Spatial temporal change for vegetation classes. b. Marsh classes changing based on mean NED DEM. . . .	67
Figure 5.1:	(a) Landsat imagery for Shatt Al-Arab River study region in Iraq; (b) SRTM 1 Arc-Second Global coverage ( 30 meters); (c) SRTM-derived slope; (d) Vegetation cover fraction (VCF) derived from Landsat 5 TM Collection 1. . . . .	73
Figure 5.2:	Transferring the error propagation model and bathtub modeling from Mississippi River Delta Region (A), to Shatt Al-Arab river region (B). . . . .	77
Figure 5.3:	The autocorrelated Gaussian covariance process and its associated convolution filter. This filter is passed over spatially random Gaussian noise to produce rasters with the desired spatial structure. . . . .	78
Figure 5.4:	Error assessment for variogram model: (a) MRDR error model residual variogram and model (line); (b) SARR variogram model (line) and variogram of simulation output (circles); (c) MRDR map of model-predicted SRTM elevation errors; (d) MRDR histogram of predicted SRTM errors; (e) SARR map of model-predicted SRTM elevation errors; (f) SARR histogram of predicted SRTM errors. . . . .	80

Figure 5.5: SRTM realizations: (a) random Gaussian noise for the SARR and spatially autocorrelated noise following convolution filtering; (b) QQ plots of random and convolution-filtered Gaussian noise; (c) DEM realization number 10; (d) bathtub modeling SRTM realization number 10. . . . . 82

Figure 5.6: (a) SARR map of regression-adjusted SRTM elevation; (b) histograms of adjusted SRTM ; (c) SARR probability map for land remaining dry following bathtub modeling of 1m inundation (d) histogram of flooding probability; (e) SARR bathtub model using raw SRTM data; (f) Proportion of SARR predicted to remain dry following 1m inundation: raw DEM is dashed line, histogram are areas across 50 realizations. . . . . 83

## KEY TO ABBREVIATIONS

CHANS	Coupled Human And Natural Systems
DEM	Digital Elevation Model
GIS	Geographic Information System
IFSAR	Interferometric Synthetic Aperture Radar
km	Kilometer
mm	Millimeter
MRDR	Mississippi River Delta Region
MSL	Mean Sea Level
NDVI	Normalized Difference Vegetation Index
NED	National Elevation Data
SARR	Shatt Al-Arab River Region
SLR	Sea Level Rise
SRTM	Shuttle Radar Topography Mission
VCF	Vegetation Cover Fraction
USGS	The United States Geological Survey

# Chapter 1

## Introduction

During the past century, global sea level has risen about  $0.17 \pm 0.05$  meter due to the increase in global average temperature (Hansen (2007); Li et al. (2009); Rahmstorf (2007)). Historically, the Earth has warmed between 1900 and 1940, cooled slightly after 1940 and then warmed markedly from 1970 onward. While global warming in the past century was estimated to be  $0.8^{\circ}\text{C}$ , the rise in temperature in the past three decades alone was  $0.6^{\circ}\text{C}$  (a rate of  $0.2^{\circ}\text{C}$  per decade) as greenhouse gases became the dominant climate forcing in recent decades (Nageswara Rao et al. (2008)). Importantly, thermal expansion of ocean water due to increasing the global warming has been responsible for about half of the sea level rise in the last century (Meyssignac and Cazenave (2012)). In addition, ice is melting in the significant ice repositories of the world.

The Greenland ice sheet is melting at a rate of  $23,923 \text{ km}^3$  per year. The extent of Arctic sea ice has been decreasing at almost 8% per decade since the middle of the last century (Nageswara Rao et al. (2008); Rahmstorf (2007)). The effect of SLR on low-lying coastal areas is tremendous. This dissertation focuses on two vulnerable areas: SARR in southern Iraq and MRDR in Louisiana, USA. SARR is estimated to have lost more than 90 % of its cultivable land between 1970 and 2002, in addition to loss of other human economic activity and environmental degradation (Singh et al. (2005); Brandimarte et al. (2015)). No comprehensive study has evaluated the role that SLR may have played in these recent

changes in the SARR. The MRDR in Louisiana has high known rates of local relative sea-level due in large part to the sinking of land, including the loss of around 4,920 square kilometers of coastal wetlands, more than one-third of its coastal plain between 1932 and 2010 (Couvillion et al. (2011)).

This study aims to investigate the influence of SLR within these sensitive and important coastal regions in two ways. First, it uses geospatial methods like bathtub modeling to estimate the position and extent of areas in these regions, which were affected by SLR from 1975 to 2017 and predict areas, which will be affected in the near future. Further, the impact of this change on land cover, u and ecosystem will be estimated. Second, since DEM data for the SARR is not very accurate, an error propagation model will be constructed to improve flooding estimates from bathtub modeling. This study will apply bathtub modeling and analyze different imagery and data sources for different time periods and will explain impacts of SLR on both regions. This study improves understanding of SLR impacts on vegetation, ecosystems and groundwater around these rivers using geospatial analysis. The temporal and spatial impact of SLR on these factors was very clear through the integration of remotely sensed land change with data on water salinity, SLR rate and rate of land subsidence in the river regions.

## **1.1 Background**

The threat of SLR has arisen due to climate change and the growth of greenhouse gas emissions leading to global warming. The global average temperature is increasing at the rate of 0.2°C per decade, which will accelerate future SLR (Dasgupta et al. (2009); Li et al. (2009)). Global SLR is due to thermal expansion of ocean water and the breakup

of the Greenland and West Antarctic ice sheets; together these might produce 1- 5m SLR by 2100 (Rahmstorf (2007); Hansen (2007); Mcleod et al. (2010)). Many research studies have attempted to assess the impact of sea level rise in coastal environments, particularly in areas with important economic activities along these coasts. An essential factor in this research is how best to characterize coastal environmental impacts over time, through both future-looking site-specific numerical modeling and past and present site-specific observational studies (Werner and Simmons (2009)). Most hydrologic studies focus on the freshwater zone density in the coastal area, which is difficult to estimate because of the lack of data about properties of water. Usually, these studies use the Ghyben-Herzberg relation equation (W. BadonGhijben (1888, 1889) and A. Herzberg (1901), Verruijt (1968)). It is a relatively uncomplicated equation, and it has been used successfully in various areas to estimate the intensity of salt water and the density of freshwater in an aquifer (Barlow (2003)). In the following equation, the density of the freshwater area above sea level is  $h$  and that below sea level is  $z$ . Both densities are related by:

$$z = PF / (Ps - PF) * h \quad (1.1)$$

Where  $PF$  represents the density of freshwater (1.000 grams per cubic centimeter ( $g/cm^3$ ) at 20°C), and  $Ps$  represents the density of saltwater (1.025 grams per cubic centimeter ( $g/cm^3$ )) (Verruijt (1968)). The equation may be simplified to  $z = 40 \times h$  (Antonellini et al. (2008); Verruijt (1968)).

Most related studies focus only on the characteristics of particular study regions, so it is hard to draw universally applicable conclusions about the impact of SLR (Werner and Simmons (2009)). For example, Sherif and Singh (1999) used numerical simulations to

model SLR-driven saltwater intrusion in two different coastal aquifers. The first was in the Nile Delta, where SLR was predicted to cause intrusion of 9.0 km. The second was in the Madras aquifer in India, where SLR in the Bay of Bengal was predicted to cause intrusion of 0.4 km in this delta (Sherif and Singh (1999)). These regions exhibited widely different conclusions in physical or more hypothesized terms. These variations do not describe a systematic comparison between these places (Werner and Simmons (2009)).

Also, a study by Bobba (2002) focused on sea level rise intrusion in Godavari Delta in India and developed numerical simulations for that delta. In this study, simulations were applied to describe an obvious risk of mixing fresh water with salt water because of sea-level rise, but it is very complicated to describe the influence of vertical intrusion of seawater into the aquifer (Bobba (2002)). The complexity of the numerical model did not allow an easy investigation of the latter influence, and the study does not express any quantitative results about the amount of seawater intrusion produced by sea-level rise (Barlow (2003); Bobba (2002)).

More uncertain too is that although many of these studies use sophisticated quantitative modeling techniques, most do not provide quantitative results about the impact of sea-level rise, probably the result of an original inability to explain the different ways contributing to both salinity effect measurement and groundwater and surface water hydraulic head (Barlow (2003)). SLR risk is high in coastal river regions with canals and drainage networks enabling saltwater intrusion from the sea to inland areas (Good and Wilson (1995)). So, good digital elevation models are essential to hydrologic processes and modeling the SLR (Poulter and Halpin (2008)). Digital elevation data with different vertical and horizontal resolutions can produce different estimates of coastal vulnerability to flooding for the same regions (Poulter and Halpin (2008)). In many coastal regions,

hydrologic complexity is increased by the presence of canals and drainage networks, features small enough to be challenging to identify. Because of that, models require DEM data with low error and high spatial resolution (Lindsay (2006)).

Finally, inundation under various SLR scenarios is commonly characterized using the bathtub model. Given the lack of hydrologic and subsurface data for more complex hydrological modeling in the SARR, the bathtub model is the best method to estimate impacts of SLR in the proposed research. SLR is treated like rising water in a bathtub, where regions with an elevation less than a targeted flood level will be predicted to be inundated (Yunus et al. (2016)). The main steps and a schematic diagram of the processing scheme followed to provide the foundation for the research from obtaining modeling the effects of SLR on near-coastal riverine regions research grade dataset through the preprocessing steps that have been followed before. The main research components of this dissertation are summarized in Figure 1.1. The conceptual model shows stages of the study process to present the foundation for the research to model the effects of SLR on near-coastal riverine regions. In chapter four and five, I use SRTM DEMs and error propagation modeling to enhance the SRTM DEMs. SRTM 30 m is the best global DEM data for bathtub modeling. Bathtub modeling is a valuable GIS-based approach for detecting and characterizing impacts from SLR on both regions. The use of bathtub modeling to identify human and environmental SLR impacts in these regions is important and to predict SLR over the next several decades.

### **1.1.1 Shatt Al-Arab River**

Shatt Al-Arab River (SAR) has received little attention, despite its potential susceptibility to SLR impacts, which are not well known. Regional SLR studies for Persian Gulf did

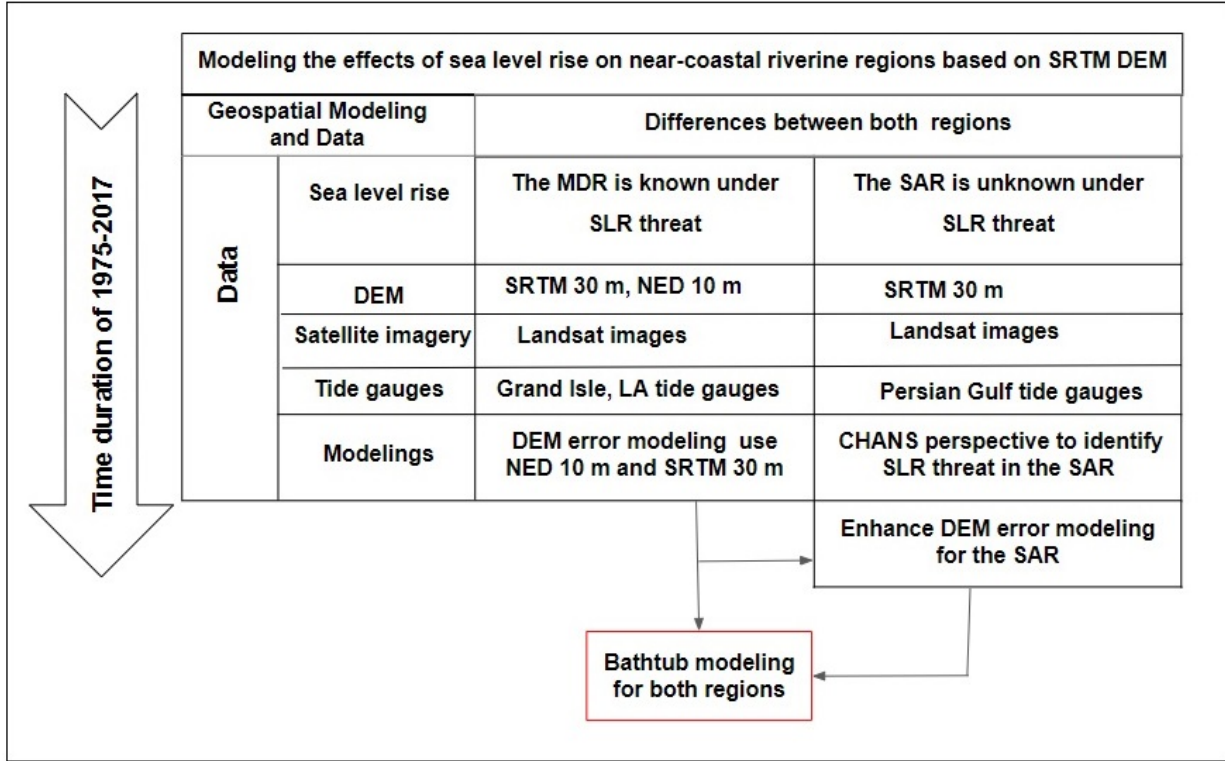


Figure 1.1: Modeling the effects of sea level rise on near-coastal riverine regions based on SRTM 30 m data preprocessing for the research work.

not discuss Iraq’s coast, arguing that this coast is a narrow area (El Raey (2010)). This study did not take into consideration Shatt Al-Arab river, which flows 193 km from the junction of Tigris and Euphrates rivers to the Gulf. The river’s width is 790 m at the coast (Al-Saaidy (2008)). A number of regional studies have used tidal gauge data in Persian Gulf to estimate relative sea level change for locations near the outlet of Shatt Al-Arab river.

Alothman (2014) constructed a time-series record from seven coastal tide gauges in this area. A relative sea level rise of  $2.2 \pm 0.5$  mm/year was observed from this record over the period 1979-2007. This result contrasts with the findings of Hassanzadeh (2007), who reported a rate of 2.8 mm/year (1990-1999) for the northern part of Persian Gulf. This study used data from tide gauges at Bandar Abbas, and Bushehr combined with

atmospheric data at both stations to investigate the mean sea level (MSL) response to meteorological forcing functions in this region. An earlier study by Sultan (1995) estimated a constant rate of  $2.1 \pm 0.1$  mm/year (1980–1990) using two-tide gauges. In an update, Sultan (2000) identified a sea level rise of 1.7 mm/year (1980-1994) using nine tide gauges. Hossein (2007) reported a mean rate of  $2.34 \pm 0.07$  mm/year (1990–1999).

The variability of these estimates of mean sea level change may be due to incomplete and inaccurate records. In addition, it can be related to the significant seasonal variation of sea level in Persian Gulf due to air pressure: water level in the Gulf is up to 26 cm higher in summer than in the winter (Sultan et al. (1995b); Hassanzadeh et al. (2007)). Nevertheless, all studies agreed that regional sea level rise is 2–2.5 mm per year from the 1980s to the 2000s.

The influence of SLR may be impactful in this region, for large areas of low-lying land have important human activities like agriculture. Lining the river is the largest date palm forest in the world. Stretching back from the riverbanks towards the desert, date plantations extend for distances varying from a few hundred meters to almost six kilometers. In the mid-1970s, the region counted some 17-18 million date palms or the fifth rank of the world's 90 million palm trees. By 2002, more than 14 million, or 80 percent, of the palms were wiped out due to salinization in Shatt Al-Arab region, which began emerging in the late 1960s (Singh et al. (2005); Brandimarte et al. (2015)). Of the 52,000 hectares of date farms fringing Shatt Al-Arab in 1975, only 11,000 hectares, or 21% remained in 2002. In total, war, salt and pests destroyed approximately 14 million palms: around 9 million in Iraq and 5 million in Iran. Moreover, of the remaining 3-4 million palms, many are in poor condition (Singh et al. (2005); Brandimarte et al. (2015)). Many studies have focused on environmental problems (Jabbar and Zhou (2011)), land change (Al-Bahili et al. (2010))

increased concentration of salt in Shatt Al-Arab (Al-Mahmood (2009); Essa (2012)) and increased concentration of salt in the land around the river (Mahmood et al. (2013)). All of these studies agree that the tide is the source of increasing salinity and its effects. However, no one mentioned the role of SLR impact on environmental problems. However, this region is affected twice daily by the tide, a source of salinity in the region which contribute to environmental problems and reduced vegetation around the river due to both increased water salinity and increased concentration of salt in soils.

### **1.1.2 Mississippi River Delta**

The MRDR has a highest relative sea-level rise in the U.S. due to the combination of global sea-level rise and local subsidence (sinking land). Land-surface altitude data collected in a region indicated mean annual subsidence of 5 mm per year during five survey epochs between 1951 and 1995 (Burkett et al. (2003)). Subsidence rates in Mississippi river delta are further increased due to a large amount of fluid withdrawal in the northern Gulf of Mexico. Oil and gas extraction leads to increased soil compaction over a short amount of time (Blum and Roberts (2009); Penland and Ramsey (1990)).

Many previous remote sensing studies have estimated MRDR flooding and how much this delta lost land because of SLR. (Couvillion et al. (2011)) based their estimate on the survey and aerial data and raised concerns about comparability of the 1932 and 1956 datasets. In contrast, (Blum and Roberts (2009)) based their estimates on aerial and satellite imagery from 1932 to 2010. Both of the studies reveal that MRDR lost more than 25% of its land area with a net change of about -1,883 square miles ( $mi^2$ ) in land area from 1932 to 2010. About 95 percent of the decrease in land area accounts for persistent losses. Trend analysis investigations from 1985 to 2010 designate a wetland loss rate of 16.57  $mi^2$  per

year (Dasgupta et al. (2009); Barras et al. (2008); Couvillion et al. (2011); Blum and Roberts (2009)). The mean sea level rise at Grand Isle, Louisiana (NOAA gauge station 8761724) is 9.03 millimeters/year based on monthly mean sea level data from 1975 to 2017 (Tides and Currents, noaa.gov).

## 1.2 Study Goals

The broad goals of this dissertation are:

1. Reveal the historic and potential future impact of SLR in SARR using geospatial data and methods.
2. Conduct an error assessment and develop statistical error modeling for Shuttle Radar Topography Mission (SRTM) 1 Arc-Second DEM. SRTM is considered the best free global digital elevation data available. This model improves the quality of elevation data in the MRDR. Inundation modeling is used on SRTM to estimate coastal vulnerability to flooding due to SLR.
3. Use the bathtub model on SRTM Global DEM 30 to measure and assess the impact of SLR on SARR and MRDR.
4. Appropriate the right error modeling to enhance the SRTM 30 m DEMs. Then apply bathtub modeling to detect and predict its future flooding over the next several decades.

## 1.3 Study Objectives

The dissertation has four objectives and these objectives are linked to each other as shown in Figure 1.1. Each objective of this study has many geospatial methods. I am using several software packages to complete each objective: GIS software (ArcGIS, ERDAS), and the R statistical software. The dissertation objectives are:

*Objective one.* Compare and contrast MRDR, SARR, and identify whether these regions have environmental degradation because SLR is based on the theoretical framework and previous studies. To achieve this objective, the following steps are used:

1. Characterize the geomorphology and climate in both regions and show how that is correlated with SLR in both regions.
2. Identify human activity and economic importance in both regions and also identify how the human system accelerates SLR risk in both regions.
3. Assess the different ways that SLR may affect both regions through rising salinity in groundwater, pressure from subsidence erosion and regional flooding.

*Objective two.* Use a CHANS perspective to characterize and delineate a clear conceptual model for factors impacting SARR and identify how human and natural systems are associated with SLR risk in this region. For achieving this objective, these steps are followed:

1. Identify primary human and environmental drivers in SARR system.
2. Characterize NDVI as a proxy for vegetation quality and quantity and measure it over a five decade period.
3. Identify spatial and temporal changes in NDVI throughout the SARR.

4. Link observed changes to dominant drivers of change in the SARR.

*Objective three.* Enhance SRTM Global DEM to better model SLR and characterize land change in MRDR. For this objective to be accomplished, certain are followed:

1. Determine how SRTM error correlates with canopy cover (derived from Landsat 7).
2. Identify the extent to which SRTM error is reduced using canopy cover and other globally available covariates.
3. Assess the effectiveness of geostatistical models in reproducing inundation model results using high-accuracy USGS NED in this region.

*Objective four.* Develop error propagation models to enhance SRTM 30 for modeling sea level rise and characterizing the land change in SARR. This is achieved via the following steps:

1. Apply the error model from objective three, developed for MRDR, to SARR.
2. Determine and map land flooding due to SLR in SARR and identify the land which will become inundated based on the bathtub model.
3. Apply a valid geostatistical model to account for SRTM error and asses uncertainty in SLR inundation model.

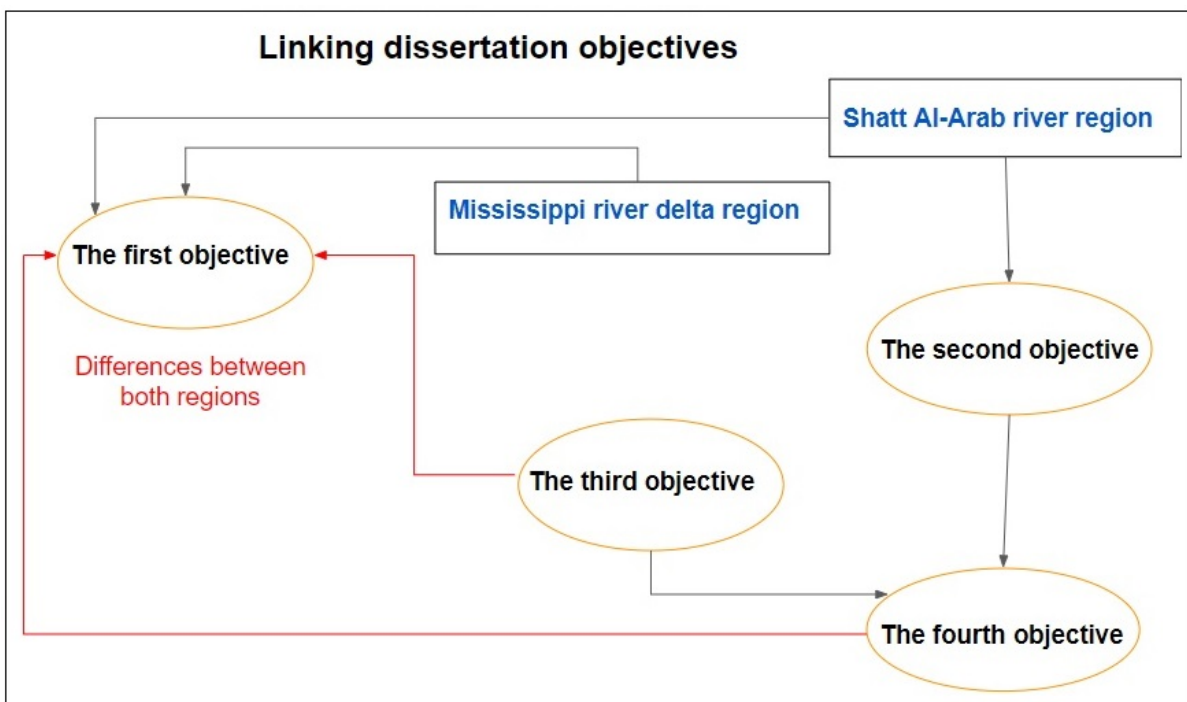


Figure 1.2: Linking dissertation objectives.

# Chapter 2

## A Comparison Between Shatt Al-Arab River Region in Southern Iraq with Mississippi River Region in Southern Louisiana, USA.

### 2.1 Introduction

SLR is a natural process greatly accelerated by humans in direct and indirect ways. For example, human activity creates greenhouse gases which cause thermal expansion of seawater and melt glaciers, ice caps, and ice sheets, directly leading to sea level increase (Pfeffer et al. (2008)). Humans also indirectly affect SLR through actions like dam building which reduces sediment supply to river deltas as in MRDR (Blum and Roberts (2012)). Dam construction also affects deltas due to reduced fresh water which encourages saltwater intrusion as in SARR (Al-Mahmood (2009); Essa (2012)). Human activities in the coastal area like oil extraction, irrigation, and groundwater mining can also be related to SLR and saltwater intrusion in these regions (Blum and Roberts (2012); Al-Mahmood (2009); Essa (2012)). According to (Nicholls and Cazenave (2010)) and Figure 2.1, there

are a range of factors contributing to global SLR:

1. Warming water in oceans which causes thermal expansion for the water and rising sea level because of global warming.
2. Increased water input to oceans because of melting glaciers in the tops of mountains due to global warming.
3. Melting ice in Greenland and Antarctica at a faster rate than ice accretion because of global warming.
4. The Earth's tectonic activity which causes land subsidence in some coastal areas (relative SLR).

The Fourth Assessment Report (AR4) of the Intergovernmental Panel on Climate Change (IPCC (2013)) projected that global SLR will exceed 1m by 2100 in response to warming oceans and melting glaciers (Rahmstorf (2007)). That means the SLR is expected to increase over time. The sea level will be rising because of ongoing temperature increase. Each decade temperatures rise 0.5 Celsius degree (Cabanis et al. (2001)). This increase in temperature will continue with the continuation of industrial pollution and deforestation by people and misuse of water sources.

According to (Clark et al. (2016)), the temperature has changed since the glacial maximum (21,000 years ago) and the mid-Holocene (6,000 years ago). Looking forward, global temperature estimates for the late 21st century are projected to be increasing more rapidly than current trends according to the IPCC scenario AR5V, as shown in Figure 2.2(c and e) (Meehl et al. (2005); Clark et al. (2016)). Anthropogenic increases in atmospheric carbon dioxide (Figure 2.2 (a and b)) is a principal driver of these changes (Clark et al. (2016)).

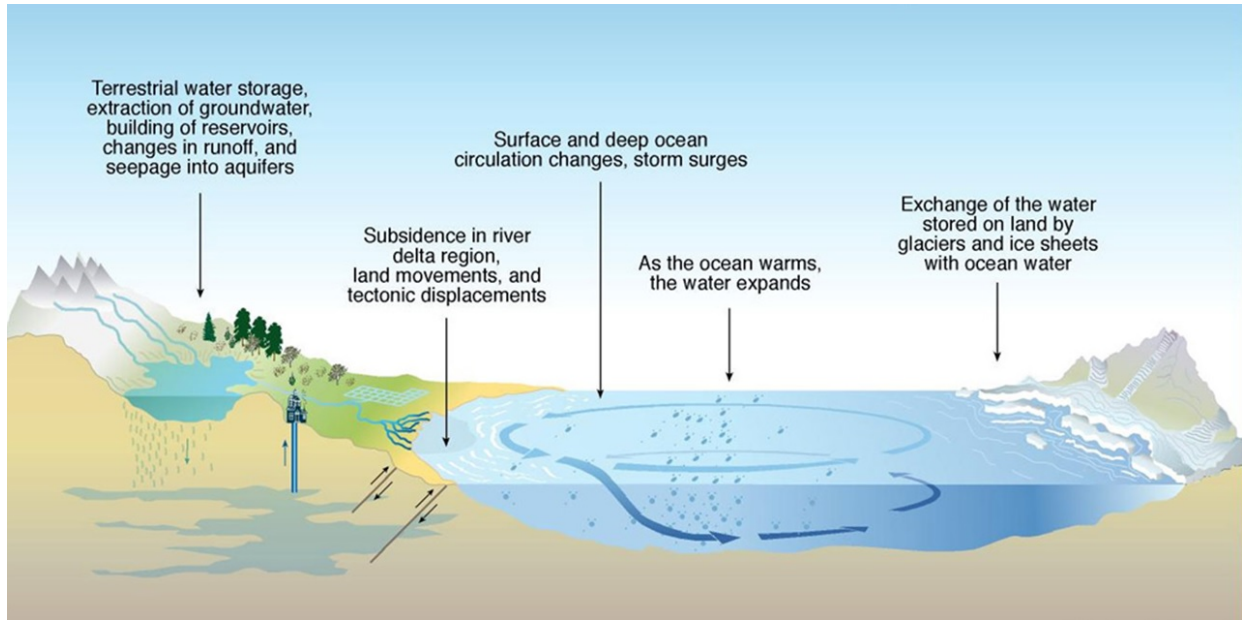


Figure 2.1: The natural system which causes the sea level to change, adopted from Brandimarte et al. (2015).

SLR is not uniform across the earth (Rahmstorf (2007); Vermeer and Rahmstorf (2009)), according to Figure 2.3:

1. The areas near the equator have higher sea level than other regions of the world due in part to greater thermal expansion in warm regions.
2. The areas which are geologically unstable along the boundaries between Earth's tectonic plates or due to isostatic rebound have higher SLR than other more stable places in the world. For example, MRDR has experienced 9 mm SLR during the last decade because the land surface is dropping.
3. The areas experiencing human activity like oil extraction and groundwater extraction can have higher relative SLR. Also, elevations of delta areas may be influenced by upstream human-built dams which store the sediment that would otherwise be deposited in these regions, leading to relative SLR (IPCC (2013)). Human manage-

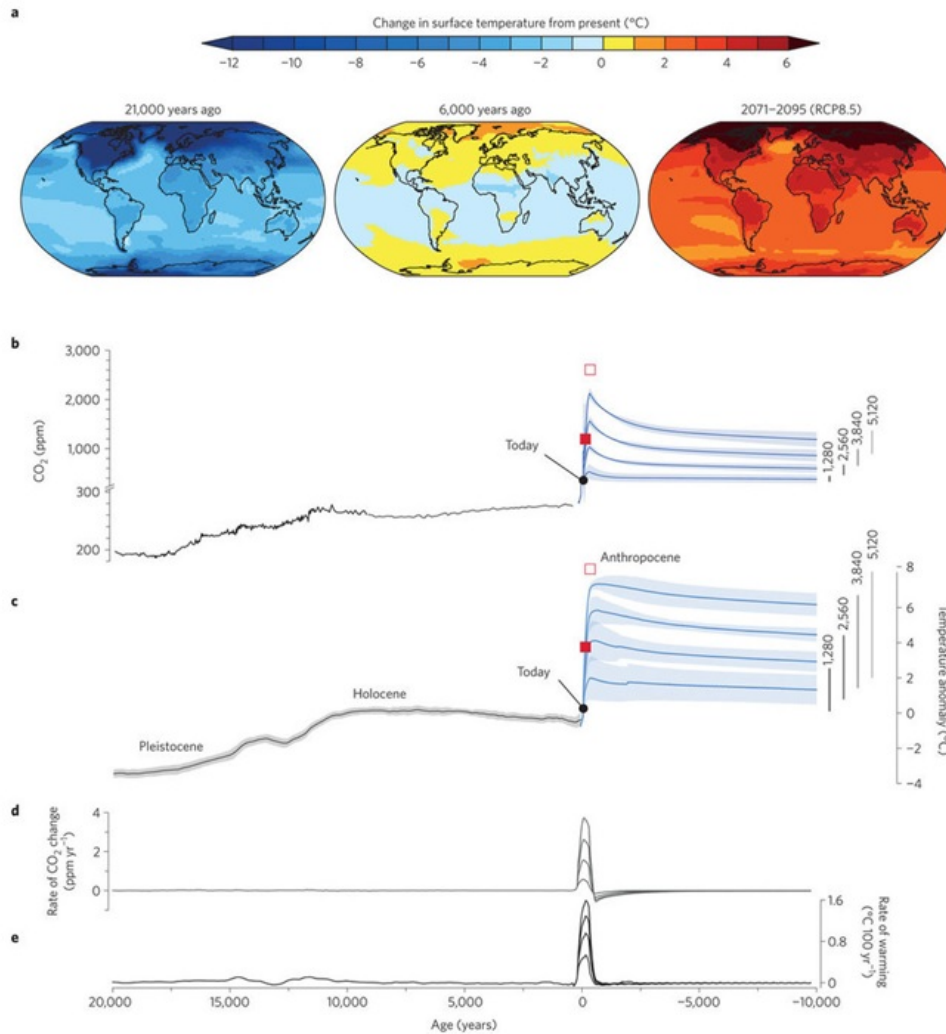


Figure 2.2: The change of the mean temperature and the carbon dioxide in the atmosphere for the global in the past and future, adopted from (Clark et al. (2016)).

ment of coastal areas is very important in protecting coastal areas from saltwater intrusion. Irrigation and drainage should be controlled and projects in these regions should be continuously maintained as well (IPCC (2013)).

4. Weather activity like hurricanes and storms can affect the coastal areas. Also, earthquakes, tsunamis, and the El Nino phenomenon can have greater effects from rising SLR and further damage coastal regions.

The SARR and the MRDR have different rates of SLR. MDR has higher SLR but the

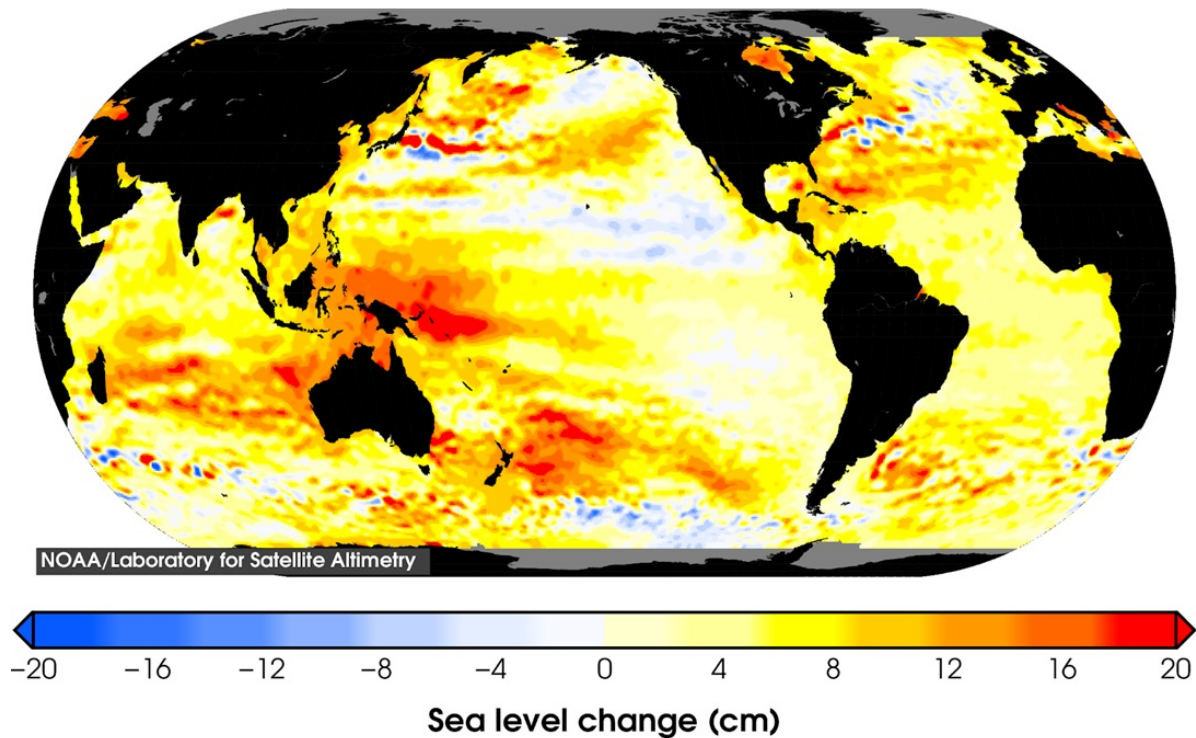


Figure 2.3: Total sea level change since 1993 based on TOPEX/Poseidon.

geographic characteristics in SARR may enhance the influence of SLR in this region.

## 2.2 The Geographical Characteristics

The study of geographical characteristics is important to clarify the risks of SLR in both regions. Table 1 compares and contrasts these general characteristics for MRDR and SARR. Both regions have important similarities and differences. A review of the characteristics in both regions can help to identify a robust and general model to detect and characterize SLR impact on these near coastal riverine areas. This chapter compares and contrasts the SLR-related social and environmental characteristics in SARR and MRDR.

Characteristics in both of the regions	Mississippi River Delta region	Shatt Al-Arab River region
Geomorphological	Land created by sediment from Mississippi River mouths in the Gulf of Mexico	Land created by sediment from Tigris, Euphrates and Karun Rivers in Persian (Arabian) Gulf
Environmental	Most region is marshes	Most region is agricultural fields
Climatic characteristics	Mild winters and hot and humid summers	Hot desert climate
Economic importance	Shipping and commercial fisheries. Oil and gas deposits	Shipping and commercial fisheries. Oil and gas deposits
Population	More than two million people	More than three million people
Cities	New Orleans	Basra

Table 2.1: Comparison of the study regions.

### 2.2.1 Topography Characteristics

Most parts of both regions are less than one meter above sea level as shown in Figure (2.4). According to SLR scenario (Williams (2009)), land with absolute elevation below one meter is very vulnerable to SLR. Many studies have presented the problem of SLR in MRDR from a variety of disciplinary perspectives, including engineering, biology and geography (Burkett et al. (2003)). There is no published study specifically investigating the impact of SLR on the SARR because of the lack of quality digital elevation data for this region. So one of the objectives of this research is to enhance the digital elevation data to show vulnerability to SLR in this region (El Raey (2010)). However, both regions are threatened by SLR and both will be flooding due to SLR inundating low elevation areas. The topographic characteristics of both regions are considered in the following subsections.

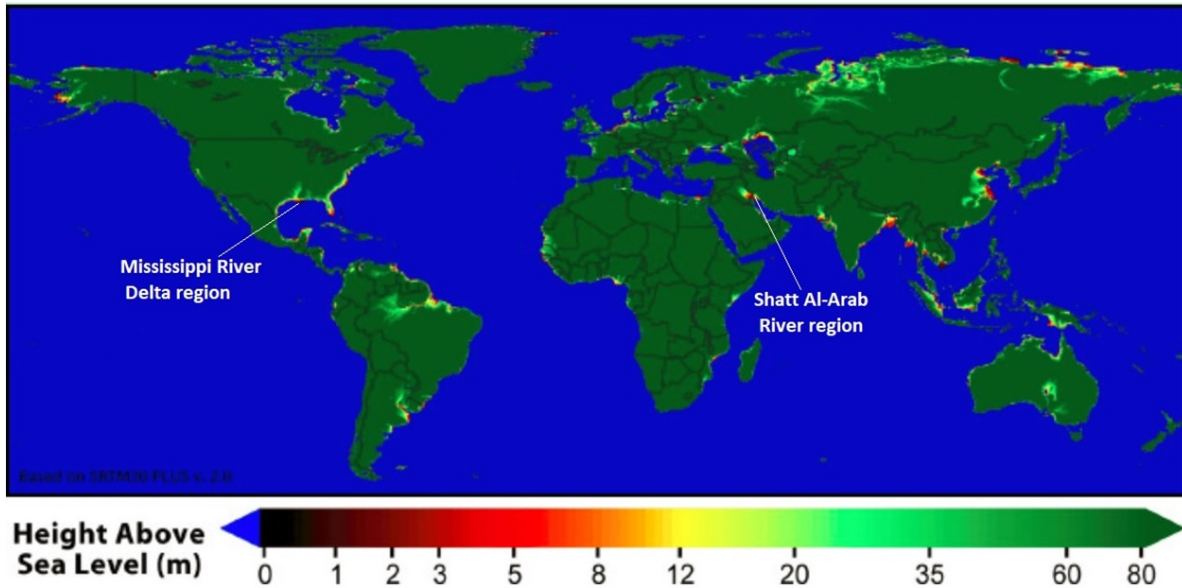


Figure 2.4: Both SARR and MRDR have high rising sea levels, adopted from (Williams (2009)).

### 2.2.1.1 Topographic Characteristics of Shatt Al-Arab River Region

This region includes land on both sides of Shatt Al-Arab south of the city of Basra to Persian (Arabian) Gulf, as shown in Figure 2.5. Elevations in Shatt Al-Arab region descend slowly from 2m in the north to 0.5 m and less in the south. Land elevation also decreases from the banks of Shatt Al-Arab 5.2 m to less than 1 millimeter in the lowlands away from the river (Al-Saaidy (2008)). The total area of Shatt Al-Arab study region is 2189 km<sup>2</sup>. River width increases from about 0.5 m at Basra to 0.8 km at its mouth. Along the settled banks there are date-palm groves, which are naturally irrigated by tidal action (Saad (1978)).

### 2.2.1.2 Topographic Characteristics of Mississippi River Delta Region

This region ranges along Mississippi from its junction with the Bayou Lafourche downriver to the Gulf of Mexico and covers 11,894 km<sup>2</sup>, as shown in Figure 2.6. This study

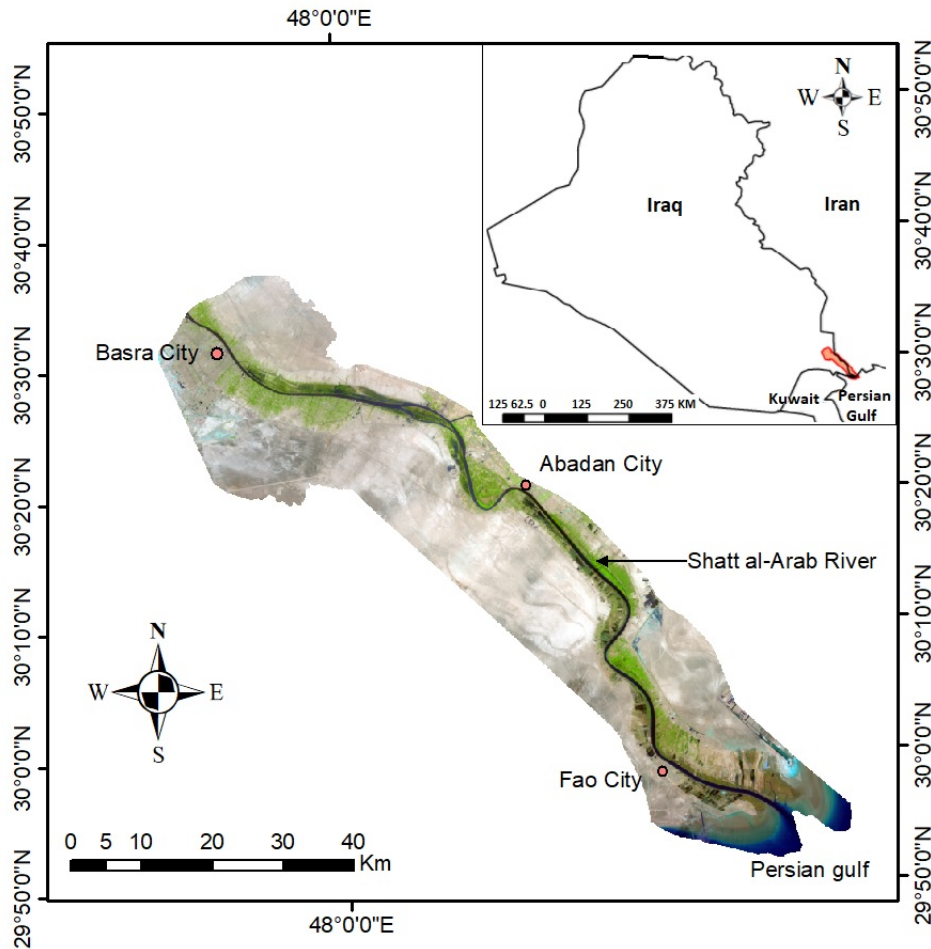


Figure 2.5: Shatt Al-Arab river region in southeastern Iraq.

focuses on an area around the river that is part of Louisiana coastal plain. This important region, which is mostly coastal wetlands, has a distinctive ecology and landscape and is rich in resources (Steyer and Llewellyn (2000)). The width of the alluvial region along MRDR from 15 to 100 km. Mississippi River flows along a ridge formed by its own natural deposits (known as a levee), from which the land elevation declines at an average fall of 33 m/km. The alluvial lands along other streams have similar terrain (Zellmer and Klein (2007)).

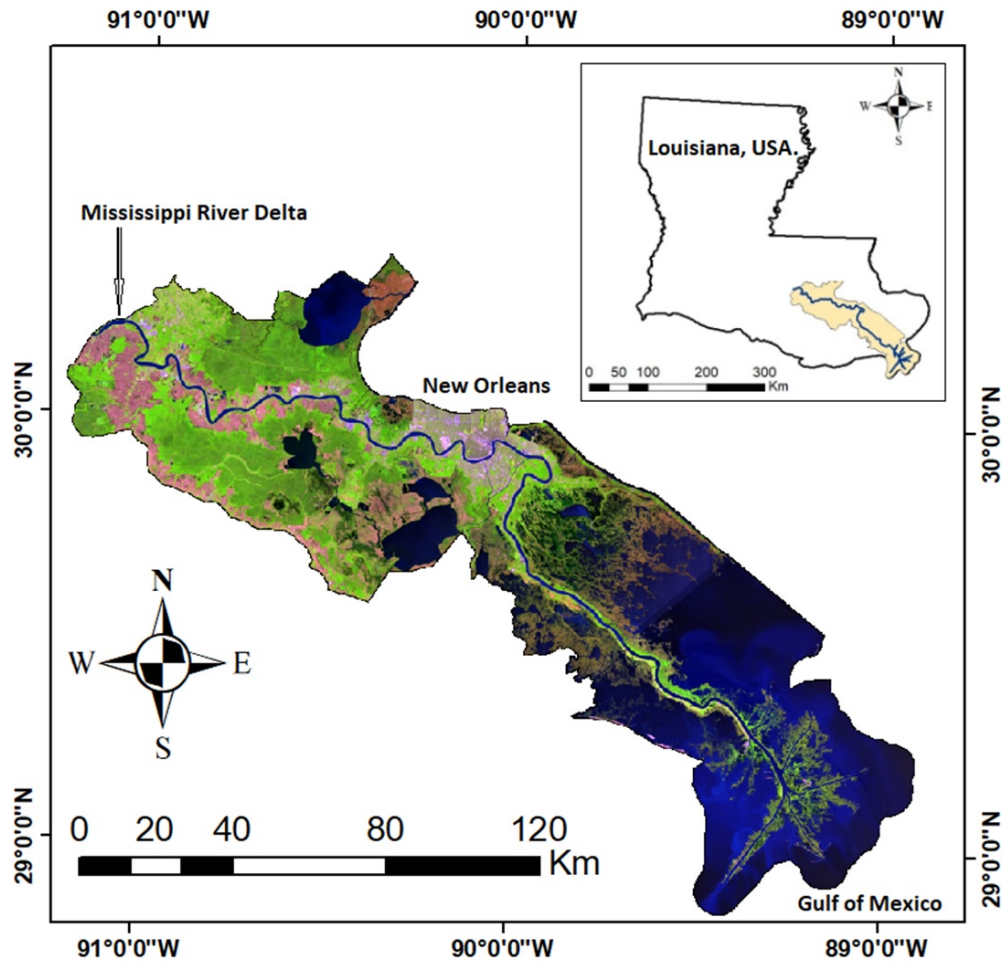


Figure 2.6: Mississippi River Delta region in Louisiana, USA.

### 2.2.2 Geology Characteristics

The coastal areas with unstable geology may experience a higher relative rate of SLR (Vermeer and Rahmstorf (2009); Rahmstorf (2007)). It is, therefore, important to understand the influence of the geologic characteristics in both regions. The following subsections report the geology of each region in this study.

### **2.2.2.1 Mississippi River Delta Geology and Ecology**

The MRDR formed 100 million years ago in the late cretaceous Period (Galloway et al. (2011)). Since the end of Cretaceous times, the central portion of North America has drained to the south into the Gulf of Mexico. Mississippi and other rivers drained of the Appalachian Mountains to the east and the Rocky Mountains at the western margin and delivered large volumes of sediment to the northern rim of the Gulf of Mexico. The ancestral Mississippi and other rivers created Progradation in sedimentary geology and geomorphology. The term progradation refers to the growth of a river delta farther out into the sea over time (Galloway and Hobday (1983)). MRDR created six delta lobes during the Holocene. These lobes are as follows: the Maringouin delta formed 7,500 to 5,500 years ago, the Teche delta created 5,500 to 3,500 years ago, the St. Bernard delta created 4,000 to 2,000 years ago, and the Lafourche delta created 2,500 to 500 years ago. The modern delta, called the Plaquemines-Balize delta or Birds Foot Delta, began forming 1,500 years ago, and the Atchafalaya and Wax Lake Deltas began forming 500 years ago (Blum and Roberts (2009)).

The dominance of this river system produces a complex branching small river width to length ratio for the delta plain. The current annual sediment discharge of 145 million metric tons marks a substantial reduction from the 400 million metric tons per year of material that built most of the delta before large-scale human activities modified the river basin with dams, locks, meander cutoffs, and other engineering structures (Giosan and Freeman (2014)). There are different kinds of swamp and marsh habitats in the delta plain: the upper delta plain has freshwater habitats, while the lower delta plain features brackish to saline marshes because of tidal inundation (Giosan and Freeman (2014)).

The MRDR is experiencing the highest relative SLR in the U.S. due to the combination of global SLR and local subsidence (sinking land) (U.S. Global Change Research Program, 2009). Great subsidence is possible in river deltas where rapid sediment accumulation traps a significant amount of water. Over time, as layers of new sediment are deposited, water is squeezed out of the underlying deposits, causing compaction and the land surface to sink. Subsidence rates in the MRDR have increased due to the presence of levees and diversions which have reduced river flooding of the marshes behind the levees, starving them of sediment. On another hand, the soil compaction from oil and gas extraction in the region cause coastal land loss (Blum and Roberts (2012)). While levees can limit flooding damage, their presence also reduces sediments that build the delta. Taken together, these factors have caused the recent loss of about 4,920 km<sup>2</sup> of coastal wetlands in the state, more than one-third of its coastal plain (Blum and Roberts (2012)). The analyses of landscape change presented in (Couvillion et al. (2011)) report the use of historical surveys, aerial data, and satellite data to track landscape changes. Summary data are presented from 1932 to 2010; trend data are presented from 1985-2010 with analysis based on satellite and aerial imagery. These findings show that Louisiana coast has undergone a net change in land area of about -3030.3948 (km<sup>2</sup>) from 1932 to 2010 (Couvillion et al. (2011)).

#### **2.2.2.2 Shatt Al-Arab Geology and Ecology**

This region includes land on both sides of Shatt Al-Arab south of the city of Basra to Persian Gulf. Shatt Al-Arab region descends slowly from 5m a.s.l. in the north to 0 in the south. Land elevation also decreases from 5m along the riverbanks to less than 1 millimeter in the lowlands away from the river (Al-Saaidy (2008)). Total area of Shatt Al-Arab

study region is 2,188.615 sq km. Its width increases from about 37 m at Basra to 0.8 km at its mouth. The water level, in at least the lower portion of the system, is considerably affected by the tides of the Gulf (Saad (1978)). SARR is located on the unstable tectonic plate (Buday et al. (1987)). SARR is part of the north of Persian Gulf. Much of the deformation and seismicity responsible for the high-relief topography of the Zagros Mountains and northeastern margin of Persian Gulf can be explained within the context of active tectonics associated with plate convergence. Known to be a tectonically quiescent region is the seismic low-relief coastal areas along the southern sideline of the Gulf. As a result, sea-level changes have been a focus in previous studies as a description of the evolution of the Pleistocene and Holocene coastline site. We hypothesize that the tectonic movement was more significant in the late-Pleistocene/Holocene shore development as opposed to the sea-level variations which also influenced this region (Wood et al. (2012)).

### **2.2.3 Hydrology Characteristics**

The flow of water through a river basin is of course important for conditions in its delta. Discharge is affected by the size of the basin, the balance of precipitation, evapotranspiration within that basin and also by water storage and diversion upstream. Human influence can play a major role because of dam construction and irrigation, as well as climate change. In this section, the hydrology of both regions in this study are discussed.

#### **2.2.3.1 Mississippi River Flow**

Mississippi River is one of the world's greatest in size, environmental diversity and natural fertility. It carries the greatest volume of water in the US, flowing 3,705 km from its origin at Lake Itasca in Minnesota, through the mid-continental United States, and to

the Gulf of Mexico Riverine Plain and its subtropical Louisiana Delta (Zellmer and Klein (2007); Blum and Roberts (2012)). Within the state of Louisiana, Mississippi River flows from north to south for a length of approximately 1,000 km and drains into the Gulf of Mexico; the Red River; the Ouachita River and its derivatives; and additional secondary streams. The extent of the alluvial area along Mississippi is of 16 to 97 km.

The study area in MRDR region ranges along Mississippi from its junction with the Bayou Lafourche downriver to the Gulf of Mexico 11894.27 sq km (Couvillion et al. (2011)). We are focusing on an area around the river that is part of the Louisiana coastal plain (Baras (2006)). This important region, which is mostly coastal wetlands, have a distinctive ecology and landscape and is rich in resources (Steyer and Llewellyn (2000)). The Mississippi River flows along a ridge formed by its natural deposits (known as a levee), from which the lands decline at an average fall of 3 m/km. The alluvial lands along other streams present similar features (Zellmer and Klein (2007)).

### **2.2.3.2 Shatt Al-Arab River Flow**

SARR is in southeastern Iraq and extends from the north to the center of Basra city until the southeastern part of it to form the international border between Iran and Iraq before flowing into Persian Gulf. SARR is formed by the junction of Tigris and Euphrates rivers at Al-Qurnah city. It continues southeastward for 193 km and flows past the Iraqi port of Basra and the Iranian port of Abadan before draining into Persian Gulf. For about the last half of its route, the river forms the boundary between Iraq and Iran; it receives a tributary, the Karun river, from the eastern (Iranian) side. Its width increases from about 40 m at Basra to 0.8 km at its mouth. Along the river banks, there are date-palm groves, which are typically irrigated by tidal action (Saad (1978); Buday et al. (1987)). However,

the water depth relatively decreases at the confluence of the Karun and Shatt al-Arab rivers, due to the continuous accumulation of large amounts of sediments transported by Karun to this locality. The water level is considerably affected by the tides of the Gulf. The water of Shatt Al-Arab may reach Hor Hammar, a large marsh lying at the northwestern sides of Sindbad Island, during the high tide, and the brackish water of this Hor may subsequently enter into Shatt al-Arab and affect its salinity. The level of Shatt al-Arab rises in spring mainly due to the increase in the levels of Tigris and Euphrates during this season. The increase in river flow follows the melting of snow in Turkey. The fresh water from this flood decreases the salinity of Shatt Al-Arab during spring (Al-Saaidy (2008); Saad (1978)).

#### **2.2.4 Climate Characteristics**

There are some distinct climatological issues in both study regions that directly affect the SLR problem. For MRDR, it is a region affected seasonally by powerful tropical storms. These storms can exacerbate SLR issues in several ways: first, during the storm itself, by pushing massive amounts of seawater into areas not normally inundated; second, after the storm, by damaging barrier islands and other features which act to reduce the intrusion of the sea into marshlands. SARR, in contrast, is affected by high seasonal variation of the height of Persian Gulf, which may bring impacts of higher sea level much earlier to the region. Also, water demand in SARR must be satisfied by rainfall in distant areas, which has consequences for the viability of human activity in the area.

Surface water is not the only water affected by SLR according to the Ghyben Herzberg relation equation (Herzberg, 1901; Badon-Ghijben, 1888; Badon-Ghijben, 1889): aquifer water will have higher concentrations of salts in regions with higher temperature. So, the

influence of the SLR on groundwater in this region will be high (Barlow (2003)). MRDR region is a Cfa climate based on the Koppen climate classification as depicted in Figure (2.7). It is a humid subtropical climate defined by mild winters and hot and humid summers which exhibit mean temperatures between 0°C (32°F) and 18°C (64°F) in the coldest month and mean temperatures between 22°C (72°F) or higher in the warmest month (Peel et al. (2007)). In contrast, SARR is a hot desert climate (BWh) according to the Koppen climate classification, as shown in Figure 2.7. BWh is an arid climate which supports little or no vegetation (Peel et al. (2007)).

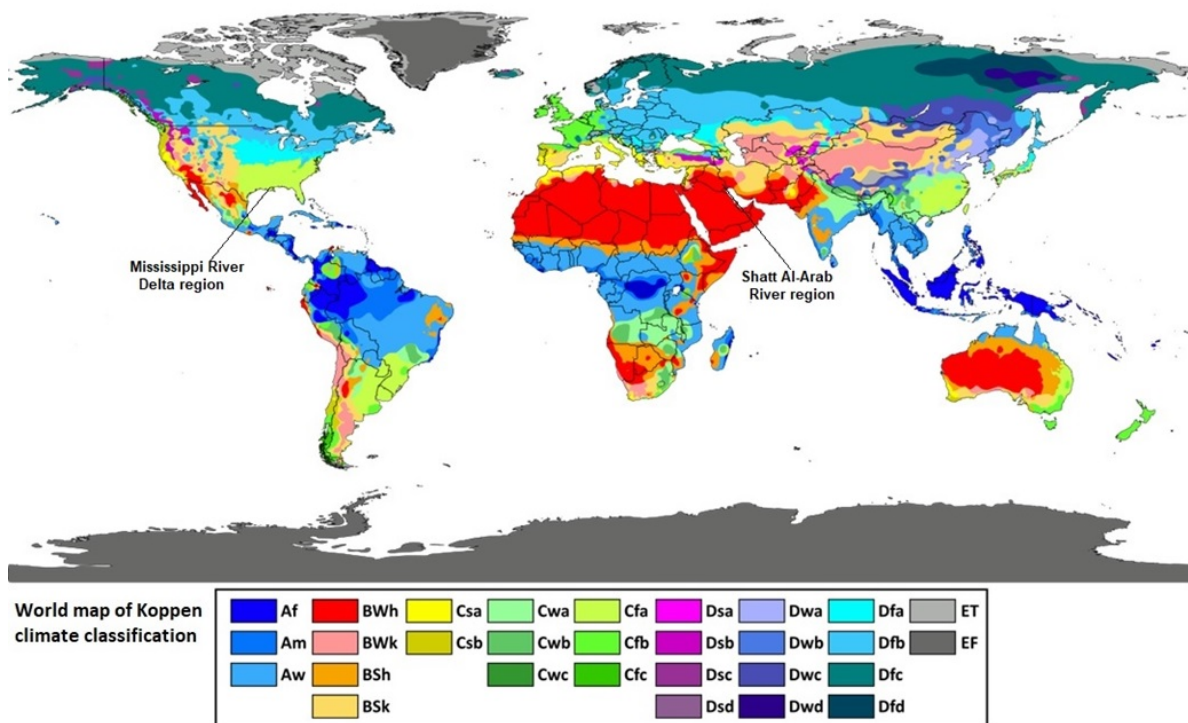


Figure 2.7: World climate regions according to Koppen-Geiger classification, adopted from (Peel et al. (2007)).

### **2.2.5 Human Activity**

There are many studies concerned with the effect of SLR on MRDR including the rise of saline groundwater levels, storm waves, and flooding. Both regions are affected more because they are connected directly with Mexican Gulf and Persian Gulf (Steyer and Llewellyn (2000)). Many studies on land change and inundation in the MRDR have identified relative SLR and land subsidence as primary factors (Blum and Roberts (2012)). In contrast, studies on environmental degradation in SARR have not diagnosed SLR as the source of the problems (Al-Saaidy (2008); Jabbar and Zhou (2011); Al Isawi (2011)). Both regions have been affected by human activities like oil extraction and irrigation which accelerate SLR effects (Blum and Roberts (2012)). There are also large differences between the regions. For example, MRDR has a lot of projects to conserve the region. Most notably, Louisiana's Coastal Protection and Restoration Authority (CPRA) was developed in 2007 to implement projects to restore and protect the region. Federal efforts like CPRA invested more than 20 billion dollars on a range of activities, including levee improvement, fill and construction of berm and barrier islands (Louisiana (2012)). Figure 2.8 is an illustration from CPRA detailing their efforts. On another hand, there is nothing spent to protect SARR.

## **2.3 Conclusion**

This chapter has outlined the Geography, Geology, Geomorphology, Climate, and Human activities in both regions and how these characteristics accelerated SLR:

1. Geologic development of both the Gulf of Mexico and Persian (Arabian) Gulf and how this relates to the general hydrology, sediment transport and solute chemistry



Figure 2.8: Projects by Louisiana’s Coastal Protection and Restoration Authority since 2007, adopted from (Louisiana (2012)).

of the two river systems.

2. Hydrology of Mississippi, Tigris and Euphrates.
3. Changes in hydrology, sediment transport and solute chemistry of both regional river systems caused by various forms of anthropogenic stress (climate and engineering structures).

Both regions are similar in geomorphological, environmental, economic and climatic characteristics. Both are geologically recent creations from the deposits of several of the world’s greatest rivers (Tigris, Euphrates, and Mississippi) flowing into gulfs (Persian Gulf and the Gulf of Mexico). Both regions are important regional economic centers for agricultural production, oil production, fishing and marine transport. Both rivers have natural deltas that have formed where the mouth of each river meets its gulf. Indeed, in recent (1000s’ of years) times, the sea extended hundreds of miles inland, and land in these regions are based on alluvium. Also, land areas on either side of these rivers are

highest along the edges of the channels and decrease in elevation farther from the river. Delta building for both rivers is an integrated and long-term process that has given both regions a unique mix of ecosystems, habitats and landforms. Both regions face increasing pressure from subsidence, erosion, sea level rise and rising salinity in groundwater, leading to coastal retreat in these regions because of the climate change and human activities there.

# Chapter 3

## Causes and Consequences of

## Environmental Degradation Along Shatt

## Al-Arab River: A Coupled Human and

## Natural System Perspective

### 3.1 Introduction

Coupled human and natural systems (CHANS) research concepts explicitly acknowledge the feedbacks between human drivers and natural processes through interactions or flows (Marina et al. (2011); Phillips (2016); Tu (2011)). Research that utilizes a CHANS approach focuses on understanding feedbacks, nonlinearities, thresholds and legacy effects across multiple spatial, temporal and organizational scales (Geri et al. (2010)). CHANS perspectives may be especially useful for the analysis of marginal geographic areas and the people who live on them, as such areas may be particularly vulnerable to social and environmental hazards. Few geographies are more marginal than the land along Shatt Al-Arab River, which begins at the marshy confluence of Euphrates and Tigris rivers in southeastern Iraq and ends 120 km away at the head of Persian Gulf. The lower portion

of the river serves as the international boundary between Iraq and Iran, dividing the region politically. Environmentally, the region is a transition zone between land and sea: most of the area is close to sea level, and in historic times, the waters of Persian Gulf have overlain the region along the river (Meehl et al. (2005)).

The environmental degradation in this region has influenced large areas around Shatt Al-Arab River that provide important human services like agriculture. Extending away from the riverbanks toward the desert, the palm tree plantation extents increase from the south to the north of the region. In the midtwentieth century, this was one of the worlds most important date palm forests, with more than 17 million trees in 1975. The region now has around 2 million palm trees. More than 14 million trees died because salinization developed starting in the late 1960s (Singh et al. (2005)). Of more than 52,000 hectares of SARR date palm plantations in 1975, (Singh et al. (2005)) found that only 11,000 hectares or 21% remained in 2002. More than 14 million palms were destroyed due to salt and pests: around 9 million in Iraq and 5 million in Iran. Moreover, of the remaining 34 million palms, many are in bad condition (Singh et al. (2005); Brandimarte et al. (2015)). A number of studies have focused on factors leading to this degradation, including land change increasing concentration of salt in the river (Al-Mahmood (2009); Jabbar and Zhou (2011); Essa (2012)), and salinization of land around the river (Mahmood et al. (2013)). All studies agree that naturally occurring tidal action is the source of salinity in the river as well as the salinity in the region. In addition, studies have implicated human activity as having played an essential role in the environmental degradation of this transitional region (Jabbar and Zhou (2011); Al Isawi (2011)), including the construction of upstream reservoirs and a high frequency of devastating war within the area.

Remote sensing-based analysis and geospatial methods can be essential to understand

CHANS at multiple spatial, temporal and organizational scales. Long-term records of satellite image data can be used to identify land cover change and key human and environmental processes driving these change (Emel et al. (2014); Liu et al. (2003); Fox et al. (2003)). To date, however, no study of SARR has comprehensively itemized the human and environmental factors that have led to degradation over the past five decades or evaluated their spatial impact. To address this gap, we develop a CHANS framework to identify conflict, water engineering, economic development policy and climate change to environmental degradation and food security in the SARR. Further, we quantify change within the region since the mid-1970s using a mix of ground and remotely sensed data to assess change in normalized difference vegetation index (NDVI). The objectives of this chapter are to:

1. Identify primary human and environmental drivers in SARR system.
2. Characterize NDVI as a proxy for vegetation quality and quantity and measure it over a five-decade period.
3. Identify spatial and temporal changes in NDVI throughout SARR.
4. Link observed changes to dominant drivers of change in SAAR.

## **3.2 Data and Methods**

### **3.2.1 Study Area**

SARR is in southeastern Iraq and southwestern Iran and includes land on both sides of Shatt al-Arab River from north of Basra City to the Persian Gulf as depicted in Figure (3.1).

Its total area is 2,189  $km^2$  (Al-Saaidy (2008)). Land elevation along the river descends gradually from five meters above sea level near Al Qurnah in the north to zero in the south. The banks of the river generally have higher elevations than interior areas. The Shatt al-Arab River flows through Iraq for about 80 km to just above the confluence with the Karun River from the east; from that point to the Gulf the river forms the border between Iran and Iraq. Cities and towns, which have more three million persons as shown in Fig. 1. interspersed with agricultural land and marshes, occupy its banks. The date-palm groves along the river are naturally irrigated by tidal action (Saad (1978)). Most studies treat the Shatt Al-Arab as a unique river because it has a tide two times during the day. Tidal movement from the Gulf controls the hydrology of the river, especially after the decline in freshwater coming from Euphrates, Tigris, and Karun rivers (Abdullah et al. (2015)) in the period evaluated in this study (1975 to 2017). Tides enter the river from Persian Gulf and reach at least as far as Basra City (Cressey (1958)).

### **3.2.2 Coupled Human and Natural System**

To understand the challenges SARR has faced in recent decades, this study develops a framework for both human and natural systems to highlight the dominant factors responsible for environmental degradation in the region. This CHANS framework is represented in the conceptual model shown in Figure (3.2). This model shows how human and natural systems affect the region and how they are linked to environmental degradation in SARR during the periods 1975, 1985, 1995, 2005, and 2017.

The concept Figure (3.2) shows how human and natural systems affect the region and how they are linked to environmental degradation in the SARR during the periods (1975, 1985, 1995, 2005 and 2017).

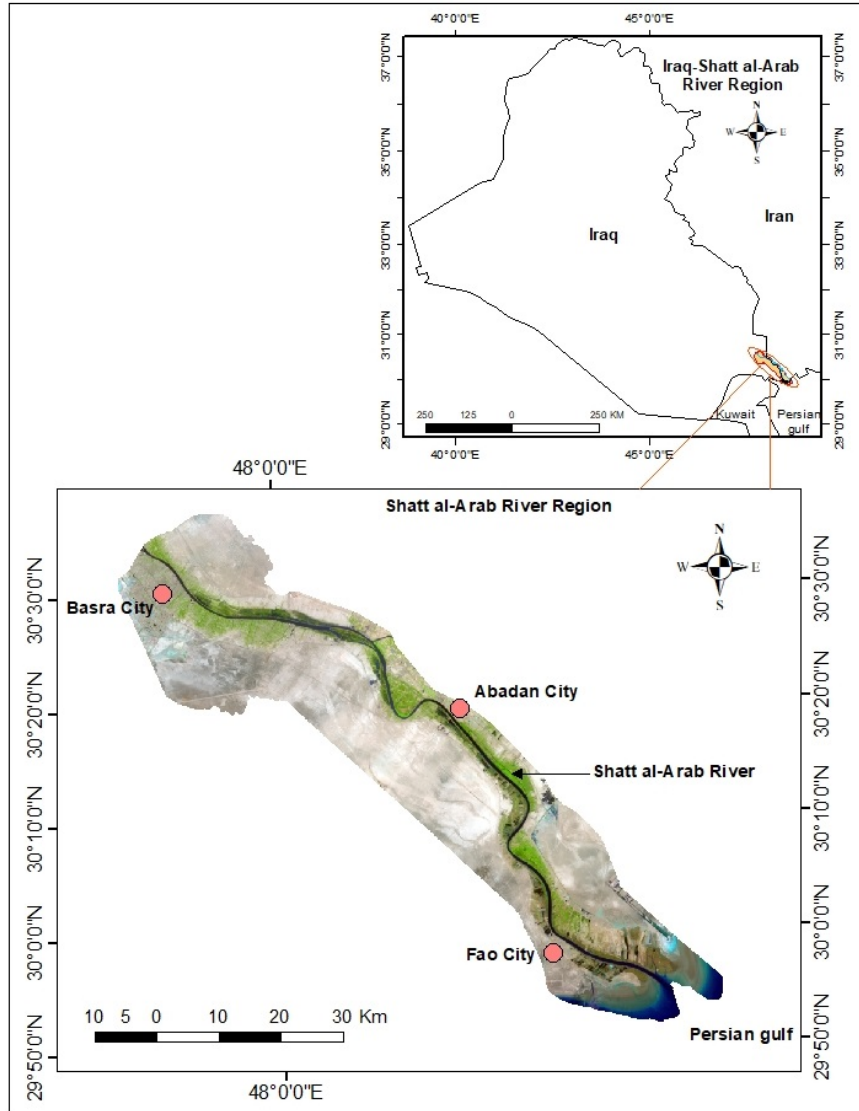


Figure 3.1: Total study area of Shatt Al-Arab river region.

### 3.2.2.1 Human Impacts

The human carbon footprint has spiked more in the last 50 years than in any other period in history, and continues to increase by 2% per year (Sohl et al. (2012); Smiley et al. (2016)). Ecosystems are negatively impacted with less biodiversity because of human interaction. Water ecosystems are responding negatively to human activities, such as pollution, habitat destruction, and overfishing and are becoming more unpredictable and less resilient

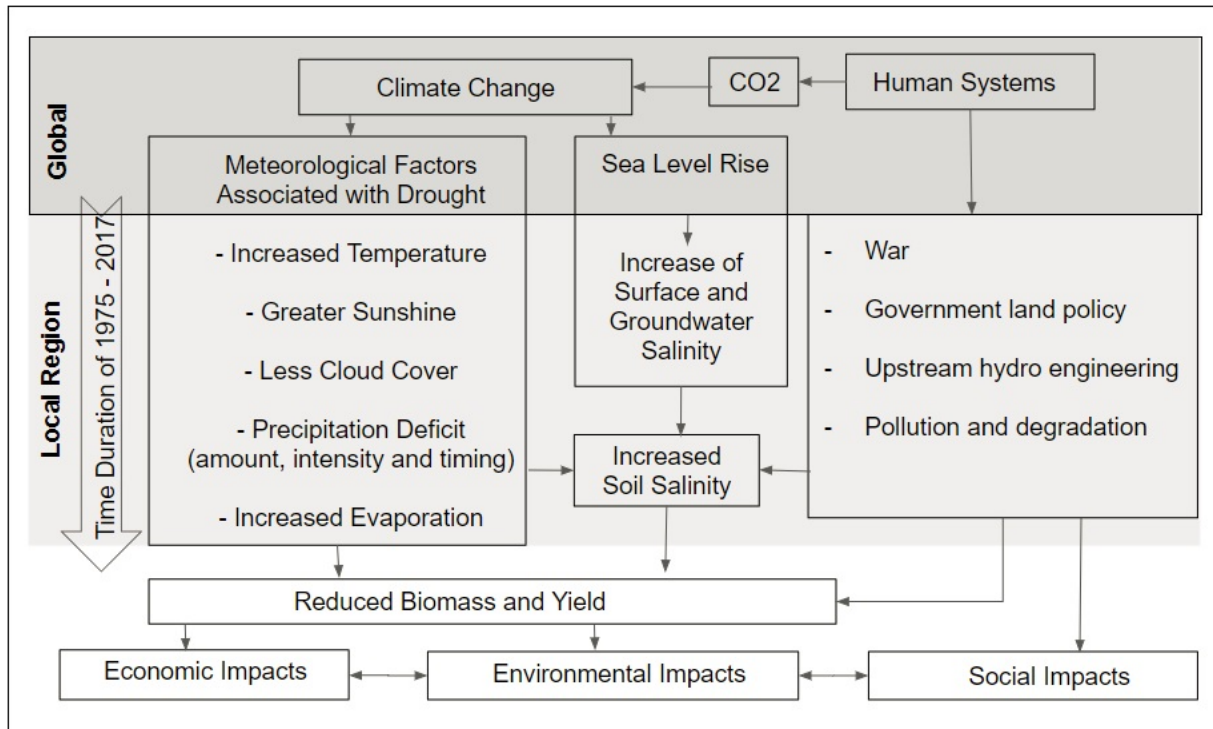


Figure 3.2: Total conceptualization of coupled human and natural systems (CHANS) in Shatt Al-Arab river region.

to external pressures (Jackson et al. (2001); Liu et al. (2007)). Human activities are responsible for global climate change and its effects on plants and animals (Liu et al. (2007); Wohlfart et al. (2017)). These influences can be seen in SARR. The main human systems directly influencing this area are:

- War
- Government land policy
- Upstream hydroengineering
- Pollution and degradation

### 3.2.2.2 Environmental Impacts

While factors like war and environmental pollution provide direct local impacts on SARR, and factors like upstream dams are a regional source of challenges in the area, climate change is the main global-scale challenge facing SARR. Climate change drives sea level rise and meteorological factors leading to regional drought, which in turn negatively impacts vegetation, agricultural productivity, and the livelihood of the people in this region (Jabbar and Zhou (2011); Al-Bahili et al. (2010)).

I identify and assess three specific environmental consequences:

- Meteorological factors associated with drought
- Sea level rise
- Groundwater salinity

### 3.2.3 Methodology

CHANS drivers and effects are complex, multi-factored, and evolving. To provide as comprehensive an assessment as possible, we collected a variety of datasets to evaluate spatial and temporal characteristics of a range of environmental properties for SARR. Long-term (1975-2017) monthly meteorological data (Minimum and Maximum Temperature, Relative Humidity, Rain Quantity) were obtained from researchers at the University of Basrah (Yassein et al. (2016)) to evaluate annual patterns and identify changes over the duration of the study period. Data on salinity of water from the Shatt Al-Arab River from 1980 to 2012 was obtained from Hamid (2014) and Abdullah (2015). I also utilized mosaicked pairs of Landsat images that cover the study area in each of the years eval-

uated (1975, 1985, 1995, 2005 and 2017). Table 3.1 lists the characteristics of each image set. All Landsat images were systematically radiometrically and geometrically corrected and transformed to a common analysis framework with standard output map projection UTM zone, image orientation, and 30 m pixel size. We calculated the normalized difference vegetation index (NDVI) at each time period. NDVI is a standard measure of vegetation intensity and a signal of land use and land cover (Fuller (1998); Justice et al. (1985); Prince (1991); Goward and Prince (1995)). It is measured on a per-pixel basis as the normalized difference between the red (RED) and near infrared (NIR) bands of an image:  $NDVI = (NIR - RED) / (NIR + RED)$ . The analysis was restricted to those areas along the Shatt Al-Arab River with a 1975 NDVI value above 0.1. Regional NDVI changes over time were evaluated, and correlations between NDVI, climatological variables, and salinity were assessed. Finally, NDVI change from 1975 to 2017 was examined within the study area. Three subareas were identified: the northwestern region above the confluence of Shatt Al-Arab and Karun Rivers, which falls almost entirely in Iraq (Upriver), the right (southern) bank below the confluence, which falls in Iraq (Downriver Iraq), and the left (northern) bank below the confluence which falls in Iran (Downriver Iran). NDVI change within each subarea is assessed to understand how degradation processes differentially affect these areas.

Sensors	Satellite	Overpass / Orbit Frequency	Data-Record (years)	Spatial Resolutions
MSS	Landsat 1-2	18 days	1975 and 1985	57 m
TM	Landsat 4-5	16 days	1995 and 2005	30 m
ETM+	Landsat 7-8	16 days	Landsat 7-8	30 m

Table 3.1: Satellite sensors utilized for the study used three sensors to cover the time (1975, 1985, 1995, 2005 and 2017).

### 3.3 Results

1. The chapters second objective is addressed by using NDVI to evaluate regional response over time in vegetation due to the drivers highlighted in the previous sections. Figure (3.3)(a)(e) present maps of SARR NDVI derived from Landsat imagery in 1975, 1985, 1995, 2005, and 2017, while 3f provides NDVI density plots for each time period. The maps qualitatively illustrate substantial changes over time in intensity and distribution of vegetated areas, which are largely date palm plantations, other agriculture, and marsh. Modal vegetation density was highest in 1975 and lowest in 1995, while the upper tails were thickest (indicating more high-NDVI pixels) in 2005. The substantial spatial and temporal variation in vegetation characterized by these findings are responses to human and environmental drivers identified in this study.

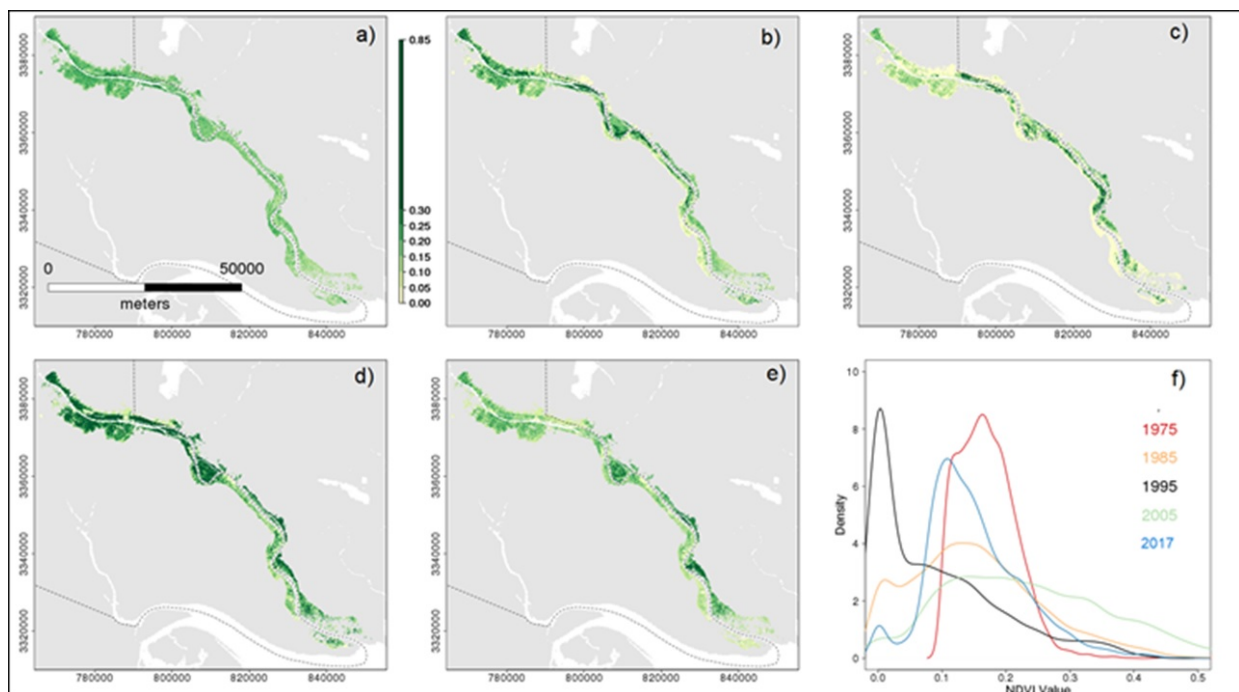


Figure 3.3: Temporal variations of NDVI (A-1975, B-1985, C-1995, D-2005 and E-2017 NDVI greenness density plot) for the Shatt Al-Arab river region.

The third objective links climate indicators to NDVI trends by regressing mean NDVI

for each year (1975, 1985, 1995, 2005, and 2017) with mean temperature, precipitation, and sea level in the same years. Figure (3.4) graphically illustrates the trends in sea level, temperature, precipitation, humidity and NDVI. This modeling indicates that: (i) there is a significant positive relationship between the NDVI trend (as an independent factor) with the SLR and precipitation variables (as dependent factors). Meanwhile, the correlation was considerably negative with the mean air temperature; (ii) these observed relationships would result in a declining trend of vegetation greenness (NDVI values), by affecting the vegetation directly (e.g., inhibiting growth due to inauspicious daily meteorological conditions) and indirectly by degrading soil characteristics (e.g. through groundwater level rise and increasing soil salinity) at such coastal/estuarine regions.

2. The fourth objective is to understand intra-regional NDVI change between 1975 and 2017. Figure 3.5 (a) maps NDVI change by pixel within the study area. In general, the region witnessed declines in NDVI, but spatial heterogeneity is apparent. Some very large decreases are evident along the riverbanks in the Upriver subarea, and in places elsewhere along the right-hand, Iraqi bank. Few substantial increases in NDVI are apparent anywhere in Iraq. In contrast, much of Lower Iran has experienced modest increases in NDVI values. The southernmost portion closest to Persian Gulf has experienced little or negative change on both sides of the river. Figure 3.5 (b) presents box plots of NDVI change distributions within each of the three subareas. The Upriver and Lower Iraq subregions experienced general declines in vegetation cover with similar, largely negative distributions. In contrast, Lower Iran experienced overall increases in NDVI change during this time, with a mean increase of 0.09. The observed changes have large magnitudes relative to the overall distribution of NDVI values, which average 0.081 and 0.13 in 1975 and 2017, respectively.

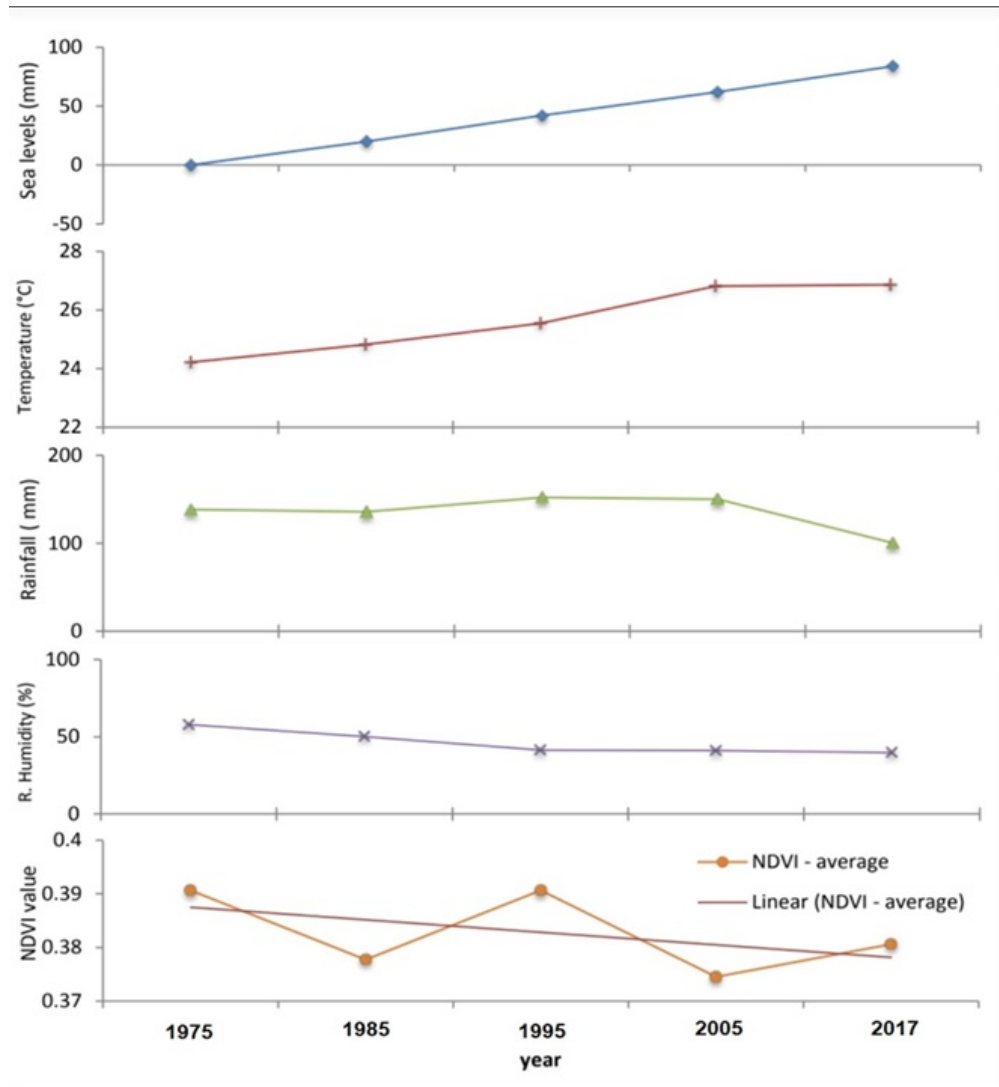


Figure 3.4: Regressing trends of temperature, precipitation, humidity, and sea levels for the periods (1975, 1985, 1995, 2005, and 2017) associated with the NDVI trends.

### 3.4 Discussion

The changes observed from 1975-2017 in vegetation cover in the SARR derive from the reciprocal interactions between natural and human components. The remote sensing and geospatial analysis reported in the previous section is valuable for understanding impacts of coupled human and natural systems, enabling the development of testable hypotheses and better policy decision making for climate change adaptation at multiple spatial, tem-

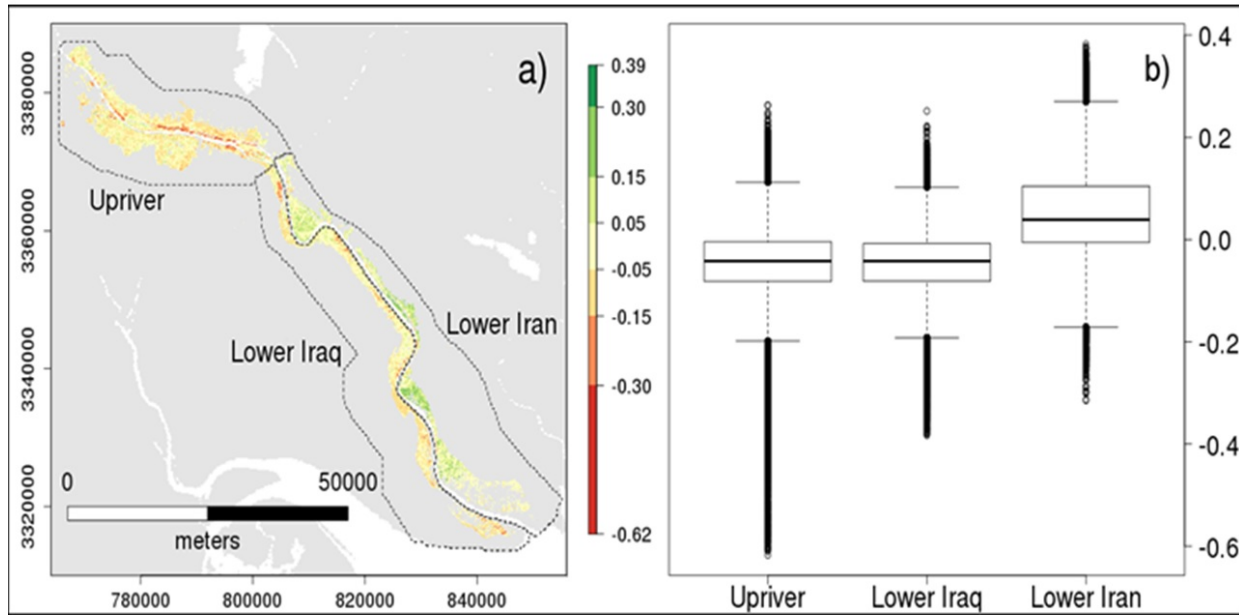


Figure 3.5: Comparative between 1975 and 2017 NDVI in Shatt Al Arab Region (a,b) which shows the difference in the density of vegetation distribution between up and down the junction of Karun river in Iraq and Iran with Shatt Al Arab river.

poral and organizational scales. In this section we consider a range of factors associated with both direct human impacts and direct environmental impacts, as presented in the conceptual model in Figure 3.2 that could explain these changes.

### 3.4.1 Human Impacts

Human activity has been influencing the region in different ways as detailed below.

#### 3.4.1.1 War and Government Policy

SARR was known for palm trees and crop cultivation; much of this agricultural resource has been lost during the time evaluated in this study because of government policies (Singh et al. (2005)). In the 1930s, the population in Iraq started relocating from rural to urban areas due to oil industry development, and consequently the agricultural sector be-

gan to suffer and become stagnant (Gibson et al. (2017)). Once Saddam Hussein became president in 1979, an effort was made to put agriculture back into the private sector. During the IranIraq War (1980 to 1988) Iraq was able to increase its production and expand crops in spite of labor resources being diverted to the war. At the same time, the war resulted in a significant economic impact causing delays in development projects and defaults to foreign contractors and loans (Springborg (1986); Gibson et al. (2017); Tripp (2007)). Much of the war was fought within SARR: the eightyyear period of the IranIraq war centered on military operations in this borderland. The war left behind many types of military waste, including mine fields, endangered the lives of the regional population, and rendered vast areas (29,000 acres) of SARR unfit for human use up to the present time (Mohammed (2008)). The inability to return the population to these areas is a source of ongoing human casualties and a major obstacle for regional agricultural and economic rehabilitation (Mohammed (2008)). In 1990, Saddam Hussein invaded Kuwait and the UN Security Council imposed sanctions against Iraq. When the sanctions failed, the UN used military force, attacking Iraqs leadership, production, infrastructure, and population. The conflict destroyed Iraqs economic infrastructure, causing extensive damage, even greater than that from the years of war with Iran (Gibson et al. (2017); Tripp (2007); Reynolds (1995)).

The comprehensive sanctions continued after military conflict ended and became stricter as Saddam Hussein remained defiant. As foreign companies were prohibited from investing in Iraq with oil exports, revenues needed for Iraq to purchase food and agricultural products were reduced. There was a ban on agricultural dual-use products including fertilizers, machinery, pesticides, and chemicals, and many countries stopped exporting food to Iraq (Gibson et al. (2017)). Consequently, increased domestic agricultural produc-

tion became a high priority, and the government created both incentives for farmers to expand their crop areas and punishments, including death, if they did not meet specified production quotas (Foote et al. (2004); Gibson et al. (2015); Gibson et al. (2017)). At the same time, a food rationing system was set up at local food stores for everyone in the country to receive distributed rations. When the effort failed to meet basic needs recommended by the World Health Organization, the UN set up the Oil-for-Food Program in 1995. Iraq was allowed to sell oil on the world market in exchange for food, medicine, and humanitarian needs. The sanctions continued until the U.S. invasion of Iraq in 2003. The effects of war and sanctions in Iraq had a devastating effect on the agricultural sector. Soil fertility was depleted, irrigation infrastructure was neglected or destroyed, and cropland suffered from salinization (Gibson et al. (2017); UN (2003) ). Once Operation Iraqi Freedom began in 2003, the Hussein regime fell without much resistance. The U.S. led operations to rebuild the country and reinstate political stability. Once the sanctions were lifted, the food imports began again. When aid organizations assisted with the food rationing systems, local farmers found it difficult to compete with the subsidized food imports (Foote et al. (2004); Gibson et al. (2017); Gibson et al. (2015)). In contrast to the 1990s, when food imports stopped, and the size of cultivated areas increased, the past fifteen years have seen a reduction in the area of cultivated land in Iraq as food imports resumed (Gibson et al. (2012); Gibson et al. (2017)).

#### **3.4.1.2 Upstream Water Demand**

The available water in the Shatt AlArab River is greatly impacted by increased water demands upstream. Its four major tributaries, the Tigris, Euphrates, Karkheh and Karun Rivers, rise in the mountains of Turkey and Iran. The entire basin is shared by Turkey,

Iran, Syria, Saudi Arabia, and Jordan, which are all neighbors of Iraq. The surface area is about 938,300  $km^2$  (with Iraq providing just 15.81% of the total water volume of the basin) (Al-Asadi (2017)) making it the largest river basin in southwest Asia. Climate change, dam construction, population growth, and increased demands for irrigation is putting added pressure on water withdrawal while the arid climate is keeping the regeneration rate low. Dam building upstream is decreasing the amount of available freshwater downstream and is significantly affecting the quality of water from Basra to the mouth of the river. International water management policies between Turkey, Iran, and Iraq are needed to avoid any further water quantity issues (Beaumont (1996); Abdullah et al. (2015)).

#### **3.4.1.3 Hydroengineering in SARR**

Figure 3.5 shows the NDVI in the southwest of the region has a clear decline of the greenness in the land cover, more than in the southeast and It appears that loss of NDVI has been very similar in the northern, Upriver subregion and the southwestern, downriver Iraq portion. The southwest close to the Persian Gulf is affected by sea level rise, and it does not have more fresh water like the northern part of the region. The southeast region has higher greenness because the Iranian Government redirection of Karun river water and used the water for irrigation in this part of the region. That might explain the different land degradation trajectories of these subareas. This study suggests that two related factors may be at work: first, a recent diversion of the systems main source of fresh water to benefit primarily fields in the Lower Iran subarea, and second, different degrees of investment by Iraq and Iran in these areas. In 2008, the Iranian government redirected the flow of Karun River to the Kashmir channel, which helped revive the vegetation and agriculture fields in this area (Hamid (2014)). On the other hand, redirecting Karun River

water caused a humanitarian catastrophe because of the high concentration of Salinity River water in the city of Fao to the south on Shatt Al-Arab River (Hamid (2014); Abdullah et al. (2015)). Given that those portions of the region reliant on Shatt Al-Arab river water experienced a decline in vegetation cover while the one area with contributions from Karun saw an increase, we maintain that decreasing water quality (largely due to rising salinity) from Shatt Al-Arab is in large part responsible for the regional vegetation decline. Other possible factors may be differing national policies in research and investment in date palm agriculture in this region (Hajian and Hamidi-Esfahani (2015); Hazzouri et al. (2015)).

#### **3.4.1.4 Pollution and Degradation**

A major source of environmental degradation in SARR is due to pollutants directly or indirectly discharged into water bodies without adequate treatment to remove harmful compounds. According to several environmental assessment studies, SARR has not made any progress in addressing its environmental issues or improving environmental quality (Nomas (2006); Al Isawi (2011)). Further, there are no regional management policies for the mitigation of human impacts on the environment, such as maintaining irrigation and drainage systems in the region or increasing natural vegetation problems in the rivers (Jabbar and Zhou (2011); Nomas (2006)). The political division of the region between Iraq and Iran complicates coordinated effort on this problem.

#### **3.4.2 Environmental Impacts**

Figure (3.4) shows that NDVI has decreased over time, as has precipitation and humidity. There have been increases in temperature and sea level from 1975 to 2017) that are

associated with the negative NDVI trends. The physical components associated with environmental degradation in the region are discussed in this section.

#### **3.4.2.1 Meteorological Factors Associated With Drought**

The study area is situated in the Subtropical Desert Koppen climate classification (BWh), characterized by warm, dry summers (Peel et al. (2007)). The mean maximum temperature can reach over 48°C in the warmest months, while the winter is cold, with the mean minimum temperature dropping to 5°C. Annual precipitation in the region is less than 100 mm and 90% of the annual rains occur between November and April (Muslih (2014)). Monthly data obtained for the Basra weather station (Basra Weather Station 2017) provide clear evidence of trends across many meteorological factors in the past five decades. Figure (3.4) illustrates consistently rising average temperature, constant precipitation, and decreasing relative humidity since 1975 to 2017. Changes in these climatic elements have direct impact on the environment in SARR.

#### **3.4.2.2 Sea Level Rise**

Sea level has risen globally in recent decades. A number of regional studies have used tidal gauge data in Persian Gulf to estimate relative sea level change for locations near the outlet of Shatt Al-Arab River. Alothman (Alothman et al. (2014)) constructed a time-series record from seven coastal tide gauges in this area. A relative sea level rise of  $2.2 \pm 0.5$  mm/year was observed from this record over the period 1979-2007. This result contrasts with the findings of Hassanzadeh (Hassanzadeh et al. (2007)), who reported a rate of 2.8 mm/year (1990-1999) for the northern part of Persian Gulf. This study used data from tide gauges at Bandar Abbas, and Bushehr combined with atmospheric data at

both stations to investigate the Mean Sea-Level (MSL) response to meteorological forcing functions in this region.

An earlier study by Sultan (1995) estimated a constant rate of sea level rise of  $2.1 \pm 0.1$  mm/year (1980–1990) using two tide gauges. In an update, Sultan (2000) identified a sea level rise of 1.7 mm/year (1980–1994) using nine tide gauges. Hossein (2007) reported a mean rate of  $2.34 \pm 0.07$  mm/year (1990–1999). The variability of these estimates of mean sea level change may be due to incomplete and inaccurate records but can also be related to the large seasonal variation of sea level in Persian Gulf due to air pressure: water level in the Gulf is up to 26 cm higher in summer than in the winter (Sultan et al. (1995a); Hassanzadeh et al. (2007)). Nevertheless, all studies are generally in agreement that regional sea level rise is 2-2.5 mm per year from the 1980s into the 2000s.

### **3.4.2.3 Groundwater Salinity**

The tide in Shatt Al-Arab happens two times during the day, which is considering the source of salinity in SARR and the salinity of the groundwater as well. The salinity of SARR has increased because of increased salt intrusion from the Gulf occasioned by reduced inflows from the upstream rivers which allow the seawater wedge to move further upstream. Data collected and reported by Hamid (2014) and Abdullah (2015) provide information on temporal changes in salinity, measured in ppm, for the Shatt Al-Arab River between Basra City and the Persian Gulf during 1980 to 2012, as illustrated in Figure (3.6). This figure shows a strongly positive and increasing trend. The cultivable areas in SARR are affected with varying degrees of soil salinity depending on the elevation of land. Recent monitoring indicates that the regions soil salinity has increased. Soil salinity is believed to be mainly responsible for low land use intensity in the area (Brandimarte

et al. (2015)).

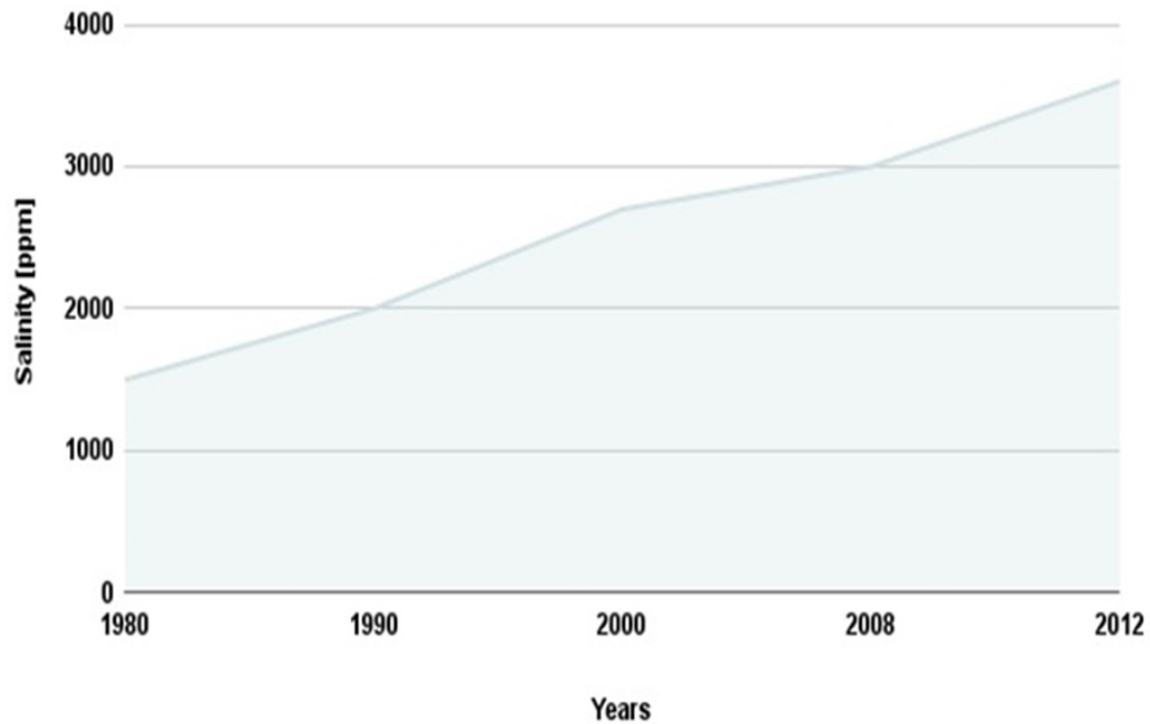


Figure 3.6: Increase in salinity (ppm) in Shatt Al-Arab river from 1980 to 2012.

### 3.4.3 Conclusions

Coupled human and natural systems are complex, presenting an interdisciplinary challenge for understanding the range of factors that shape the trajectories of such systems. This study developed a CHANS framework to understand the factors driving the past five decades of environmental degradation along Shatt Al-Arab River. Through processing of Landsat imagery across that span, the geographic distribution of vegetation quantity (largely in the form of date palm agriculture) was assessed and linked to regional environmental data. We identified a range of factors that have contributed to degradation of vegetation in this dynamic, marginal area. The most important factors are directly or indi-

rectly driven by global climate change. We believe that climate change is the greatest and most challenging problem now facing SARR: dealing with this is of course a tremendous challenge because climate change is a global problem.

Better water, land, food and energy management will reduce costs and increase benefits for both humans and the environment in SARR and everywhere on Earth, but important scientific and policy questions remain. If developed and implemented correctly, complex systems models, tools and analysis should advance the human development and environmental sustainability agenda but achieving this will require concerted action from all sectors and actors ranging from academia to the government to the private sector (Bizikova et al. (2013)).

From the geographers point of view, the CHANS framework is groundbreaking for its potential to understand and suggest solutions for geographic problems like environmental degradation that operate over multiple spatial and temporal scales. CHANS can account for the reciprocal interactions between human and natural components in the SARR and identify the most relevant variables that have an essential role in this system. The present study has shown that these variables (meteorological conditions, sea level rise and human conduct) are consequences of climate change as in Shatt Al-Arab river region. Of course, humans are primarily responsible for climate change, but the people in the study area are also victims of climate change. They have played little role in the regional and global factors driving environmental degradation in SARR. As sea level rise accelerates in this century, threats to this low-lying coastal region will only become more acute.

# Chapter 4

## Flooded With Error: Handling

## Uncertainty in SRTM For The

## Assessment of Sea Level Rise in

## Mississippi River Delta

### 4.1 Introduction

SLR is one of the biggest threats to coastal habitats and communities worldwide (Mcleod et al. (2010)) posing critical scientific and management challenges (Gesch (2009)). Estuarine wetlands like MRD are characterized by complex interactions between surface water fluxes, vegetation type and poor water movement. The tidal wetlands are very sensitive to very small changes in topography within this tidal regime (Wang et al. (2007)). To understand the ecology of these environments, it is important to understand the hydrology, and to recognize feedbacks from the ecology to the hydrological balance as well. Because of the intimate relationship between estuarine wetland ecology and hydrology, knowledge of wetland hydrology is critical if I am to predict and manage changes in wetland environments. Long-term drivers such as climate change and sea level rise, as well as

human interferences of hydraulic modification of water flow are critical for these systems as well (Hughes et al. (1998)).

Mississippi river delta located north of the Gulf of Mexico in southern Louisiana is most noted for its extensive low-lying topography and its economic activities. MRDR has the highest relative sea-level rise in the U.S. due to the combination of global sea-level rise and local subsidence (sinking land). Based on analysis roughly corresponds with measured water level changes: the mean sea level rise at Grand Isle, Louisiana (NOAA gauge station 8761724) is 9.03 millimeters/year based on monthly mean sea level data from 1975 to 2017 (Tides and Currents. noaa.gov).

Land-surface altitude data collected in this region indicated mean annual subsidence of 5 mm per year during five survey epochs between 1951 and 1995 (Burkett et al. (2003)). Subsidence rates in Mississippi River Delta are even further increased due to the large amount of fluid withdrawal in the northern Gulf of Mexico. Oil and gas extraction leads to increased soil compaction over a short amount of time (Blum and Roberts (2009); Penland and Ramsey (1990)).

In addition, river dominated deltas such as MRDR have a different morphology than wave or tidally influenced deltas such as the Nile and Ganges deltas. Mississippi delta reflects primarily on the sediment input from rivers, which can be distinguished from wave or tidal dominated deltas such as the Nile and Ganges deltas (W. van de Lageweg et al. (2017)). Many previous remote sensing studies estimates MRDR flooding and how much this delta lost land because of SLR. Couvillion et al. (2011) was based on survey and aerial data and addressed concerns about comparability of the 1932 and 1956 datasets. Blum and Harry (2009) was based on aerial and satellite imagery taken from 1932 to 2010. Both studies reveal MRDR lost more than 25% of its land with a net change of about 4,000

$km^2$  in land area from 1932 to 2010. About 95% of the decrease in land area accounts for persistent losses, while the remainder of the area that has converted to water is not classified as loss because it does not exhibit the persistence necessary to be classified as such. Trend analysis investigations of wetland loss from 1985 to 2010 identify a rate of 43  $km^2$  per year (Barras et al. (2008); Couvillion et al. (2011); Blum and Roberts (2009)).

There are different kinds of hydrologic models that could be used for inundation. The advantage of GIS inundation models is inexpensive to run and doesn't need a lot of time either. In addition, these inundation models are based on elevation datasets which are available in a different kind resolution. Some of these data are free. There are various of inundation model studies for local, regional and global scale appropriate to mapping of a coastal region based on digital elevation modeling and sea level rise modeling (Mcleod et al. (2010); Titus and Richman (2001)). The inundation model which used high resolution as lidar data is suitable to determine the risks of SLR (Kulp and Strauss (2016); Titus and Richman (2001)). On another hand, the lidar data doesn't available to cover all the earth because SRTM is the best digital elevation modeling for the low and flat topography (Tara et al. (2010); Kulp and Strauss (2016)).

Many studies focused on error propagation modeling to enhance (SRTM in different types of land cover (Tara et al. (2010); Shortridge (2006); Hofton et al. (2006); Bhang et al. (2007); Rodriguez et al. (2006); Gamba et al. (2002); Kulp and Strauss (2016)). Our study is creating correlated surfaces in near coastal riverine regions to achieve the main aims of our study, which are: first, using propagation error model to reduced (SRTM) 1 Arc-Second Global elevation error as global DEM available correlate the error with global land use cover vegetation cover fraction (VCF) in near coastal riverine regions. Two, applying this modeling (reduce (SRTM) 1 Arc-Second Global error) in the global near coastal river-

ine regions which are potentially vulnerable to inundation. This chapter concerns with the accurate modeling of (SRTM) 1 Arc-Second Global in near coastal riverine regions. The modeling in this chapter possesses excellent efficiency for Mississippi River delta region in southern Louisiana and it can apply in near coastal riverine regions. I address several key questions for developing globally applicable error models for inundation assessment:

1. How does SRTM error correlate with global canopy cover (Landsat 5)?
2. To what extent is SRTM error reduced using Landsat 5 and other global covariates?
3. How effective are geostatistical models at reproducing inundation model results using high-accuracy USGS NED in this region?

## **4.2 Data and Methods**

### **4.2.1 Study Area**

The study focuses on the Louisiana coastal plain around Mississippi River from its junction with the Bayou Lafourche downriver to the Gulf of Mexico and covers  $11,894 \text{ km}^2$  as shown in Figure (4.1)(a). This important region, which is mostly coastal wetlands, has a distinctive ecology and landscape and is rich in resources (Steyer and Llewellyn (2000)). The alluvial generally ranges from 15 to 100 km in width, which is supported by the findings of the region along Mississippi. Mississippi River flows along a ridge formed by its own natural deposits (known as a levee), from which the lands decline at an average fall of 3 m/km (Zellmer and Klein (2007)).

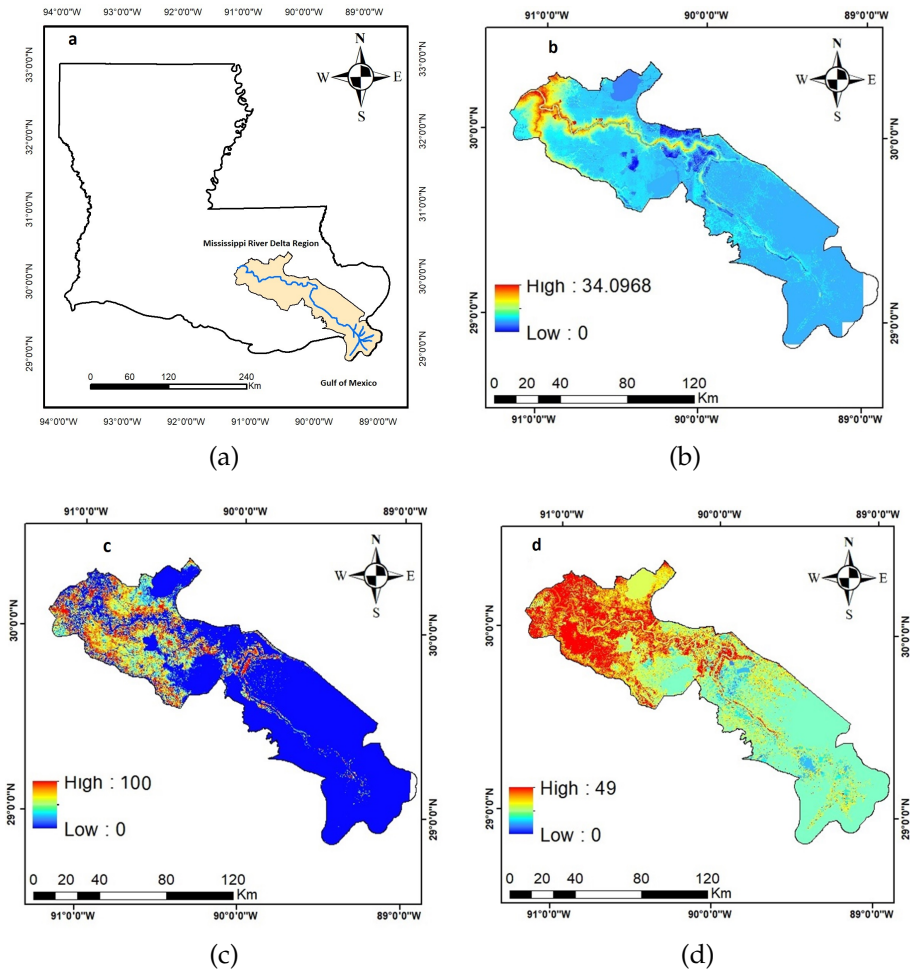


Figure 4.1: (a) study area (Mississippi River Delta region in Louisiana state); (b) NED 1/3 arc-second (approximately 10 meters); (c) VCF Landsat 5 TM Collection 1 products 30 m and (d) SRTM 1 Arc-Second Global coverage ( 30 meters).

## 4.2.2 Data

### 4.2.2.1 National Elevation Dataset (NED)

In this study, I used the National Elevation Dataset (NED) 1/3 arc-second (approximately 10 meters) DEM, which is the best publicly available high-resolution elevation DEM for most of the US at this time as shown in Figure (4.1),(b). The 1/3 series is produced and distributed by the U.S. Geological Survey (USGS) and is one of many seamless datasets. These data are available through the Earth Explorer portal (<https://earthexplorer.usgs.gov/>),

(Gesch et al. (2002)). I use NED 1/3 arc-second data because it has been edited and to remove structures and vegetation to produce a bare-surface DEM suitable for modeling the water plane. I downloaded two one-degree tiles to cover the study area. These tiles were mosaicked and then projected UTM zone 16N, WGS84 with a cell size of 10 m, and finally resampled to 30 m resolution to match the SRTM 1 DEM.

#### **4.2.2.2 SRTM 1 Arc-Second Global Coverage ( 30 meters)**

The Shuttle Radar Topography Mission (SRTM), collected interferometric synthetic aperture radar (IFSAR) data in February of 2000 covering 80% of the earth's land surface. The importance of this data stems from the vast areas of the world it covers, especially regions with little or no free terrain data at medium to high resolution. The advantages of this data for scientific and research applications for such regions are substantial. Accuracy is one important issue with SRTM DEMs (Shortridge (2006)). 1 arc second SRTM was downloaded from Earth Explorer: three tiles were required to cover the study site. I did subsite and mosaic of these images to get MRDR SRTM, and then projected to UTM zone 16 N referenced to the WGS 1984 datum; final cell size was 30 meters as shown in Figure (4.1),(d).

#### **4.2.2.3 Vegetation Data**

Since SRTM error is positively associated with vegetation cover (Shortridge (2006)), I used vegetation cover fraction (VCF) as a secondary variable to correct the SRTM error. VCF has been used in many global land process models as earth surface change and climate change in regional and global studies (Barlage and Zeng (2003); Zhang et al. (2013); Jia-paer et al. (2011); Baret et al. (2013)). I produce VCF Landsat 5 TM Collection 1 products

are available for download (Earth Explorer). I used four images (Path 21, 22,23 Row 39,40) to cover the study area. All these images acquisition date: 19 / February / 02, and these images are 30-m resolution, the same as the SRTM resolution. The observation of the earth was conducted at the same time too as shown in Figure (4.1),(c). VCF mean the percentage of green vegetation spatial distribution to the total statistical region (Jing et al. (2011); Barlage and Zeng (2003); Zhang et al. (2013)). I created the normalized difference vegetation index (NDVI) image first and I determined two values from this NDVI which bare soil and NDVI value full canopy. The VCF is of two components: vegetation and soil. I estimate VCF percentage by the following equation:

$$VCF = (NDVI - NDVI_{baresoil}) / (NDVI_{fullcanopy} - NDVI_{baresoil}) \quad (4.1)$$

where  $NDVI$  is normalized difference vegetation index,  $NDVI_c$  is NDVI for a full canopy pixel, and  $NDVI_b$  is bare soil NDVI value pixel (Wang et al. (2017)) (Estimating Fractional Vegetation Cover from Landsat 5 TM Collection 1 products reflectance data in Mississippi river delta).

### 4.2.3 Methodology

SRTM error can be characterized by models that combine correlated environmental variables and spatial autocorrelation. In this study, I investigate the utility of vegetation index from Landsat along with elevation and slope to account for SRTM error in MRDR. SRTM error can be characterized by models that combine correlated environmental variables and spatial autocorrelation. I use error model based on a set of 10K points, validated and then used to adjust SRTM, and that gets applied to a bathtub model.

In the first step, 10,000 random point samples from reference NED are extracted. These were used to develop measures of SRTM error across the region. Also, I apply regression kriging to fitting an OLS regression model with covariates to SRTM error, and then modeling the spatial autocorrelation of the residuals via simple kriging and combining those into a single raster of SRTM error. The steps for SRTM error modeling and estimation of inundation are summarized in Figure 4.2.

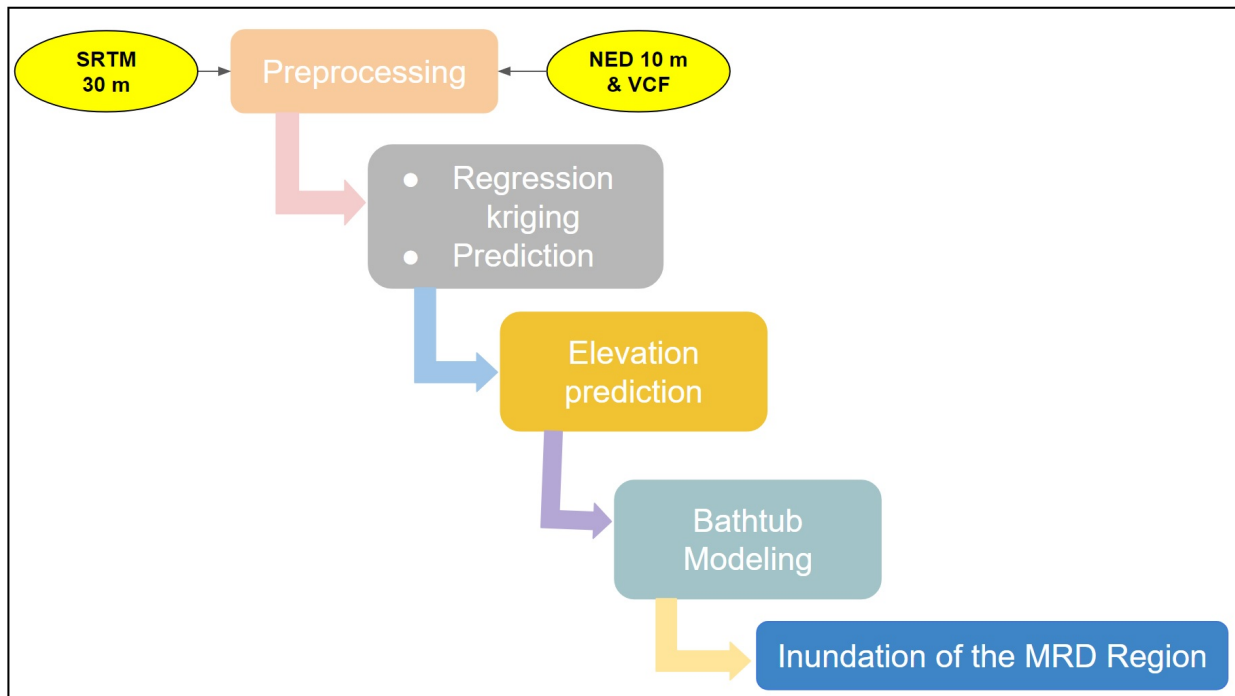


Figure 4.2: Error modeling and bathtub modeling for Mississippi River Delta Region.

#### 4.2.3.1 Regression Kriging

I used regression-kriging models to generate estimates of SRTM error for every cell in MRDR. Regression-kriging is the best linear interpolation calculating a universal model of spatial difference, and the best linear predictive unbiased predictor of spatial data was performing. The result of this model has high accursed simulations, and the topography elevation values represent more details about spatial distribution. See (Leon et al.

(2014); Hengl et al. (2008); Christensen (2001)) for more details about the regression-kriging model. Regression-kriging prediction is calculated as follows (Leon et al. (2014)):

$$\hat{z}(s_0) = \hat{m}(s_0) + \hat{e}(s_0) = \sum_k^p \hat{\beta}_k \times X_k(s_0) + \sum_{i=1}^n \lambda_i \cdot e(s_i) \quad (4.2)$$

where  $\hat{z}(s_0)$  is the predicted SRTM error,  $\hat{m}(s_0)$  is the fitted linear regression of SRTM error using *VCF*, SRTM elevation, and slope as independent variables, and  $\hat{e}(s_0)$  is the simple kriging interpolated residual at the prediction location  $s_0$ . The  $\hat{\beta}_k$  are the estimated regression coefficients and  $X_k$  are explanatory variables. The  $\lambda_i$  are kriging weights for the residuals, where  $e(s_i)$  is the residual at measurement location  $s_i$ , that is, the difference between the elevation error and the fitted trend at  $s_i$ . The regression coefficients  $\hat{\beta}_k$  are estimated using generalized least squares (Leon et al. (2014)).

Spatial structure of the residuals from the regression model was fit using a combination of two Gaussian variogram models to fit both short range and long-range structure. Parameters of the first variogram model were: partial sill = 0.1, range = 800, and nugget = 0.04, while those for the second variogram model were partial sill = 0.12, range = 4000, and nugget = 0. The regression model was validated by drawing a new set of 10,000 random locations and predicting SRTM error for those locations.

#### 4.2.3.2 Inundation Modeling

I used inundation modeling which can be filled with hydrological connectivity or without hydrological connectivity. The vertical and horizontal resolution of digital elevation data used to estimate coastal vulnerability will impact estimates of flooding. Despite, the high resolution of digital elevation models (DEM) used in environmental evaluation

can be important to the exposure of topographic characteristics and the measurement of hydrological processes (Poulter and Halpin (2008)). I apply inundation modeling to determine which area from the region will suffer from flooding due to SLR. The Function to implement the bathtub inundation model is:

$$Flooded_j = \begin{cases} 2 & \text{if } DEM_j > f \\ 1 & \text{if } f \geq DEM_j \geq 0 \\ 0 & \text{if } DEM_j \leq 0 \end{cases} \quad (4.3)$$

where  $Flooded_j$  is a binary variable indicating the flooding status of cell  $j$ ,  $DEM_j$  is the elevation of cell  $j$ , and  $f$  is the flood elevation above sea level.

In this experiment, the original SRTM DEM, the NED DEM, and an adjusted SRTM DEM based on the error model were all used as inputs to an inundation model set to flood all land less than 1m in absolute elevation above sea level. The geostatistical modeling of the SRTM elevation error and the inundation model were calculated using the R statistical package and the following libraries: `gstat`, `raster`, and `grdevices` (R Core Team (2017); Bivand (2017) ; Robert J. Hijmans (2017)).

## 4.2.4 Results

Results will be linked to the three research questions the paper intends to address.

### 4.2.4.1 Parameter Estimation For SRTM 1 Error Regression Model

To address question one, I evaluated the relationship between Landsat-based VCF and SRTM error at a random sample of 10,000 points across the study region while also ac-

counting for relationships between error and SRTM slope and raw elevation. Figure 4.3 shows a map of SRTM error across the MRDR along with scatterplots of relationships with VCF, SRTM elevation itself, and SRTM slope. Table 4.1 summarizes the regression coefficients: SRTM error model with (VCF, SRTM elevation, and SRTM slope) by variogram modeling is positive regression coefficients. The estimate of SRTM error with SRTM elevation was 0.800835, and the estimate of SRTM error with VCF was 0.0054241, indicating that mean parameter estimation SRTM error is positive. The T value was positive for SRTM elevation (159.976) and VCF (7.991). Figure 4.4 provides a range of model visualizations. Regression model performance took advantage of the strong relationship between SRTM elevation and the error. Histogram of model predictions was around one meter. A variogram of regression model residuals was fit. The spatial structure for first variogram model of SRTM errors conferred (partial sill = 0.1, range = 800 and nugget = 0.04) and the second variogram model was (partial sill = 0.12, range = 4000 and nugget = 0).

Adjusted SRTM elevation predictions for the entire study region ranged between 20 m and 25 m. The regression model R-square is 0.8342, indicating the model effectively predicts SRTM error in this region. The SRTM1 error model was used to predict error across the entire MRDR region as shown in (4.3),(a) and visual investigation proposed that error was not spread randomly in this region. However, the spatial characteristics of SRTM1 error and geographical variability exhibit low correlations with the spatial error distribution in Figure 4.3. Scatterplots of raw SRTM error with SRTM slope and VCF exhibit low correlations (Figure (4.3),(b), (d)), but raw SRTM error and SRTM elevation are highly positively correlated (Figure 4.3 (c). Visual analyses between SRTM1 and VCF in Figures (4.3), (a) and Figure (4.1),(b), (d) show VCF segmented the results of accuracy

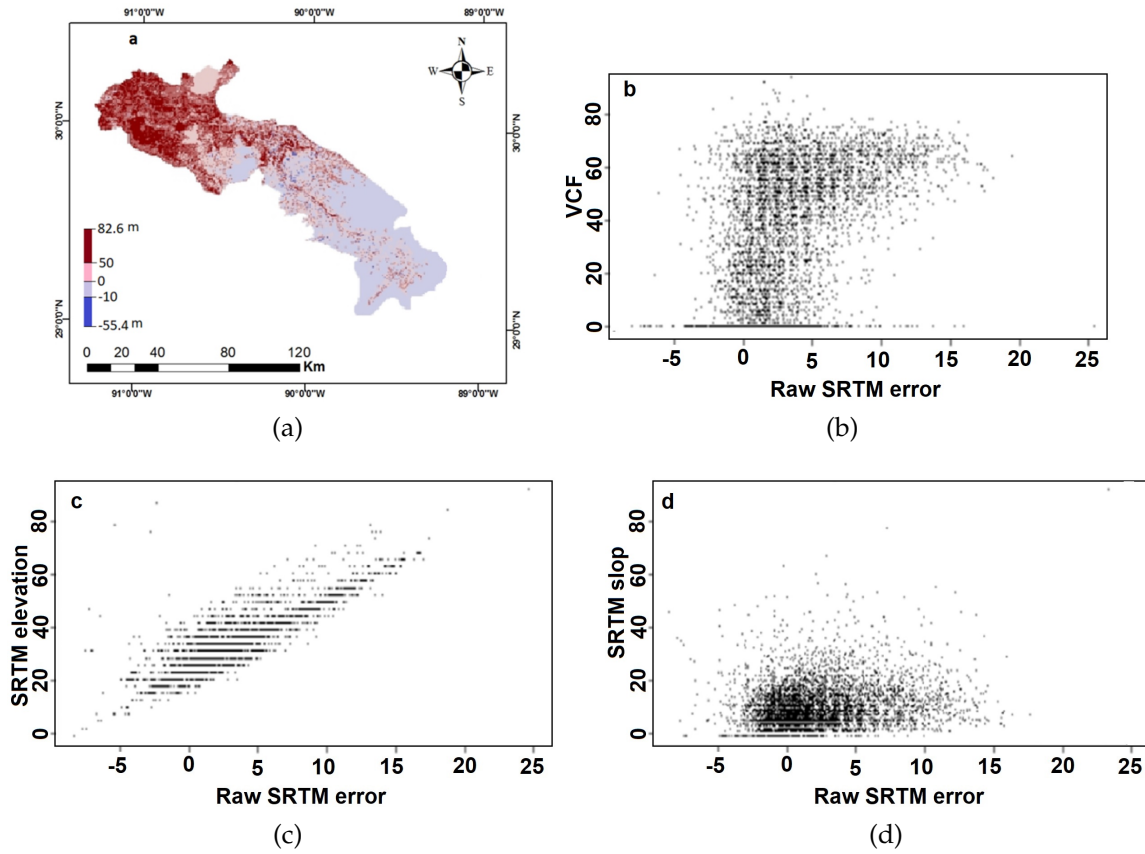


Figure 4.3: SRTM error: (a) Regression original SRTM error and raw SRTM error versus: (b) VCF; (c) SRTM elevation; (d) SRTM slope.

assessment.

#### 4.2.4.2 Regression and Variogram Results

The regression kriging model was validated on a second sample of points to determine model capability for the composition of the SRTM errors and the variogram of regression model residuals. The efficient model included the following key predictors: VCF, SRTM, SRTM slope, and intercept (Figure 4.3(a), (b), and Table 4.1).

The result of the variogram modeling is the adjustment of SRTM elevation errors. Figure (4.3)( e ), (f) shows two meters adjustment, and the modified errors distribution was between 20 and 25 meters.

Parameter	Estimate	Std. Error	t value	$P_r(>  t )$
Intercept	-0.1381996	0.0188362	-7.337	2.36e-13 ***
SRTM elevation	0.8008351	0.0050060	159.976	< 2e-16 ***
VCF	0.0054241	0.0006788	7.991	1.49e-15 ***
SRTM Slope	-0.0803025	0.0103973	-7.723	1.24e-14 **

Table 4.1: Regression coefficients of SRTM error model with NED and VCF.

#### 4.2.4.3 Inundation Modeling

The regression kriging predicted SRTM error surface for MRDR was subtracted from the original SRTM data to produce an adjusted SRTM elevation to develop a DEM with lower error. This adjusted SRTM DEM, along with NED (as the reference DEM) and the original SRTM, was used as input to the inundation modeling experiment. Figure 4.5 compares the spatial extent of 1m sea level rise in MRDR using the original SRTM DEM before error modeling and the adjusted SRTM DEM. Each map shows three classes: water, areas which were at or below 0m of elevation; land, areas which are above 1m; flooded areas between 0 and 1m which are inundated by this amount of flooding. Differences are stark: only 8.8% of the land surface is flooded using the original SRTM, while nearly 52% is flooded in the adjusted SRTM.

In contrast, Figure 4.6 shows the inundation of the reference NED DEM in comparison to the adjusted SRTM. The DEMs produced similar inundation model results meaning that the error model performed very well. Inundation area estimates are relatively similar between the NED (42.1%) and the SRTM (51.8%).

#### 4.2.5 Discussion

Topography is a key factor that influences the processes of coastal change, so up-to-date, high-resolution, high-accuracy elevation data is required to model the coastal environ-

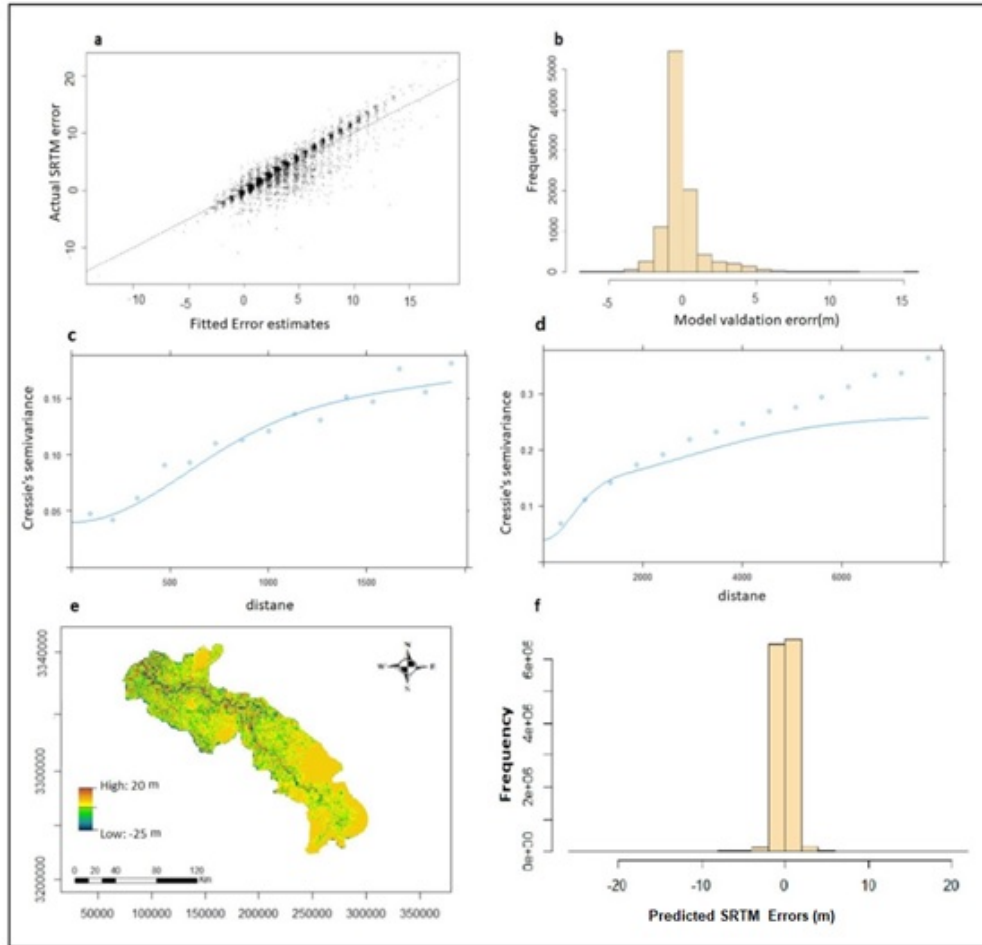


Figure 4.4: Error assessment for variogram model: (a) Regression model performance; (b) histogram of validation error of the regression model; (c) variogram and model of regression model residuals over short distances; (d) variogram and model of regression model residuals over long distances; (e) map of model-predicted SRTM elevation errors and (f) histograms of predicted SRTM errors).

ment (Gesch (2009)). Lower elevation, marshes, irrigation canals and drainage networks allow saltwater intrusion from the gulf to near-coastal riverine regions (River-dominated deltas) (Good and Wilson (1995)). The high resolution of digital elevation models (DEM) is used in environmental evaluation and can significantly influence the detail of topographic characteristics, creating varying results in inundation and the measurement of hydrological processes (Poulter and Halpin (2008)). Topographic detail increases in coastal regions with the presence of canals, marshes and drainage networks (Lindsay (2006)),

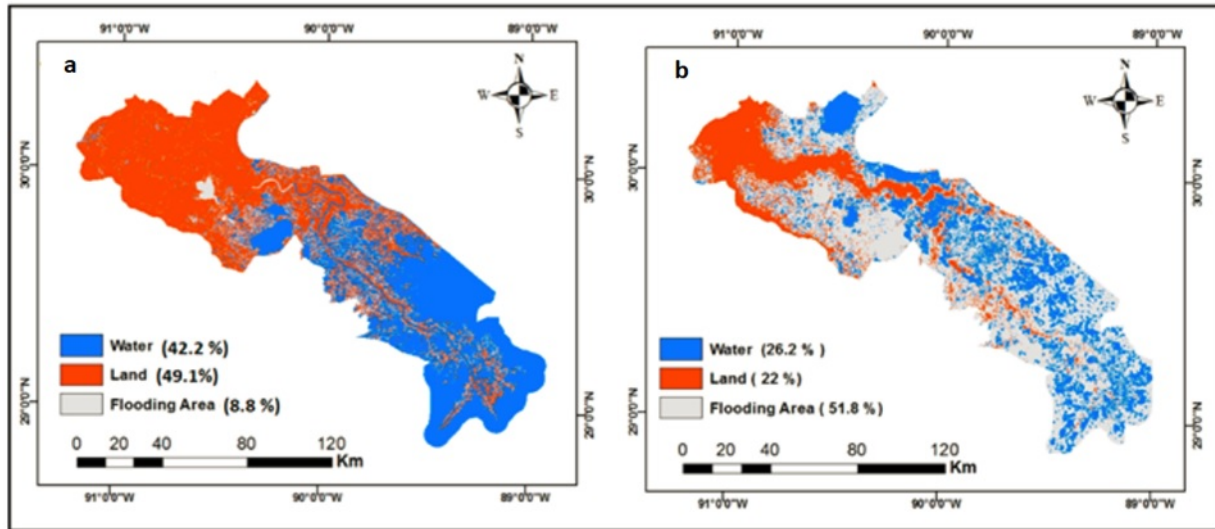


Figure 4.5: Inundation models (predicting the spatial extent of a 1m sea level rise in the MRD region: (a) initial SRTM and (b) adjusted SRTM DEM after the error modeling.

therefore, DEM is a valuable resource to provide horizontal resolution to measure hydrological processes. (Poulter and Halpin (2008)).

Chabreck describes the major habitats in the coastal Louisiana region based on a vegetation survey of more than 5000 stations (Chabreck (1972)). Chabreck (1970, 1972) delineated and mapped four vegetation zones (fresh, intermediate, brackish, and saline) mainly based on Penfound and Hathaway (1938) descriptions of the major vegetation types of the MRDR (Visser et al. (1998)). The topography elevation was used to determine the spatial distribution of these marshes (low elevation is open water) and Saline (Saltwater) marsh and higher elevation is Intermediate marsh and brackish (Figure (4.6)), ( 1). Zonal statistics were used as the table to summarize the values of the NED 10m within the zones of the marshes dataset (USGS, BRD, NWRC, LDWF), and I reported the results to a table.

These analyses show that Mississippi River Delta Region has undergone a net change in the land area of spatial and temporal from 1978 to 2016. This net change is illustrated

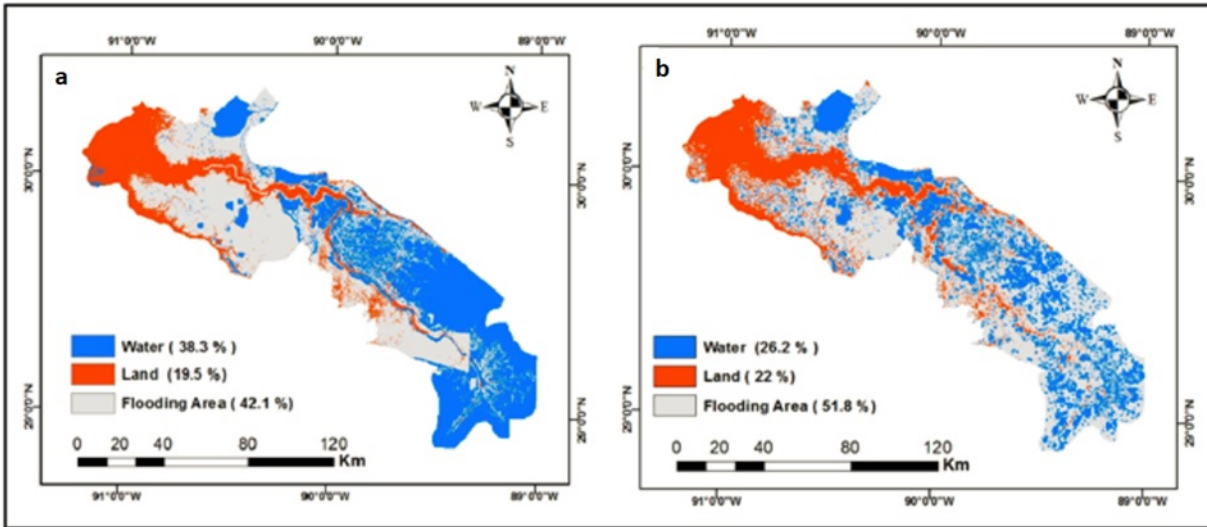


Figure 4.6: Inundation model predicting the spatial extent of a 1m sea level rise in the MRDR: (a) NED 10m DEM and (b) adjusted SRTM DEM.

and mapped in five vegetation zones on NED (fresh (-20.57 %), intermediate (10.97 %), brackish (-13.09%), open water (20.93 %) and saline (-26.19 %) and other which is inside levees (-20.29 %) Figure (4.6) , (2). However, The DEM data which has high accuracy as NED DEM 10m is so important to explain the land change as near coastal riverine regions, but unfortunate NED is not available just in the US. Because of that, I developed a globally applicable SRTM error model for inundation assessment. Also, I have presented the analysis of the topographic vulnerability of the MRDR based on SRTM DEM 30m, which covers most of the world, adjusted to account for high sea level rise. This adjustment carries significant consequences of estimating the region flooding due to sea level rise.

#### 4.2.6 Conclusion

In this study, I created an error assessment and developed a regression kriging error model for SRTM1. Inundation modeling using SRTM and the regression kriging-adjusted SRTM was employed to estimate the regional vulnerability to flooding due to SLR. The

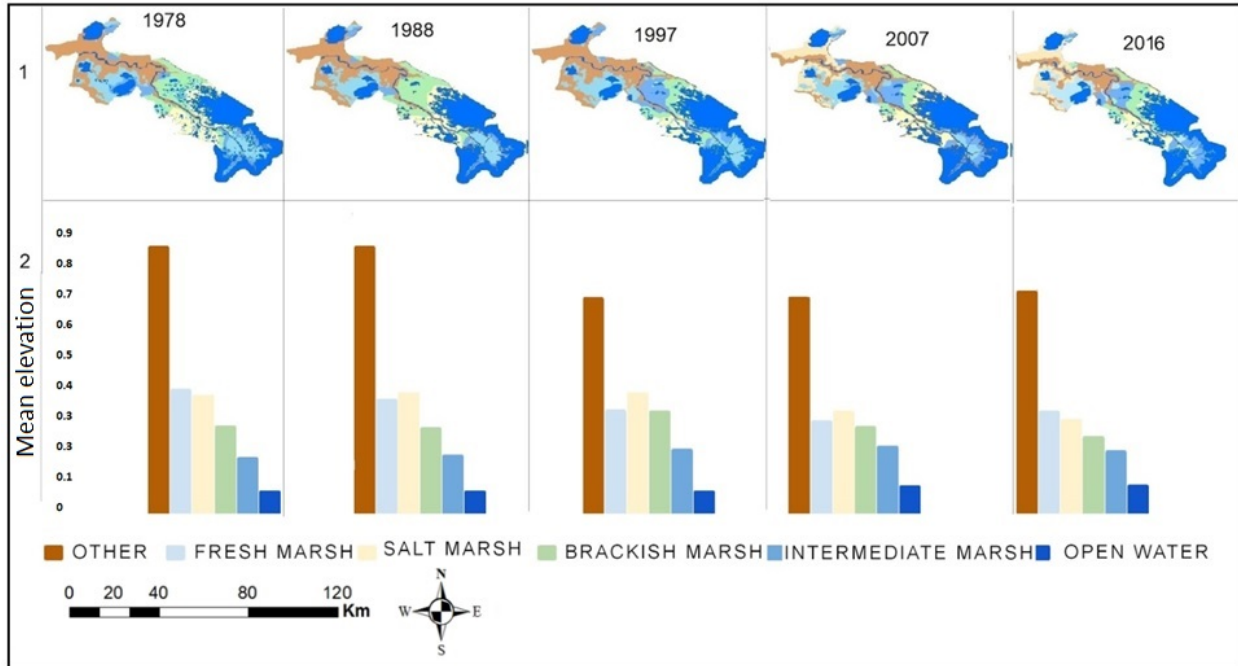


Figure 4.7: Marsh classes in Mississippi river delta region: a. Spatial temporal change for vegetation classes. b. Marsh classes changing based on mean NED DEM.

error assessment found that SRTM error in the MRDR is correlated with Landsat-derived canopy cover, SRTM slope and SRTM elevations. The regression model showed that these correlations can be used to develop reliable, high accuracy predictions of SRTM error. Regression kriging took further advantage of the spatial autocorrelation of the regression residuals to closely reproduce the reference NED elevation surface. Key findings and implications of the chapter include:

1. SLR inundation can be accurately modeled and forecast for coming decades on a global scale with SRTM 30m with good geostatistical models and error propagation.
2. Using SRTM is helpful in inundation modeling (bathtub modeling), as it is a freely available global dataset. It saves time and money when it is applied to other global regions without high-resolution, high accuracy DEMs.

3. There are promising results from adjusted SRTM bathtub modeling that correlate well with NED data. In contrast, raw SRTM greatly underestimated the inundation threat.
4. The method developed to remove SRTM error works well in our study area and it will be possible to apply the same model to other regions with similar geographical features.

# Chapter 5

## Accounting for DEM Error in Sea Level

## Rise Assessment for Shatt Al-Arab River

## Region

### 5.1 Introduction

Sea level rise varies regionally around the world: in Persian (Arabian) Gulf the rate is similar that in south Asia which is  $2.2 \pm 0.5$  mm/year (Allothman et al. (2014); Hassanzadeh et al. (2007)). As the Persian Gulf experiences high temperatures in the summer, the mean sea level is lower in winter and higher in summer with an inter-annual range of 26 cm (Hassanzadeh et al. (2007); Sultan et al. (1995a)). As a consequence, tidal wetlands and nearby low elevation areas are extremely sensitive to even slight changes in altitude (Wang et al. (2007)) or sea level. Hydrology plays a key role in understanding the ecology of these environments: predicting and managing changes in near coastal environments requires an understanding of the linkages between estuarine wetland ecology and hydrology. Also critical for these systems are the long-term drivers of climate change, sea level rise, and human interferences of hydraulic modification of water flow (Hughes et al. (1998)). In the Shatt al-Arab River Region (SARR), low-lying areas support impor-

tant human activities such as settlements and agriculture, the influence of SLR may have substantial human impact in this region. The SARR has supported the largest cultivated date palm forest in the world, which stretches from the riverbanks towards the desert for distances varying from a few hundred meters to almost six kilometers. A fifth of the world's palm trees were cultivated in this region in the mid-1970s, amounting to 17-18 million date palms. By 2002, salinization wiped out more than 80 percent of the SARR palm forest, a total of 14 million palms (Singh et al. (2005); Brandimarte et al. (2015)). Environmental problems have been a major focus of several studies in this region, in particular land change due to an increased salinity in both the river water and the soil (Jabbar and Zhou (2011); Al-Bahili et al. (2010); Al-Bahili et al. (2010); Essa (2012); Mahmood et al. (2013)).

Decreasing levels of freshwater in this river as a primary driver of many problems in the region (Abdullah et al. (2015)). However, there are two main reasons for the lack of fresh water. The first involves the concentration of Shatt Al-Arab salinization, which is increasing from the south due to being so close to the source of salinization, which comes from the Gulf. The northern part of Shatt Al-Arab river is less affected by salinization due to the fact that it is moving away from its source (the Gulf). The second problem involves the vegetation area around Shatt Al-Arab river, which is notably disappearing from the south, yet there is still some of vegetation in the northern part of the river. SLR plays a major role in the environment as well as the land change problems as it measures the impact of the previous years on this region as well as estimates their impact on the future of SARR.

In this study, I used a digital elevation model (DEM), the Shuttle Radar Topography Mission (SRTM). This DEM was produced from data collected during a US Space Shuttle

mission in February of 2000 that covered 80% of the global land surface (Farr et al. (2007)). It is the first global DEM with 30m resolution, but this DEM data has large vertical errors in densely vegetated and urban areas (Shortridge (2006); Rabus et al. (2003); Shortridge and Messina (2011)). To apply geospatial inundation which is widely used to model SLR (e.g., Titus and Richman (2001); Kulp and Strauss (2016); Tara et al. (2010); Mcleod et al. (2010)) while accounting for these errors, I must apply error propagation modeling. I use geostatistical simulations and the Monte Carlo method to understand the effect of SRTM error on inundation likelihood. More specifically, kriging is used to develop linear estimates of parameters for the SRTM error distribution for each cell in DEM, then sample from that distribution to generate error, and hence true elevation, realizations. I do not have actual elevations for this region, so I will use parameters from an error model constructed on the SRTM 1" data in the MRDR. The study will create correlated, statistical DEM error realizations in the study regions to achieve the main aims of my research, which are:

1. Develop an error propagation model to enhance (SRTM) 1 Arc-Second Global elevation model for the region.
2. Transfer parameters like vegetation cover and slope for error assessment of SRTM.
3. Apply this model to identify areas which are potentially vulnerable to inundation in SARR.
4. The error model will be calibrated and validated using MRDR and applied in SARR.
5. Understand the impact of error on inundation models in low-lying coastal regions.

## 5.2 Data and Methods

### 5.2.1 Study Area

SARR is in southeastern Iraq and southwestern Iran and includes land on both sides of Shatt al-Arab River from north of Basra City to the Persian Gulf as depicted in Figure 5.1. Its total area is 2,189 km<sup>2</sup> (Al-Saaidy (2008)). Land elevation along the river descends gradually from five meters above sea level near Al Qurnah in the north to zero in the south. The banks of the river generally have higher elevations than interior areas. The Shatt al-Arab River flows through Iraq for about 80 km to just above the confluence with the Karun River from the east; from that point to the Gulf the river forms the border between Iran and Iraq. Cities and towns, which together are home to more than three million persons as shown in Figure 5.1 interspersed with agricultural land and marshes, occupy its banks. The date-palm groves along the river are naturally irrigated by tidal action (Saad, 1978). Most studies treat the Shatt Al-Arab as a unique river because it has a tide two times during the day. Tidal movement from the Gulf controls the hydrology of the river, especially after the decline in freshwater coming from the Euphrates, Tigris, and Karun rivers (Abdullah et al. (2015)) in the period evaluated in this study (1975 to 2017). Tides enter the river from Persian Gulf and reach at least as far as Basra City (Cressey (1958)). The region includes a portion of the Governate of Basra in southeast Iraq, and of Abadan County, located in western Iran as shown in Figure 5.1 (a). This region is rich in economically important agricultural resources, including crops, vegetables and palm trees (Jabbar and Zhou (2011); Al-Bahili et al. (2010)). Elevation typically ranges from 5 to 0 meters in the lowlands away from the river. The size of the total area is 2,189 km<sup>2</sup> as shown Figure 5.1(a) and (b). Various studies found that Shatt Al-Arab is

distinctive in that it has two tide sequences during the day such that the water level of Shatt Al-Arab is directly affected by the water in the Gulf (Abdullah et al. (2015)). It is the tidal movement that regulates the hydrology of the river, especially after the reduction in freshwater approaching from Euphrates, Tigris and Karun rivers (Abdullah et al. (2015)) in the phase evaluated in this study (1975 to 2017). Tides are found to come into the river from Persian Gulf and will spread at least as far as Basra city (Cressey (1958)).

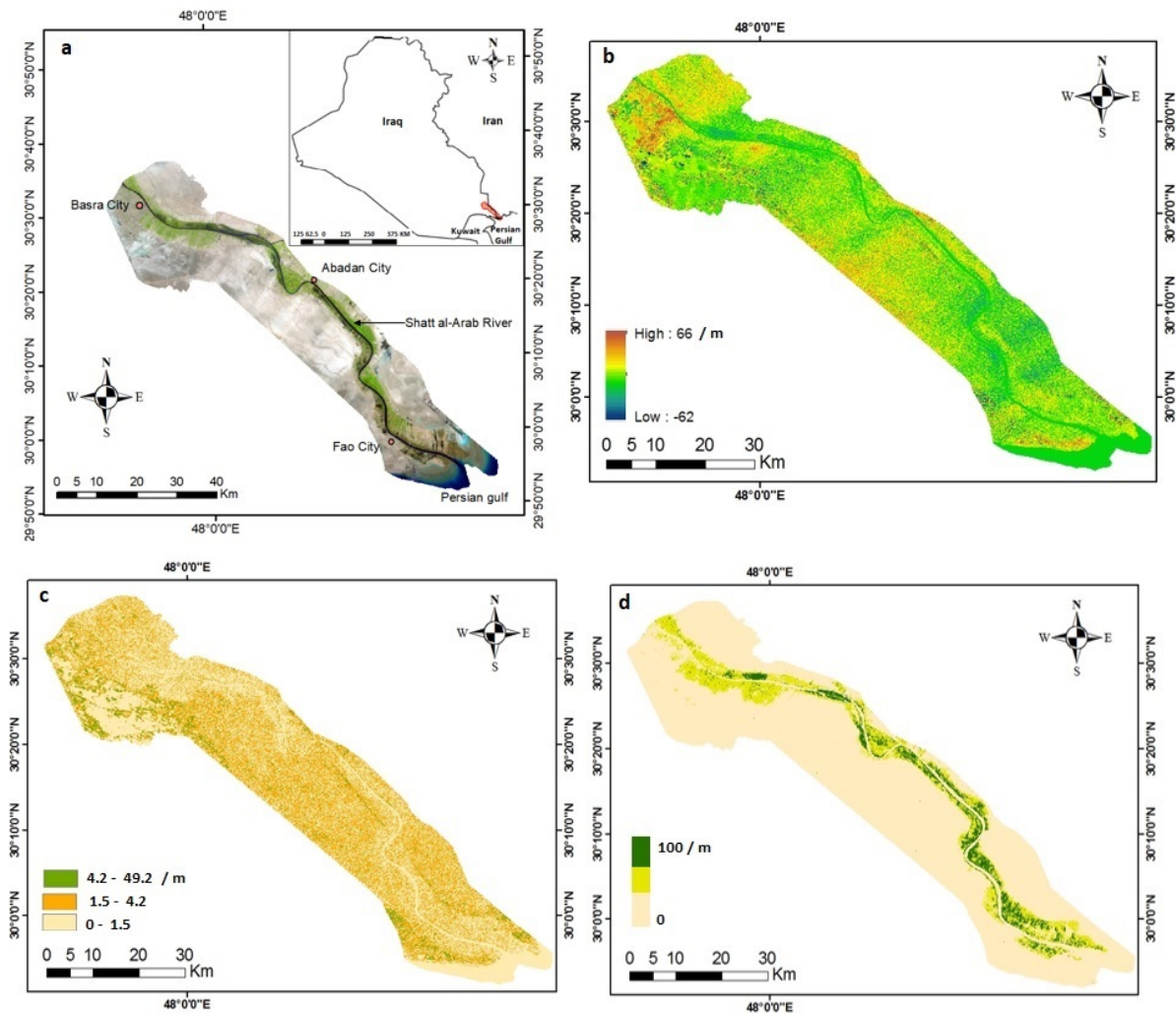


Figure 5.1: (a) Landsat imagery for Shatt Al-Arab River study region in Iraq; (b) SRTM 1 Arc-Second Global coverage (30 meters); (c) SRTM-derived slope; (d) Vegetation cover fraction (VCF) derived from Landsat 5 TM Collection 1.

### **5.2.2 SRTM 1 Arc-Second Global Coverage ( 30 meters)**

In February of 2000, interferometric synthetic aperture radar (IFSAR) data was collected by the Shuttle Radar Topography Mission (SRTM) covering 80% of the earth's land surface (Rabus et al. (2003)). The data collected brings substantial significance with it, especially in regions with little or no free terrain data at medium to high resolution. SRTM DEMs are not without issues, of which accuracy is particularly important here (Shortridge (2006)). SRTM one arc second data were downloaded from USGS Earth Explorer, then clipped and mosaicked in ArcGIS to get a DEM for SARR. This DEM was then projected to UTM zone 15 N referenced to WGS 1984 datum; final cell size was 30 meters as shown in Figure 5.1, (b).

### **5.2.3 Vegetation Data**

In regional and global studies, vegetation cover fraction (VCF) has been used as a variable in global land process models for earth surface change and climate change assessment (Zhang et al. (2013); Barlage and Zeng (2003); Jing et al. (2011)). This study also required the use of VCF as a variable since SRTM error is associated with vegetation cover (Shortridge (2006); Barlage and Zeng (2003); Zhang et al. (2013); Jiapaer et al. (2011); Baret et al. (2013)). Since VCF Landsat 5 TM Collection 1 products are available for download from USGS Earth Explorer, four images, which were acquired on February 19, 2002, were used in this study (Path 165,166 and Row 39). Since the SRTM resolution was 30 m, the downloaded images were also projected and resampled to 30m resolution. All of the images also had the same time observation of the earth as shown in Figure 5.1, (d). It is important to note that the percentage of green vegetation spatial distribution to the total statistical

region is the definition of VCF (Jing et al. (2011); Barlage and Zeng (2003); Zhang et al. (2013)). As part of this study, the normalized difference vegetation index (NDVI) image was created first, and it was determined to have two values, which are bare soil and NDVI value full canopy. The NDVI allowed for a conclusion that VCF is made up of two components, vegetation and soil. The VCF percentage was estimated by the following equation:

$$VCF = (NDVI - NDVI_s) / (NDVI_c - NDVI_b) \quad (5.1)$$

where  $NDVI$  is normalized difference vegetation index,  $NDVI_c$  is NDVI for a full canopy pixel, and  $NDVI_b$  is bare soil NDVI value pixel (Wang et al. (2017)).

## 5.2.4 Methods

### 5.2.4.1 Monte Carlo Error Propagation

I use Monte Carlo simulation which is one of the main approaches to error propagation modeling as a technique to determine how spatially autocorrelated error affects applications using spatial data. The Monte Carlo simulation operation is repeated many times to generate a sample for the input probability distribution (Leon et al. (2014); Hengl et al. (2008)). SRTM error for SARR is expected to have a mean component, that is associated with available covariates (SRTM elevation, VCF and SRTM slope) and a spatially autocorrelated, mean-zero residual component. I developed the error model (raw error  $\sim$  SRTM elevation + VCF + SRTM slope) in a separate study for the Mississippi River Delta Region (MRDR). I then did validation which is fitted error estimates versus actual SRTM error and finally I made a variogram of these residuals. I use regression kriging to fit the model

and handle its spatially autocorrelated residuals (Hengl et al. (2003)).

$$\hat{z}_{RK}(s_0) = \sum_{k=0}^p \hat{\beta}_k \times q_k(s_0) + \sum_{i=1}^n w_i(s_0) \cdot e(s_i) \quad (5.2)$$

Where:  $\hat{\beta}_k$  is estimated drift model coefficients,  $w_i$  is the semi-variance function determine weights and  $e$  is the regression residuals

Predictions for the residual error surface in SARR must be unconditional, meaning that residual realizations match spatial properties of MRDR model but don't account for ground truth, since I do not have reference elevation data for SARR. The error realizations are used to enhance SARR SRTM 30 m DEM, and I apply SLR inundation model to detect and characterize the flooding impact of SLR for the study region, as shown in Figure 5.2.

#### 5.2.4.2 Unconditional Simulation with Convolution Filtering

This study has a large amount of data, too computationally intensive for standard simulation methods. I employed process convolution (Oksanen and Sarjakoski (2005)) to develop the residual simulations in an efficient manner. The convolution filter reproduces a spatial Gaussian covariance function:

$$\rho(h) = \exp\left[-3\left(\frac{h^2}{r^2}\right)\right] \quad (5.3)$$

where  $h$  is the correlation coefficient and  $r$  is the specified range of the DEM error. The convolution filter method works as follows. I generate a vector of locations for each SRTM pixel to simulate values  $z : (s_i), i = 1, \dots, n$  in the following steps, itemized here and as shown in Figure 5.3 (Oksanen and Sarjakoski (2005)):

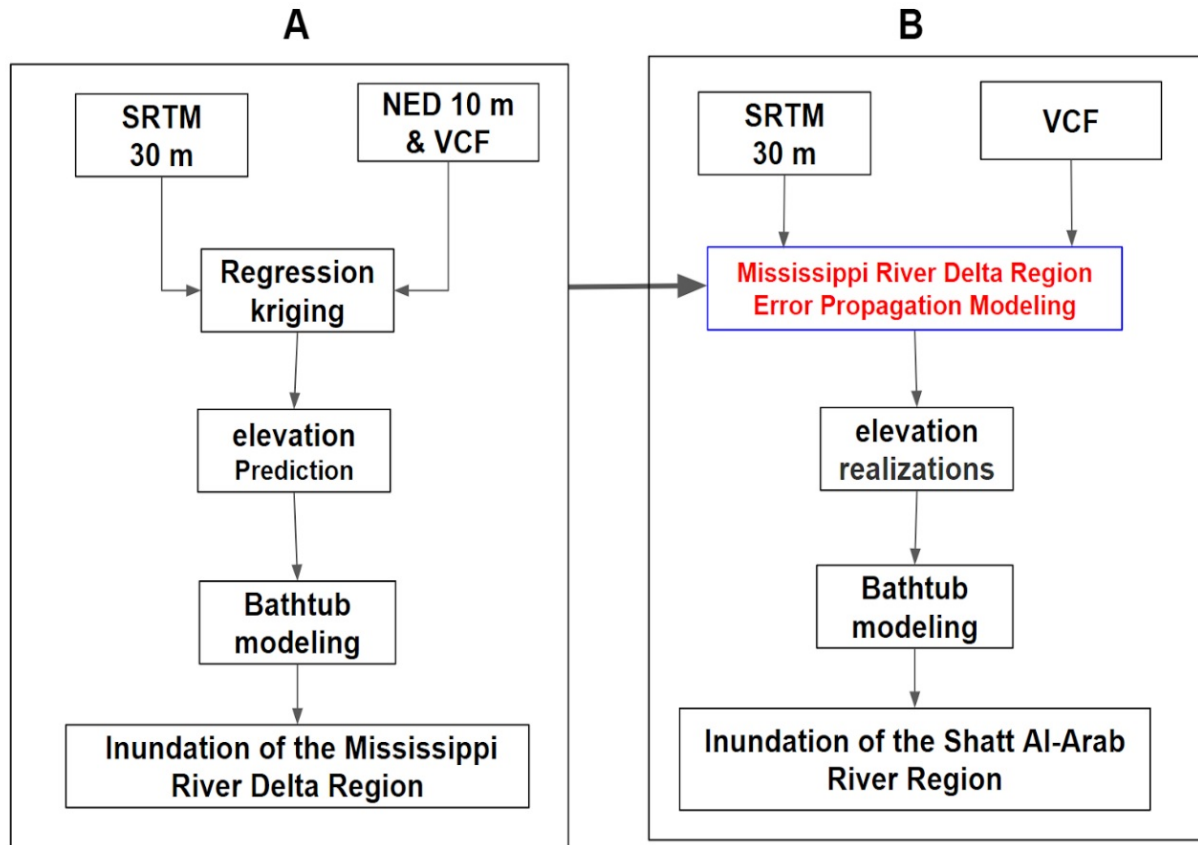


Figure 5.2: Transferring the error propagation model and bathtub modeling from Mississippi River Delta Region (A), to Shatt Al-Arab river region (B).

### 5.2.4.3 Inundation Modeling

Many previous studies on geospatial inundation modeling (bathtub modeling) used either high resolution digital elevation data like lidar data or medium resolution SRTM 30 and used error modeling to remove an error from SRTM based on the truth data that has high resolution (Yassein et al. (2016); W. van de Lageweg et al. (2017); Leon et al. (2014); Kulp and Strauss (2016); Sande et al. (2012)). In SARR, I do not have reference elevation data, so this study uses the error propagation model developed for the MRDR and applies it to the SARR. In this study, a basic inundation model (without considering surface hydrological connectivity) was coded by hand in the R statistical package using the following

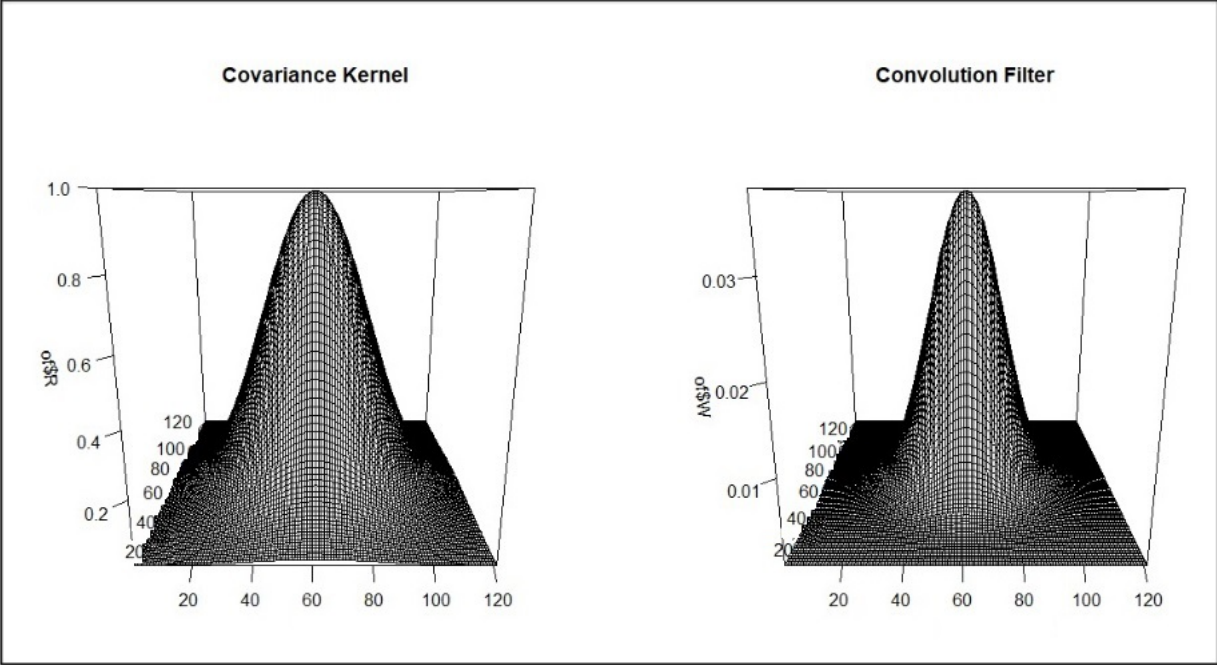


Figure 5.3: The autocorrelated Gaussian covariance process and its associated convolution filter. This filter is passed over spatially random Gaussian noise to produce rasters with the desired spatial structure.

libraries: `sp`, `gstat`, `raster`, `grdevices` and `gstat` (Bivand (2017); R Core Team (2017); Robert J. Hijmans (2017)). A sea level rise of 1 m, a value often cited in the literature as possible by the end of the 21st century (IPCC (2013)), is projected, and inundation modeling is applied to the exhibition area from the region which will be flooding in 1m of SLR. The inundation model function is:

$$\text{Flooded}_j = \begin{cases} 2 & \text{if } DEM_j > f \\ 1 & \text{if } f \geq DEM_j \geq 0 \\ 0 & \text{if } DEM_j \leq 0 \end{cases} \quad (5.4)$$

where  $\text{Flooded}_j$  represents cell  $j$  in the DEM, the cell elevation value for  $j$  is represented with  $DEM_j$ , and  $f$  is the inundation elevation. The inundation model will be applied to

every DEM realization in SARR, resulting in dozens of output maps. The distribution of inundated area across these maps is calculated and portrayed in a histogram. Finally, the probability of inundation for each cell is computed and a map of inundation probability for SARR is produced.

## **5.3 Results**

### **5.3.1 Regression Kriging-Based Error Modeling**

The error model was developed and validated using data from MRDR and transferred to SARR. Validation in the MRDR was positive: the regression model shows high significance and explanatory power, and the residuals were spatially autocorrelated. The variogram model of SRTM errors was a Gaussian model with range = 800, partial sill = 0.1 and nugget = 0.04, as shown in Figure 5.4(a) and Table 5.1. I transferred the error model to SARR to model SRTM error for this region and produce realizations of the potential DEM surface, accounting for uncertainty in SRTM associated with vegetation, slope, elevation values and spatially autocorrelated residuals. Figure 5.4(b) illustrates the predicted SRTM error surface from the regression model for MRDR, while Figure 5.4(d) shows the predicted error surface for SARR. Histograms of both are shown in Figure 5.4(c) and (e), illustrating that these are centered just above zero with a bell-shaped distribution with long tails.

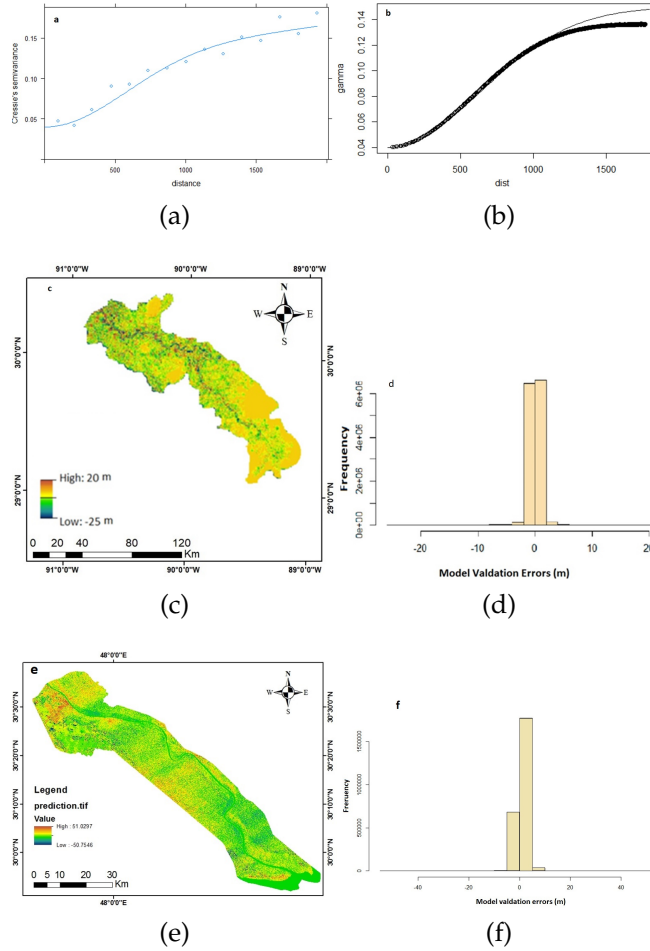


Figure 5.4: Error assessment for variogram model: (a) MRDR error model residual variogram and model (line); (b) SARR variogram model (line) and variogram of simulation output (circles); (c) MRDR map of model-predicted SRTM elevation errors; (d) MRDR histogram of predicted SRTM errors; (e) SARR map of model-predicted SRTM elevation errors; (f) SARR histogram of predicted SRTM errors.

### 5.3.2 Realizations

To better understand the effect of DEM data uncertainty on inundation modeling, DEM realizations were constructed from the SRTM data and the error model as shown below:

$$DEM_{real} = SRTM - Regression - predictederror - Residualrealization \quad (5.5)$$

The regression kriging predicted SRTM error for SARR was subtracted from the orig-

Parameter	Estimate	Std. Error	t value	$P_r(>  t )$
Intercept	-0.1381996	0.0188362	-7.337	2.36e-13 ***
SRTM Elevation	0.8008351	0.0050060	159.976	< 2e-16 ***
VCF	0.0054241	0.0006788	7.991	1.49e-15 ***
SRTM Slope	-0.0803025	0.0103973	-7.723	1.24e-14 **

Table 5.1: Regression coefficients for regression model variables

inal SRTM data. Unconditional error model residual realizations were generated and subtracted as well. QQ plots were used to check the normality assumptions of the error model. The QQ plot for an initial Gaussian random noise realization as shown in Figure 5.5(a) and (b) is straight and, therefore, matches expectations, while that for the filtered realization is not as normal, but its shorter tails are acceptable. I generated 50 realizations of error model residual maps and used the equation above to produce DEM realizations for SARR; one of these is depicted in Figure 5.5(c).

### 5.3.3 Inundation Modeling

The spatial extent of inundation for a 1m sea level rise in SARR region was calculated using the original SRTM DEM as mapped in Figure 5.6, (c),(e). In this comparison, each map shows three classes: water, where areas were at or below 0m of elevation; land, where areas are above 1m; flooded, where areas are between 0 and 1m due to being inundated by this amount of flooding. While only 28% of the land surface is indicated as flooded using the raw SRTM, DEM realizations show a substantial difference with nearly 50% of the land area being flooded for all realizations. Figure 5.6,(d),(f) depicts a histogram of the proportion of land area that remains dry for these realizations as well as that for the raw SRTM.

In this study, I used the inaccurate but globally available SRTM as the base elevation

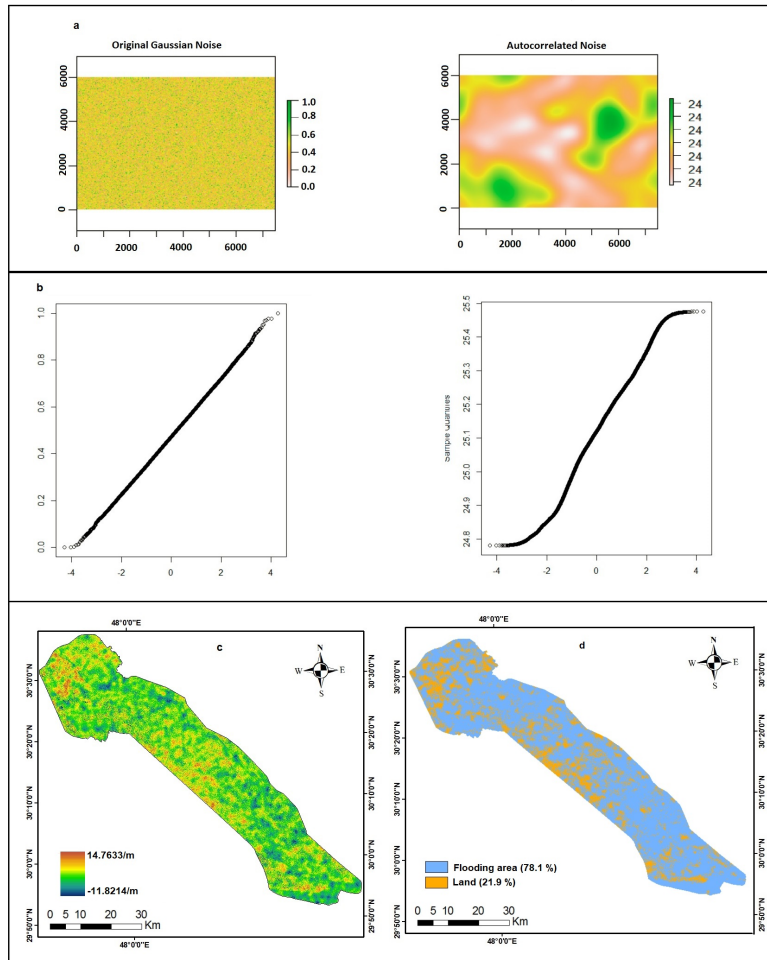


Figure 5.5: SRTM realizations: (a) random Gaussian noise for the SARR and spatially autocorrelated noise following convolution filtering; (b) QQ plots of random and convolution-filtered Gaussian noise; (c) DEM realization number 10; (d) bathtub modeling SRTM realization number 10.

data for SARR and transfer a SRTM regression kriging error model from the MRDR. This model could account for SRTM error due to vegetation and topographic factors while also characterizing the spatial autocorrelation of the regression residuals. I applied a standard geospatial bathtub model to multiple realizations of this elevation model to assess and visualize the impact of one meter of SLR in SARR. The key principle was to employ regression kriging modeling with unconditional simulation of the residual process via convolution filtering to create propagate the impact of SRTM error to the geospatial

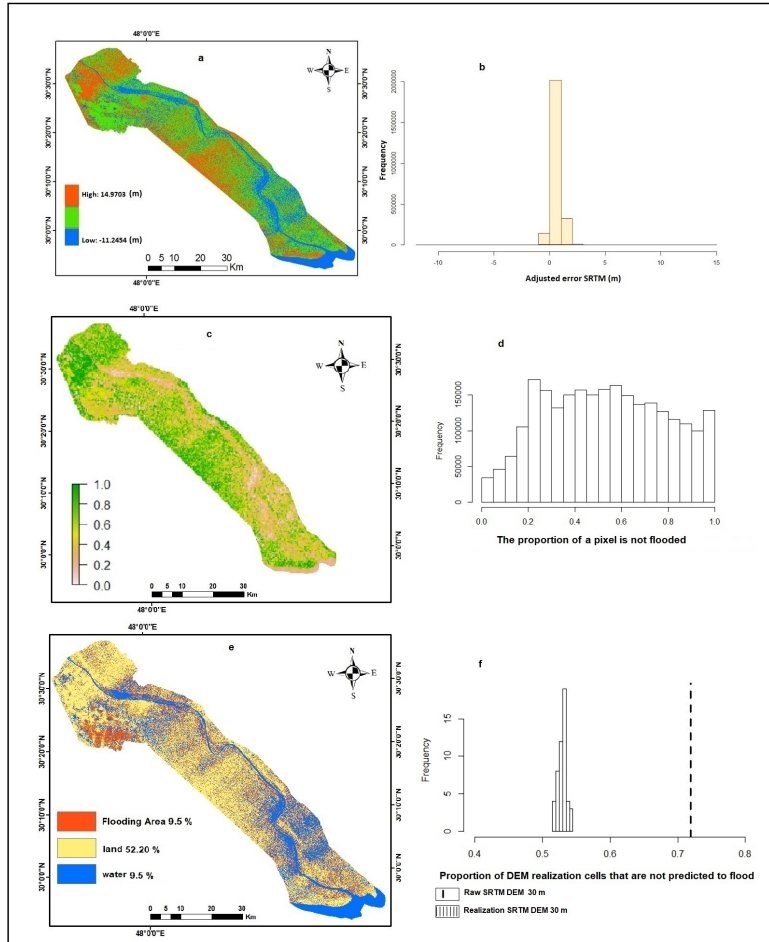


Figure 5.6: (a) SARR map of regression-adjusted SRTM elevation; (b) histograms of adjusted SRTM ; (c) SARR probability map for land remaining dry following bathtub modeling of 1m inundation (d) histogram of flooding probability; (e) SARR bathtub model using raw SRTM data; (f) Proportion of SARR predicted to remain dry following 1m inundation: raw DEM is dashed line, histogram are areas across 50 realizations.

inundation model in SARR. To ensure robust results, 50 realizations of the elevation surface were generated. This study is the first one to transfer an error propagation model for bathtub modeling between different places in the world and to evaluate the effects of SRTM error on SLR inundation of near-coastal riverine regions. I think that the use of the MRDR error model in SARR is justified for several reasons:

1. SRTM 30 is a global DEM product that covers both regions. I assume that, because the sensors that produced it are the same, its error properties in both areas are simi-

lar.

2. The topography of both regions is similar. Both regions are low elevation between 0 to 35m. Elevation is relatively high around the rivers and lower away from the rivers. The northwestern parts of both regions are higher than the southeastern, which both end in gulfs.
3. I can get the parameters to explain SRTM error in both regions like vegetation cover and the slope from SRTM itself and from Landsat imagery.
4. I have surface reference elevation data for MRDR, but I don't have any reference elevation data for SARR.

Geostatistical simulation is computationally expensive, especially over large regions. In this study, a Gaussian convolution filter was applied to random noise raster, which rapidly generated spatially autocorrelated DEM error realizations. The results showed that the methodology improved simulation efficiency while guaranteeing a relative normality of residuals in each simulation. The comparison of geospatial inundation modeling for raw SRTM 30 m and adjusted SRTM 30 m, as shown in Figure 5.6,(f) for 1m SLR, and the impact of SRTM error on flooding estimation is stark. The raw SRTM was flooded around 28%, but adjusted SRTM will be more than 45% flooded. This finding has potential implications for other studies that use SRTM to estimate SLR. were just one study (Kulp and Strauss (2016)). This study used SRTM to assess the performance of NOAA's Global Land 1-km Base Elevation Project (GLOBE) in the US, but this study didn't reach any definitive conclusion because of the spatial heterogeneity in Shuttle Radar Topography Mission (SRTM) 30 m modeling quality which used in this study<sup>4</sup>(Kulp and Strauss (2016)).

## 5.4 Limitations

A major limitation for conducting SLR modeling in SARR is the data. For comparison, MRDR has high-resolution, high accuracy 10 m DEMs derived from lidar, while tide station gauges in the MRDR can give regular sea level elevations in this region at high temporal frequency over many years (NOAA (2018)). In contrast, in SARR there are several studies concerned with the intrusion of seawater in the region and how the river became salty because of a lack of fresh water from upstream water, local demand, and seawater intrusion, but there is no reliable, long term gauge or station to provide the data I can use to measure SLR, or high-quality, freely available DEM. This study was the first about SLR impact in SARR. In SARR I have just SRTM 30m, a global data product with substantial error. After developing the regression kriging error propagation for the MRDR, I duplicate the modeling and fitting the model to the mean and handles spatially auto-correlated residual. The residual error surface is unconditional and residual realizations match properties of the model but do not have local reference data for validation. I must assume that error properties truly are similar between the two regions; if this is not the case, then the effects of error on inundation model are misspecified. Second, the resulting surface in the regression kriging, like any interpolation procedure, does not represent slope and aspect. In both regions, the surface is smoother than depicted, as slopes and aspect are poorly represented.

Another limitation of the study is the methods described in this study can only be applied in near-coastal riverine regions. Therefore, any differences between enforcement methods at the propagation regression kriging modeling can only be said to be transferable to other areas with similar geographical characteristics, especially topography and

vegetation cover. There are multiple SLR models available for the data-rich MRDR, including more formal hydrological modeling, but this study is limited to bathtub modeling in order provide a fair comparison between MRDR and SARR.

## 5.5 Conclusion

The study results presented in this paper furnished valuable information on the error propagation modeling of SRTM 1 to characterize sea level rise in SARR. It is the first to apply error propagation modeling in this context. Model output included a probability of inundation for each location in the SARR, and a comparison of total inundated area. The approach was effective for determining and mapping the land which would be inundated in the region from a 1m rise in sea level based on bathtub modeling. Most critically, in SARR, error propagation modeling found much larger areas were at risk of flooding than would be estimated with raw SRTM. SRTM, with its global coverage, can be used to model SLR if error propagation modeling is applied properly. The approach will give reasonable flooding risk for regions facing SLR. This research provides an appropriate example of the successful application of transferring a geostatistical error model for error propagation modeling to assess SLR inundation on near-coastal riverine regions.

# Chapter 6

## Conclusion

The threat of global warming and changing sea level rise has led to many studies on its impact in some areas, like the MRDR in southern Louisiana, USA. However, it is also necessary to assess the impact in other coastal areas like the SARR in southern Iraq. Consequences of sea level rise in the coastal regions investigated in this dissertation are complex, with a range of indicators and impacts. The most important indicators of SLR in both regions are loss of land within the MRDR, declining vegetation cover within both regions, reduction in land-based human activity such as agriculture and settlement within both regions, ecosystem change around both regions, increase in groundwater salinity around both regions, and increase in water salinity in both rivers. In this research, I sought to explore the potential impacts of SLR on the SARR in southern Iraq and conduct a comparison with the MRDR in southern Louisiana, USA. To accurately model and predict SLR impact in the near-coastal riverine regions of the world, high quality, high-resolution elevation data is needed, especially for geospatial inundation modeling (bathtub modeling). Unfortunately, there is no freely available high-resolution data for all of the world and therefore enhancing SRTM 1 Arc Second by developing error propagation models is important for those regions.

Previous studies of geospatial inundation modeling (bathtub modeling) for SLR using high-resolution data such as LiDAR were applied for limited geographical areas around

coastal cities which are vulnerable to increasing flood risks, including the Greater London region (United Kingdom), the Lagos State area (Nigeria) and Brighton, the northernmost suburb of Brisbane City (Australia) (Yunus et al. (2016); Leon et al. (2014); Sande et al. (2012)). In contrast there is a study which used SRTM to assess the performance of NOAAs Global Land 1-km Base Elevation Project (GLOBE) in the US, but this study does not reach any definitive conclusion because of the spatial heterogeneity in SRTM quality for data used in this study (Kulp and Strauss (2016)).

In this research, I clarify the connections between the environmental degradation in the SARR and SLR. These connections are complex, and the range of potential drivers present challenges for understanding the causes, consequences, and trajectories of this marginal region. A coupled human and natural systems framework was established in an effort to better comprehend the factors influencing the previous five decades of environmental degradation in the SARR. I used decadal Landsat imagery across that region to assess the geographic distribution of vegetation, how it is associated with the regional environment, and how it has been changing. Additionally, an array of factors was identified as contributing to the degradation of vegetation in this dynamic, peripheral area. Global climate change plays a critical part in directly and indirectly driving the most important factors and presents the most serious problem now facing the SARR. The scope of this problem is significant due to the fact that climate change is a global problem as opposed to a regional problem, and is not directly addressable by regional policy. In the second case, I created error propagation modeling to assess SRTM 1 Arc Second error in the MRD region. Following this assessment, I applied inundation modeling to determine the flooding area due to SLR. The modeling developed for the MRD region appears to have a viable application in similar near coastal riverine regions around the world.

In addition, I transferred error propagation modeling from the MRDR to the SARR, in an effort to understand the impact of SLR in this region by applying inundation modeling. The error propagation model is comprised of three phases. First, several parameters from the MRDR, which is used to produce an expected DEM error surface for the SARR. The result for the SARR is obtained by subtracting the surface from the SRTM DEM. Second, spatially autocorrelated, mean-zero rasters with a Gaussian covariance model capture residuals from the error model, which are replicated for the SARR. My goal here was to better characterize the extent of flooding in the SARR associated with 1 m of SLR using an inundation modeling (bathtub model) by enhancing the SRTM 1 Arc Second DEMs by duplicating with an SRTM error model.

## **6.1 Methods**

### **6.1.1 Coupled human and natural systems (CHANS)**

CHANS is a popular, recent approach for investigators to understand responses, nonlinearities, thresholds, and legacy effects across many spatial, temporal, and organizations scales. The CHANS framework has been enormously valuable as it permits a nontraditional interdisciplinary approach. I used a CHANS framework to measure SLR indicators in SARR and the associations of SLR with the human system (war, government land policy, upstream hydroengineering, pollution, and degradation) and natural system (meteorological factors associated with drought and groundwater salinity). In this study, I utilized numerous measures of ecological, economic and social systems following a review of the CHANS concept.

### **6.1.2 The inundation model (bathtub modeling) and error propagation**

DEM error was in part removed and in part accounted for by utilizing the error propagation model, which fed into an inundation model that allowed for an assessment of the SLR influences in the SARR. To understand the impact of the SLR, I have to apply the inundation model in this complex region, I conducted an error assessment and developed statistical error modeling for SRTM for the MRDR and implemented this model to the SARR in an effort to improve the quality of elevation data. In this study, the vegetation index derived from Landsat combined with elevation and slope are used to account for SRTM error in the MRDR. Based on a set of 10 thousand points in the MRDR, an error model was developed, which then was authenticated and used to adjust the SRTM, and then was used to generate an enhanced DEM for an inundation model. The regression kriging-based SRTM error model effectively captures error through correlated environmental variables and residual spatial autocorrelation collectively.

Next, I developed error propagation models to enhance SRTM 1 Arc Second for modeling SLR in the SARR by applying the model from chapter four, developed for the MRD region, to the SARR. I employed process convolution to develop the residual simulations in an efficient manner. The convolution filter reproduces a spatial Gaussian covariance function matching that observed in the MRDR. The MRDR predictions of the SRTM elevation shows the error between 20 m and 25m, and the histogram of model predictions was approximately one meter. In the second prediction, SRTM elevation SARR depicts the error between 51 m and -50 m, and the histogram of model predictions was again approximately one meter. The adjusted SRTM elevation errors were on two meters, and the modified errors distribution ranged between 15 m and -11 meters. Fifty simulations

of 2-D autocorrelated Gaussian noise process were produced, which was used as input to the inundation modeling experiment. In SARR I dont have reference digital elevation data, so this study is transferred the error propagation modeling from the MRDR, which has reference NED data digital elevation, to the SARR.

## 6.2 Dissertation Objectives

This dissertation has four objectives each of which uses many geospatial methods. The dissertation objectives are:

*Objective one.*

Compare and contrast MRDR, SARR, and identify whether these regions have environmental degradation because of SLR, based on the theoretical framework and findings from previous studies. To achieve this objective, the following steps are used:

1. Characterize the geomorphology and climate in both regions and show how that is correlated with SLR in both regions.
2. Identify human activity and economic importance in both regions and also identify how the human system accelerates SLR risk in both regions.
3. Assess the different ways that SLR may affect both regions through rising salinity in groundwater, pressure from subsidence erosion and regional flooding.

With respect to the two chapter, I found that both regions are similar in important geomorphological, environmental, economic and climatic characteristics. For example, both are geologically recent creations from the deposits of several of the worlds greatest rivers (Tigris, Euphrates and the Mississippi Rivers) flowing into gulfs (the Persian Gulf and

the Gulf of Mexico). Both regions are important regional economic centers for agricultural production, oil production, fishing, and marine transport. Both rivers have natural deltas that have formed where the mouth of each river meets its gulf. Also, land areas on either side of these rivers are highest along the edges of the channels and decrease in elevation farther from the river. Delta development for both rivers is an integrated and long-term process that has given both regions a unique mix of ecosystems, habitats and landforms. In this chapter I show that both regions face increasing pressure from subsidence, erosion, sea-level rise and rising salinity in groundwater, leading to coastal retreat in these regions because of the climate change and human activities there. SLR affects these regions in somewhat different through flooding, pressure from subsidence and erosion, and rising salinity in groundwater.

*Objective two.* Use a CHANS perspective to characterize and delineate a clear conceptual model for factors impacting SARR and identify how human and natural systems are associated with SLR risk in this region. For achieving this objective, these steps are followed:

1. Identify primary human and environmental drivers in SARR system.
2. Characterize NDVI as a proxy for vegetation quality and quantity and measure it over a five decade period.
3. Identify spatial and temporal changes in NDVI throughout the SARR.
4. Link observed changes to dominant drivers of change in the SARR.

Chapter three's findings in this objective are: this chapter supports the importance of the CHANS viewpoint because it recognizes not only the difficulties of this region but also the solutions needed. First, the study outlines a distinct view of the SAR region in an

effort to identify the facts needed so that CHANS can be applied for a deeper understanding of the problems and solutions needed. Second, my research identified the significance of the SLR, which a primary natural systems driver for this region, and how the impacts of SLR have accelerated over time. This study supported the importance of CHANS by allowing for confirmation and understanding that the Shatt al-Arab River region is suffering. Environmental degradation occurred in the SARR from 1975 to 2017, and this study concentrates on both the human and natural complications while determining which one is accountable for the environmental degradation.

*Objective three.* Enhance SRTM Global DEM to better model SLR and characterize land change in MRDR. For this objective to be accomplished, these steps are followed:

1. Determine how SRTM error correlates with canopy cover (derived from Landsat 7).
2. Identify the extent to which SRTM error is reduced using canopy cover and other globally available covariates.
3. Assess the effectiveness of geostatistical models in reproducing inundation model results using high-accuracy USGS NED in this region.

Chapter four followed an extensive process to address this objective: The first phase was to extract the 10,000 random point sample from reference NED elevations, SRTM, and NDVI, and then use the outcome to develop a regression model for SRTM error across the region. The residuals of spatial structure from the regression model were spatially modeled to fit both short-range and long-range structure of two Gaussian variogram models. The first variogram model parameters were: partial sill = 0.1, nugget = 0.04 and range = 800, whereas partial sill = 0.12, nugget = 0 and range = 4000, were parameters for the

second variogram model. The regression model was validated using 10,000 other random locations. I applied the inundation model of 1m SLR for the adjusted SRTM DEM and the original SRTM DEM before error modeling. The output of the modeling maps shows three classes: land areas which are higher than 1m; water areas which were at or under 0m of elevation; and flooded areas between 1m and 0 which are flooded by this quantity of inundation. The difference between models is unambiguous: around 52% in the adjusted SRTM will be flooded, while in the original SRTM 8.8% will be flooded.

*Objective four.* Develop error propagation models to enhance SRTM 30 for modeling sea level rise and characterizing the land change in SARR. This is achieved via the following steps:

1. Apply the error model from objective three, developed for MRDR, to SARR.
2. Determine and map land flooding due to SLR in SARR and identify the land which will become inundated based on the bathtub model.
3. Apply a valid geostatistical model to account for SRTM error and assess uncertainty in SLR inundation model.

Chapter five's findings on this objective are as follows. After unconditional simulation with convolution filtering for SRTM, I applied the inundation model with SLR set to 1 m to each realization. This produced fifty output flooding maps, enabling an understanding of the likelihood of flooding for each cell in the region. The output maps show the areas below 1m and therefore flooded by this volume of water. Around 45% of the region's land will be flooded for all realizations. For the raw SRTM, 27% of the land surface is shown as flooded. SRTM error seems to give conservatively biased estimates of the flooded area.

## 6.3 Future Research

Modeling SLR impact in near-coastal riverine regions is essential for these sensitive areas, so focus should be on this problem. By assessing the utility of geospatial methods for monitoring and modeling these impacts through the integration of land changes that appear through DEM and satellite imagery analysis for different periods of time with the values of water salinity, SLR rate, and land subsidence rate in the river regions, analysts can understand what the effects of these changes may be. For my future research, the error models should be tested in areas with similar geographical characteristics and data like that in the Mississippi River Delta region. That will help determine if the error modeling can be used other sensitive coastal regions in the world. Another important direction is to use relationships between SRTM DEMs 1 Arc Second and classified satellite imagery of land change on the SARR over recent decades, e.g., 1975, 1985, 1995, 2005, and 2018, to predict the impact of SLR on land use over the next several decades. The coming decades will see important changes in many understudied near coastal areas like the SARR, and the use of spatial data, while accounting for error, will play an important role in helping to understand and manage those changes.

## **BIBLIOGRAPHY**

## BIBLIOGRAPHY

- C. H. Chabreck. Vegetation, water and soil characteristics of the Louisiana coastal region. *LSU Agricultural Experiment Station Reports*, 664, 1972. ISSN 0036-8075. URL <https://digitalcommons.lsu.edu/agexp/147/>.
- A. D. Abdullah, I. Masih, P. van der Zaag, U. F. Karim, I. Popescu, and Q. A. Suhail. Shatt al arab river system under escalating pressure: a preliminary exploration of the issues and options for mitigation. *International Journal of River Basin Management*, 13(2): 215–227, 2015. doi: 10.1080/15715124.2015.1007870. URL <https://doi.org/10.1080/15715124.2015.1007870>.
- S. Al-Asadi. The future of freshwater in shatt al- arab river (southern iraq). *Journal of Geography and Geology*, 9(2):24, 2017. ISSN 1916-9787. doi: 10.5539/jgg.v9n2p24. URL <http://ccsenet.org/journal/index.php/jgg/article/view/68135>.
- N. Al-Bahili, J. Al-Maliki, and A. Al-Rubaye. The effect of vegetation on the stream bank erosion of shatt al-arab river, south iraq. *Marsh Bulletin*, 5(1):1–13, 2010. URL <http://pubs.er.usgs.gov/publication/pp1815>.
- I. Al Isawi. The geographic potentialities in shatt al-arab district and their suitability for planting the suggested field produce. *Dissertation, University of Basrah, College of Arts*, 2011.
- H. Al-Mahmood. The monthly variations of discharge and effect that on a total dissolved suspended and salinity in shatt al-arab river (south of iraq). *Iraqi Journal of Science*, 50: 355–368, 2009. URL <http://repository.uobaghdad.edu.iq/ArticlePrint.aspx?ID=2170>.
- Z. Al-Saaidy. The potentials and the agricultural production in basrah during (1990-2006) and it's developing procedures in future. Graduate Thesis and Dissertations, The University of Basrah, College of Administration and Economics., 2008.
- A. Alothman, M. Bos, R. Fernandes, and M. Ayhan. Sea level rise in the north-western part of the arabian gulf. *Journal of Geodynamics*, 81:105 – 110, 2014. ISSN 0264-3707. doi: <https://doi.org/10.1016/j.jog.2014.09.002>. URL <http://www.sciencedirect.com/science/article/pii/S0264370714001264>.
- M. Antonellini, P. Mollema, B. Giambastiani, K. Bishop, L. Caruso, A. Minchio, L. Pellegri, M. Sabia, E. Ulazzi, and G. Gabbianelli. Salt water intrusion in the coastal aquifer of the southern po plain, italy. *Hydrogeology Journal*, 16(8):1541, Jun 2008. ISSN 1435-0157. doi: 10.1007/s10040-008-0319-9. URL <https://doi.org/10.1007/s10040-008-0319-9>.

- F. Baret, M. Weiss, R. Lacaze, F. Camacho, H. Makhmara, P. Pacholczyk, and B. Smets. Geov1: Lai and fapar essential climate variables and fcover global time series capitalizing over existing products. part1: Principles of development and production. *Remote Sensing of Environment*, 137:299 – 309, 2013. ISSN 0034-4257. doi: <https://doi.org/10.1016/j.rse.2012.12.027>. URL <http://www.sciencedirect.com/science/article/pii/S0034425713000813>.
- M. Barlage and X. Zeng. The impact of fractional vegetation cover and leaf area index on warm season precipitation variability in global ensemble simulations. *Arizona Journal of Hydrometeorology*, 01 2003.
- P. M. Barlow. Ground water in freshwater-saltwater environments of the atlantic coast. *Tech. Report, U.S. Department of the Interior*, 2003. URL <http://pubs.er.usgs.gov/publication/cir1262>. Report.
- J. A. Barras. Land area changes in coastal louisiana after the 2005 hurricanes: A series of three maps. *U.S. Department of the Interior — U.S. Geological Survey*, 2006. ISSN 2006-1274. URL <http://pubs.er.usgs.gov/publication/ofr20061274>. Report.
- J. A. Barras, J. C. Bernier, and R. A. Morton. Land area change in coastal louisiana: A multidecadal perspective (from 1956 to 2006). *Tech. Report, U.S. Department of the Interior*, 2008. URL <http://pubs.er.usgs.gov/publication/sim3019>. Report.
- P. Beaumont. Agricultural and environmental changes in the upper euphrates catchment of turkey and syria and their political and economic implications. *Applied Geography*, 16(2):137 – 157, 1996. ISSN 0143-6228. doi: [https://doi.org/10.1016/0143-6228\(95\)00033-X](https://doi.org/10.1016/0143-6228(95)00033-X). URL <http://www.sciencedirect.com/science/article/pii/014362289500033X>.
- K. J. Bhang, F. W. Schwartz, and A. Braun. Verification of the Vertical Error in C-Band SRTM DEM Using ICESat and Landsat-7, Otter Tail County, MN. *IEEE Transactions on Geoscience and Remote Sensing*, 45:36–44, Jan. 2007. doi: 10.1109/TGRS.2006.885401.
- R. Bivand. spgwr: Geographically weighted regression. *CRAN Task View: Analysis of Spatial Data*, 01 2017. URL <https://cran.r-project.org/web/packages/spgwr/index.html>.
- L. Bizikova, D. Roy, D. Swanson, H. D. Venema, and M. McCandless. The water energy food security nexus : Towards a practical planning and decision-support framework for landscape investment and risk management. In *The International Institute for Sustainable Development (IISD)*, 2013.
- M. D. Blum and H. H. Roberts. Drowning of the mississippi delta due to insufficient sediment supply and global sea-level?rise. *Nature Geoscience*, 2:488 EP –, Jun 2009. URL <http://dx.doi.org/10.1038/ngeo553>.
- M. D. Blum and H. H. Roberts. The mississippi delta region: Past, present, and future. *Annual Review of Earth and Planetary Sciences*, 40(1):655–683,

2012. doi: 10.1146/annurev-earth-042711-105248. URL <https://doi.org/10.1146/annurev-earth-042711-105248>.
- A. G. Bobba. Numerical modelling of salt-water intrusion due to human activities and sea-level change in the godavari delta, india. *Hydrological Sciences Journal*, 47(sup1): S67–S80, 2002. doi: 10.1080/02626660209493023. URL <https://doi.org/10.1080/02626660209493023>.
- L. Brandimarte, I. Popescu, and N. K. Neamah. Analysis of fresh-saline water interface at the shatt al-arab estuary. *International Journal of River Basin Management*, 13(1):17–25, 2015. doi: 10.1080/15715124.2014.945092. URL <https://doi.org/10.1080/15715124.2014.945092>.
- T. Buday, I. Kassab, and S. Jassim. *The Regional Geology of Iraq: Tectonism, magmatism and metamorphism*. The Regional Geology of Iraq. State Organization for Minerals, Directorate General for Geological Survey and Mineral Investigations, 1987. URL <https://books.google.com/books?id=2VxPAQAIAAJ>.
- V. R. Burkett, D. B. Zilkoski, and D. Hart. Sea-level rise and subsidence: Implications for flooding in new orleans, louisiana. *U.S. Geological Survey Subsidence Interest Group Conference: proceedings of the Technical Meeting, Galveston, Texas, November 27-29, 2001*, 06 2003. URL <http://pubs.er.usgs.gov/publication/2000794>.
- C. Cabanes, A. Cazenave, and C. Le Provost. Sea level rise during past 40 years determined from satellite and in situ observations. *Science*, 294(5543):840–842, 2001. ISSN 0036-8075. doi: 10.1126/science.1063556. URL <http://science.sciencemag.org/content/294/5543/840>.
- C. H. Chabreck. Vegetation, water and soil characteristics of the louisiana coastal region. *LSU Agricultural Experiment Station Reports*, 664, 1972. ISSN 0036-8075. URL <https://digitalcommons.lsu.edu/agexp/147/>.
- R. Christensen. Advanced linear modeling. multivariate, time series, and spatial data; nonparametric regression and response surface maximization. 2nd ed. *Springer Science and Business Media*, 01 2001.
- P. U. Clark, J. D. Shakun, S. A. Marcott, A. C. Mix, M. Eby, S. Kulp, A. Levermann, G. A. Milne, P. L. Pfister, B. D. Santer, D. P. Schrag, S. Solomon, T. F. Stocker, B. H. Strauss, A. J. Weaver, R. Winkelmann, D. Archer, E. Bard, A. Goldner, K. Lambeck, R. T. Pierrehumbert, and G.-K. Plattner. Consequences of twenty-first-century policy for multi-millennial climate and sea-level change. *Nature Climate Change*, 6:360 EP –, Feb 2016. URL <http://dx.doi.org/10.1038/nclimate2923>. Perspective.
- B. R. Couvillion, J. A. Barras, G. D. Steyer, W. Sleavin, M. Fischer, H. Beck, N. Trahan, B. Griffin, and D. Heckman. "land area change in coastal louisiana from 1932 to 2010. *Tech. Report*, U.S. Department of the Interior, 2011. URL <https://pubs.usgs.gov/sim/3164>. Report.

- G. B. Cressey. The shatt al-arab basin. *Middle East Journal*, 12(4):448–460, 1958. ISSN 00263141, 19403461. URL <http://www.jstor.org/stable/4323054>.
- S. Dasgupta, B. Laplante, C. Meisner, D. Wheeler, and J. Yan. The impact of sea level rise on developing countries: a comparative analysis. *Climatic Change*, 93(3):379–388, Apr 2009. ISSN 1573-1480. doi: 10.1007/s10584-008-9499-5. URL <https://doi.org/10.1007/s10584-008-9499-5>.
- M. El Raey. Impact of sea level rise on the arab region. *University of Alexandria and Regional Center for Disaster Risk Reduction, Arab Academy of Science, Technology and Maritime Transport*, 2010. URL [http://www.arabclimateinitiative.org/Countries/egypt/ElRaey\\_Impact\\_of\\_Sea\\_Level\\_Rise\\_on\\_the\\_Arab\\_Region.pdf](http://www.arabclimateinitiative.org/Countries/egypt/ElRaey_Impact_of_Sea_Level_Rise_on_the_Arab_Region.pdf).
- J. Emel, J. Plisinski, and J. Rogan. Monitoring geomorphic and hydrologic change at mine sites using satellite imagery: The geita gold mine in tanzania. *Applied Geography*, 54:243 – 249, 2014. ISSN 0143-6228. doi: <https://doi.org/10.1016/j.apgeog.2014.07.009>. URL <http://www.sciencedirect.com/science/article/pii/S0143622814001659>.
- A. M. Essa. The use of diatom indices for the assessment of shatt al-arab river water quality. *Journal of Basrah Researches ((Sciences))*, 38:114–124, 2012. URL <https://bit.ly/2NIdnD1>.
- T. G. Farr, P. A. Rosen, C. Edward, C. Robert, D. Riley, H. Scott, K. Michael, P. Mimi, R. Ernesto, R. Ladislav, S. David, S. Scott, S. Joanne, U. Jeffrey, W. Marian, O. Michael, B. Douglas, and A. Douglas. The shuttle radar topography mission. *Reviews of Geophysics*, 45(2), May 2007. doi: 10.1029/2005RG000183. URL <https://agupubs.onlinelibrary.wiley.com/doi/abs/10.1029/2005RG000183>.
- C. L. Foote, K. Crane, W. Block, and S. Gray. Economic policy and prospects in iraq (may 4, 2004). *FRB of Boston Public Policy Discussion Paper No. 04-1*, pages 47–70, 2004. URL <http://dx.doi.org/10.2139/ssrn.887920>.
- J. Fox, R. R. Rindfuss, S. J. Walsh, and V. Mishra. People and the environment: Approaches for linking household and community surveys to remote sensing and gis. *Springer Science and Business Media*, 2003. URL <https://www.springer.com/us/book/9781402073229>.
- D. O. Fuller. Trends in ndvi time series and their relation to rangeland and crop production in senegal, 1987-1993. *International Journal of Remote Sensing*, 19(10): 2013–2018, 1998. doi: 10.1080/014311698215135. URL <https://doi.org/10.1080/014311698215135>.
- W. E. Galloway and D. K. Hobday. Coal. in: Terrigenous clastic depositional systems. *Terrigenous Clastic Depositional Systems*, pages 253–297, 1983.
- W. E. Galloway, T. L. Whiteaker, and P. Ganey-Curry. History of cenozoic north american drainage basin evolution, sediment yield, and accumulation in the gulf of mexico basin. *Geosphere*, 7(4):938, 2011. doi: 10.1130/GES00647.1. URL <http://dx.doi.org/10.1130/GES00647.1>.

- P. Gamba, F. Dell'Acqua, and B. Houshmand. Srtm data characterization in urban areas. *International Archives of Photogrammetry Remote Sensing and Spatial Information Sciences.*, 34, 05 2002.
- F. Geri, V. Amici, and D. Rocchini. Human activity impact on the heterogeneity of a mediterranean landscape. *Applied Geography*, 30(3):370 – 379, 2010. ISSN 0143-6228. doi: <https://doi.org/10.1016/j.apgeog.2009.10.006>. URL <http://www.sciencedirect.com/science/article/pii/S0143622809000721>.
- D. B. Gesch. Analysis of lidar elevation data for improved identification and delineation of lands vulnerable to sea-level rise. *Journal of Coastal Research*, pages 49–58, 2009. doi: 10.2112/SI53-006.1. URL <https://doi.org/10.2112/SI53-006.1>.
- D. B. Gesch, M. J. Oimoen, S. K. Greenlee, C. A. Nelson, M. J. Steuck, and D. J. Tyler. The national elevation data set. *Photogrammetric Engineering and Remote Sensing*, 68(1):5–11, 2002. URL <http://pubs.er.usgs.gov/publication/70156331>.
- G. R. Gibson, J. B. Campbell, and R. H. Wynne. Three decades of war and food insecurity in iraq. *Photogrammetric Engineering and Remote Sensing*, 78(8):885–895, 2012. ISSN 0099-1112. doi: [doi:10.14358/PERS.78.8.895](https://doi.org/10.14358/PERS.78.8.895). URL <https://www.ingentaconnect.com/content/asprs/pers/2012/00000078/00000008/art00008>.
- G. R. Gibson, J. B. Campbell, and C. E. Zipper. Sociopolitical influences on cropland area change in iraq, 20012012. *Applied Geography*, 62:339 – 346, 2015. ISSN 0143-6228. doi: <https://doi.org/10.1016/j.apgeog.2015.05.007>. URL <http://www.sciencedirect.com/science/article/pii/S0143622815001277>.
- G. R. Gibson, N. L. Taylor, N. C. Lamo, and J. K. Lackey. Effects of recent instability on cultivated area along the euphrates river in iraq. *The Professional Geographer*, 69(2): 163–176, 2017. doi: 10.1080/00330124.2016.1194216. URL <https://doi.org/10.1080/00330124.2016.1194216>.
- L. Giosan and A. M. Freeman. *How Deltas Work: A Brief Look at the Mississippi River Delta in a Global Context*, pages 29–32. Springer Netherlands, Dordrecht, 2014. ISBN 978-94-017-8733-8. doi: 10.1007/978-94-017-8733-8\_3. URL [https://doi.org/10.1007/978-94-017-8733-8\\_3](https://doi.org/10.1007/978-94-017-8733-8_3).
- J. B. D. M. J. R. K. R. Good, B. and R. Wilson. Louisiana's major coastal navigation channels. *Louisiana Department of Natural Resources, Baton Rouge, LA 70802*, 1995. URL <http://coastal.la.gov/a-common-vision/2012-coastal-master-plan/>.
- S. N. Goward and S. D. Prince. Transient effects of climate on vegetation dynamics: Satellite observations. *Journal of Biogeography*, 22(2/3):549–564, 1995. ISSN 03050270, 13652699. URL <http://www.jstor.org/stable/2845953>.
- S. Hajian and Z. Hamidi-Esfahani. *Date Palm Status and Perspective in Iran*, pages 19–47. Springer Netherlands, Dordrecht, 2015. ISBN 978-94-017-9707-8. doi: 10.1007/978-94-017-9707-8\_2. URL [https://doi.org/10.1007/978-94-017-9707-8\\_2](https://doi.org/10.1007/978-94-017-9707-8_2).

- R. A. M. Hamid. The concentration of salt in shatt al-arab. *Journal of Basrah researchers (The Humanities)*, 39, 2014. ISSN 18172695.
- J. E. Hansen. Scientific reticence and sea level rise. *Environmental Research Letters*, 2(2): 024002, 2007. URL <http://stacks.iop.org/1748-9326/2/i=2/a=024002>.
- S. Hassanzadeh, A. Kiasatpour, and F. Hosseinibalam. Sea-level response to atmospheric forcing along the north coast of persian gulf. *Meteorology and Atmospheric Physics*, 95 (3):223–237, Feb 2007. ISSN 1436-5065. doi: 10.1007/s00703-006-0213-8. URL <https://doi.org/10.1007/s00703-006-0213-8>.
- K. M. Hazzouri, J. M. Flowers, H. J. Visser, H. S. M. Khierallah, U. Rosas, G. M. Pham, R. S. Meyer, C. K. Johansen, Z. A. Fresquez, K. Masmoudi, N. Haider, N. El Kadri, Y. Idagh-dour, J. A. Malek, D. Thirkill, G. S. Markhand, R. R. Krueger, A. Zaid, and M. D. Purugganan. Whole genome re-sequencing of date palms yields insights into diversification of a fruit tree crop. *Nat Commun*, 6:8824, Nov 2015. ISSN 2041-1723. doi: 10.1038/ncomms9824. URL [http://www.ncbi.nlm.nih.gov/pmc/articles/PMC4667612/26549859\[pmid\]](http://www.ncbi.nlm.nih.gov/pmc/articles/PMC4667612/26549859[pmid]).
- T. Hengl, G. Heuvelink, and A. Stein. Comparison of kriging with external drift and regression-kriging. *Technical Note*, 08 2003.
- T. Hengl, B. Bajat, D. Blagojevi, and H. I. Reuter. Geostatistical modeling of topography using auxiliary maps. *Computers and Geosciences*, 34(12):1886 – 1899, 2008. ISSN 0098-3004. doi: <https://doi.org/10.1016/j.cageo.2008.01.005>. URL <http://www.sciencedirect.com/science/article/pii/S0098300408001106>.
- M. Hofton, R. Dubayah, J. B. Blair, and D. Rabine. Validation of srtm elevations over vegetated and non-vegetated terrain using medium footprint lidar. *Photogrammetric Engineering and Remote Sensing*, 72(3):279–285, 2006. ISSN 0099-1112. doi: [doi:10.14358/PERS.72.3.279](https://doi.org/10.14358/PERS.72.3.279). URL <https://www.ingentaconnect.com/content/asprs/pers/2006/00000072/00000003/art00005>.
- C. E. Hughes, P. Binning, and G. R. Willgoose. Characterisation of the hydrology of an estuarine wetland. *Journal of Hydrology*, 211(1):34 – 49, 1998. ISSN 0022-1694. doi: [https://doi.org/10.1016/S0022-1694\(98\)00194-2](https://doi.org/10.1016/S0022-1694(98)00194-2). URL <http://www.sciencedirect.com/science/article/pii/S0022169498001942>.
- IPCC. *Climate Change 2013: The Physical Science Basis. Contribution of Working Group I to the Fifth Assessment Report of the Intergovernmental Panel on Climate Change*. Cambridge University Press, Cambridge, United Kingdom and New York, NY, USA, 2013. ISBN ISBN 978-1-107-66182-0. doi: 10.1017/CBO9781107415324. URL [www.climatechange2013.org](http://www.climatechange2013.org).
- M. T. Jabbar and X. Zhou. Eco-environmental change detection by using remote sensing and gis techniques: a case study basrah province, south part of iraq. *Environmental Earth Sciences*, 64(5):1397–1407, Nov 2011. ISSN 1866-6299. doi: 10.1007/s12665-011-0964-5. URL <https://doi.org/10.1007/s12665-011-0964-5>.

- J. B. C. Jackson, M. X. Kirby, W. H. Berger, K. A. Bjorndal, L. W. Botsford, B. J. Bourque, R. H. Bradbury, R. Cooke, J. Erlandson, J. A. Estes, T. P. Hughes, S. Kidwell, C. B. Lange, H. S. Lenihan, J. M. Pandolfi, C. H. Peterson, R. S. Steneck, M. J. Tegner, and R. R. Warner. Historical overfishing and the recent collapse of coastal ecosystems. *Science*, 293(5530):629–637, 2001. ISSN 0036-8075. doi: 10.1126/science.1059199. URL <http://science.sciencemag.org/content/293/5530/629>.
- G. Jiapaer, X. Chen, and A. Bao. A comparison of methods for estimating fractional vegetation cover in arid regions. *Agricultural and Forest Meteorology*, 151(12):1698 – 1710, 2011. ISSN 0168-1923. doi: <https://doi.org/10.1016/j.agrformet.2011.07.004>. URL <http://www.sciencedirect.com/science/article/pii/S0168192311002176>.
- X. Jing, W.-Q. Yao, J.-H. Wang, and X.-Y. Song. A study on the relationship between dynamic change of vegetation coverage and precipitation in beijings mountainous areas during the last 20 years. *Mathematical and Computer Modelling*, 54(3):1079 – 1085, 2011. ISSN 0895-7177. doi: <https://doi.org/10.1016/j.mcm.2010.11.038>. URL <http://www.sciencedirect.com/science/article/pii/S0895717710005297>. Mathematical and Computer Modeling in agriculture (CCTA 2010).
- C. O. Justice, J. R. G. Townshend, B. N. H. HOLBEN, and C. J. Tucker. Analysis of the phenology of global vegetation using meteorological satellite data. *International Journal of Remote Sensing*, 6(8):1271–1318, 1985. doi: 10.1080/01431168508948281. URL <https://doi.org/10.1080/01431168508948281>.
- S. Kulp and B. H. Strauss. Global dem errors underpredict coastal vulnerability to sea level rise and flooding. *Frontiers in Earth Science*, 4:36, 2016. ISSN 2296-6463. doi: 10.3389/feart.2016.00036. URL <https://www.frontiersin.org/article/10.3389/feart.2016.00036>.
- J. X. Leon, G. B. M. Heuvelink, and S. R. Phinn. Incorporating dem uncertainty in coastal inundation mapping. *PLoS One*, 9(9):e108727, Sep 2014. ISSN 1932-6203. doi: 10.1371/journal.pone.0108727. URL <http://www.ncbi.nlm.nih.gov/pmc/articles/PMC4177217/>.
- X. Li, R. Rowley, J. Kostelnick, D. Braaten, J. Meisel, and K. Hulbutta. Gis analysis of global impacts from sea level rise. *Photogrammetric Engineering and Remote Sensing*, 75: 807–818, 07 2009.
- J. B. Lindsay. Sensitivity of channel mapping techniques to uncertainty in digital elevation data. *International Journal of Geographical Information Science*, 20(6):669–692, 2006. doi: 10.1080/13658810600661433. URL <https://doi.org/10.1080/13658810600661433>.
- J. Liu, L. An, S. S. Batie, R. E. Groop, Z. Liang, M. A. Linderman, A. G. Mertig, Z. Ouyang, and J. Qi. *Human Impacts on land Cover and Panda Habitat in Wolong Nature Reserve*, pages 241–263. Springer US, Boston, MA, 2003. ISBN 978-0-306-48130-7. doi: 10.1007/0-306-48130-8\_9. URL [https://doi.org/10.1007/0-306-48130-8\\_9](https://doi.org/10.1007/0-306-48130-8_9).

- J. Liu, T. Dietz, S. R. Carpenter, M. Alberti, C. Folke, E. Moran, A. N. Pell, P. Deadman, T. Kratz, J. Lubchenco, E. Ostrom, Z. Ouyang, W. Provencher, C. L. Redman, S. H. Schneider, and W. W. Taylor. Complexity of coupled human and natural systems. *Science*, 317(5844):1513–1516, 2007. ISSN 0036-8075. doi: 10.1126/science.1144004. URL <http://science.sciencemag.org/content/317/5844/1513>.
- T. S. o. Louisiana. Louisianas comprehensive master plan for a sustainable coast. *Coastal Protection and Restoration Authority*, 2012. URL <http://coastal.la.gov/a-common-vision/2012-coastal-master-plan/>.
- A. A. Mahmood, A. M. Eassa, H. Mohammed, Muayad, and Y. Shubbar, Israa. Assessment of ground water quality at basrah, iraq by water quality index (wqi). *Journal of Babylon University/Pure and Applied Sciences*, 21:2531–2543, 2013. URL <https://bit.ly/2NIZsMS>.
- A. Marina, A. Heidi, B. L. A., B. Nicholas, D. L. E., D. S. A., J. C. A., F. Jos, H. D. S., K. T. T. A., L. J. (Jack), M. W. J., M. H. D. G., M. J. D. A., M. Michael, P. Guillermo, P. R. Gilmore, R. C. L., R. N. J., S. David, and U. Gerald. Research on coupled human and natural systems (chans): Approach, challenges, and strategies. *The Bulletin of the Ecological Society of America*, 92(2):218–228, 2011. doi: 10.1890/0012-9623-92.2.218. URL <https://esajournals.onlinelibrary.wiley.com/doi/abs/10.1890/0012-9623-92.2.218>.
- E. Mcleod, B. Poulter, J. Hinkel, E. Reyes, and R. Salm. Sea-level rise impact models and environmental conservation: A review of models and their applications. *Ocean and Coastal Management*, 53(9):507 – 517, 2010. ISSN 0964-5691. doi: <https://doi.org/10.1016/j.ocecoaman.2010.06.009>. URL <http://www.sciencedirect.com/science/article/pii/S0964569110000852>.
- G. A. Meehl, W. M. Washington, W. D. Collins, J. M. Arblaster, A. Hu, L. E. Buja, W. G. Strand, and H. Teng. How much more global warming and sea level rise? *Science*, 307(5716):1769–1772, 2005.
- B. Meyssignac and A. Cazenave. Sea level: A review of present-day and recent-past changes and variability. *Journal of Geodynamics*, 58:96 – 109, 2012. ISSN 0264-3707. doi: <https://doi.org/10.1016/j.jog.2012.03.005>. URL <http://www.sciencedirect.com/science/article/pii/S0264370712000464>.
- A. J. Mohammed. Remnants of war in the province of basra (a study of geography). *Basra studies journal*, 5:115–150, 2008. ISSN 1994-4721. URL <https://bit.ly/2KYkNnb>.
- K. D. Muslih. Identifying the climatic conditions in iraq by tracking down cooling events in the north atlantic ocean in the period 30000 bc. *Miscellanea Geographica*, 18(3):40 – 46, 2014. URL <https://content.sciendo.com/view/journals/mgrsd/18/3/article-p40.xml>.
- K. Nageswara Rao, P. Subraelu, T. Venkateswara Rao, B. Hema Malini, R. Ratheesh, S. Bhattacharya, A. S. Rajawat, and Ajai. Sea-level rise and coastal vulnerability: an

- assessment of andhra pradesh coast, india through remote sensing and gis. *Journal of Coastal Conservation*, 12(4):195–207, Nov 2008. ISSN 1874-7841. doi: 10.1007/s11852-009-0042-2. URL <https://doi.org/10.1007/s11852-009-0042-2>.
- R. J. Nicholls and A. Cazenave. Sea-level rise and its impact on coastal zones. *Science*, 328(5985):1517–1520, 2010. ISSN 0036-8075. doi: 10.1126/science.1185782. URL <http://science.sciencemag.org/content/328/5985/1517>.
- NOAA. *Data Integration Visualization Exploration and Reporting (DIVER)*. National Oceanic and Atmospheric Administration, US Department of Commerce, 2018. URL <https://www.diver.orr.noaa.gov/>.
- H. Nomas. The concentration of salt in shatt al-arab. *Arts Basra Magazine*, 2006.
- J. Oksanen and T. Sarjakoski. Error propagation of dem-based surface derivatives. *Computers and Geosciences*, 31(8):1015 – 1027, 2005. ISSN 0098-3004. doi: <https://doi.org/10.1016/j.cageo.2005.02.014>. URL <http://www.sciencedirect.com/science/article/pii/S0098300405000701>.
- M. C. Peel, B. L. Finlayson, and T. A. McMahon. Updated world map of the kppen-geiger climate classification. *Hydrology and Earth System Sciences*, 11(5):1633–1644, 2007. doi: 10.5194/hess-11-1633-2007. URL <https://www.hydrol-earth-syst-sci.net/11/1633/2007/>.
- S. Penland and K. E. Ramsey. Relative sea-level rise in louisiana and the gulf of mexico: 1908-1988. *Journal of Coastal Research*, 6(2):323–342, 1990. ISSN 07490208, 15515036. URL <http://www.jstor.org/stable/4297682>.
- W. T. Pfeffer, J. T. Harper, and S. O’Neel. Kinematic constraints on glacier contributions to 21st-century sea-level rise. *Science*, 321(5894):1340–1343, 2008. ISSN 0036-8075. doi: 10.1126/science.1159099. URL <http://science.sciencemag.org/content/321/5894/1340>.
- J. Phillips. Climate change and surface mining: A review of environment-human interactions and their spatial dynamics. *Applied Geography*, 74:95 – 108, 2016. ISSN 0143-6228. doi: <https://doi.org/10.1016/j.apgeog.2016.07.001>. URL <http://www.sciencedirect.com/science/article/pii/S0143622816301746>.
- B. Poulter and P. N. Halpin. Raster modelling of coastal flooding from sealevel rise. *International Journal of Geographical Information Science*, 22(2):167–182, 2008. doi: 10.1080/13658810701371858. URL <https://doi.org/10.1080/13658810701371858>.
- S. D. Prince. Satellite remote sensing of primary production: comparison of results for sahelian grasslands 1981-1988. *International Journal of Remote Sensing*, 12(6): 1301–1311, 1991. doi: 10.1080/01431169108929727. URL <https://doi.org/10.1080/01431169108929727>.
- R Core Team. *R: A Language and Environment for Statistical Computing*. R Foundation for Statistical Computing, Vienna, Austria, 2017. URL <http://www.R-project.org/>.

- B. Rabus, M. Eineder, A. Roth, and R. Bamler. The shuttle radar topography mission: a new class of digital elevation models acquired by spaceborne radar. *ISPRS Journal of Photogrammetry and Remote Sensing*, 57(4):241 – 262, 2003. ISSN 0924-2716. doi: [https://doi.org/10.1016/S0924-2716\(02\)00124-7](https://doi.org/10.1016/S0924-2716(02)00124-7). URL <http://www.sciencedirect.com/science/article/pii/S0924271602001247>.
- S. Rahmstorf. A semi-empirical approach to projecting future sea-level rise. *Science*, 315(5810):368–370, 2007. ISSN 0036-8075. doi: 10.1126/science.1135456. URL <http://science.sciencemag.org/content/315/5810/368>.
- R. T. Reynolds. Heart of the storm, the genesis of the air campaign against iraq. *Air University Press, Maxwell Air Force Base, Alabama*, 1995. URL <http://www.au.af.mil/au/awc/awcgate/au/reynolds.pdf>.
- J. C. M. M. S. J. A. G. O. P. L. A. B. E. B. R. A. S. A. G. Robert J. Hijmans, Jacob van Etten. *raster: Geographic Data Analysis and Modeling*, 2017. URL <https://cran.r-project.org/web/packages/raster/index.html>.
- E. Rodriguez, C. S. Morris, and J. E. Belz. A global assessment of the srtm performance. *Photogrammetric Engineering and Remote Sensing*, 72(3):249–260, 2006. ISSN 0099-1112. doi: doi:10.14358/PERS.72.3.249. URL <https://www.ingentaconnect.com/content/asprs/pers/2006/00000072/00000003/art00002>.
- M. A. Saad. Seasonal variations of some physicochemical conditions of shatt arab estuary, iraq. *Estuarine and Coastal Marine Science*, 6(5):503 – 513, 1978. ISSN 0302-3524. doi: [https://doi.org/10.1016/0302-3524\(78\)90027-0](https://doi.org/10.1016/0302-3524(78)90027-0). URL <http://www.sciencedirect.com/science/article/pii/0302352478900270>.
- B. Sande, J. Larsen, and C. Hoyng. Sensitivity of coastal flood risk assessments to digital elevation models. *Water*, 4(3):568–579, 2012. ISSN 2073-4441. doi: 10.3390/w4030568. URL <http://www.mdpi.com/2073-4441/4/3/568>.
- M. M. Sherif and V. P. Singh. Effect of climate change on sea water intrusion in coastal aquifers. *Hydrological Processes*, 13(8):1277–1287, 1999. doi: 10.1002/(SICI)1099-1085(19990615)13:8<1277::AID-HYP765>3.0.CO;2-W. URL <https://onlinelibrary.wiley.com/doi/abs/10.1002/%28SICI%291099-1085%2819990615%2913%3A8%3C1277%3A%3AAID-HYP765%3E3.0.CO%3B2-W>.
- A. Shortridge. Shuttle radar topography mission elevation data error and its relationship to land cover. *Cartography and Geographic Information Science*, 33(1):65–75, 2006. doi: 10.1559/152304006777323172. URL <https://doi.org/10.1559/152304006777323172>.
- A. Shortridge and J. Messina. Spatial structure and landscape associations of srtm error. *Remote Sensing of Environment*, 115(6):1576 – 1587, 2011. ISSN 0034-4257. doi: <https://doi.org/10.1016/j.rse.2011.02.017>. URL <http://www.sciencedirect.com/science/article/pii/S0034425711000678>.

- A. Singh, T. R. Loveland, D. Del Pietro, H. Partow, P. Peduzzi, and W. C. Silverio Torres. One planet many people: Atlas of our changing environment, 2005. URL <https://archive-ouverte.unige.ch/unige:32650>. ID: unige:32650.
- B. Smiley, J. Trofymow, and K. Niemann. Spatially-explicit reconstruction of 100 years of forest land use and disturbance on a coastal british columbia douglas-fir-dominated landscape: Implications for future watershed-scale carbon stock recovery. *Applied Geography*, 74:109 – 122, 2016. ISSN 0143-6228. doi: <https://doi.org/10.1016/j.apgeog.2016.06.011>. URL <http://www.sciencedirect.com/science/article/pii/S014362281630162X>.
- T. L. Sohl, B. M. Sleeter, Z. Zhu, K. L. Sayler, S. Bennett, M. Bouchard, R. Reker, T. Hawbaker, A. Wein, S. Liu, R. Kanengieter, and W. Acevedo. A land-use and land-cover modeling strategy to support a national assessment of carbon stocks and fluxes. *Applied Geography*, 34:111 – 124, 2012. ISSN 0143-6228. doi: <https://doi.org/10.1016/j.apgeog.2011.10.019>. URL <http://www.sciencedirect.com/science/article/pii/S0143622811002220>.
- R. Springborg. Infitah, agrarian transformation, and elite consolidation in contemporary iraq. *Middle East Journal*, 40(1):33–52, 1986. ISSN 00263141, 19403461. URL <http://www.jstor.org/stable/4327247>.
- G. D. Steyer and D. W. Llewellyn. Coastal wetlands planning, protection, and restoration act: A programmatic application of adaptive management. *Ecological Engineering*, 15(3): 385 – 395, 2000. ISSN 0925-8574. doi: [https://doi.org/10.1016/S0925-8574\(00\)00088-4](https://doi.org/10.1016/S0925-8574(00)00088-4). URL <http://www.sciencedirect.com/science/article/pii/S0925857400000884>.
- S. Sultan, F. Ahmad, N. Elghribi, and A. Al-Subhi. An analysis of arabian gulf monthly mean sea level. *Continental Shelf Research*, 15(11):1471 – 1482, 1995a. ISSN 0278-4343. doi: [https://doi.org/10.1016/0278-4343\(94\)00081-W](https://doi.org/10.1016/0278-4343(94)00081-W). URL <http://www.sciencedirect.com/science/article/pii/027843439400081W>.
- S. Sultan, F. Ahmad, N. Elghribi, and A. Al-Subhi. An analysis of arabian gulf monthly mean sea level. *Continental Shelf Research*, 15(11):1471 – 1482, 1995b. ISSN 0278-4343. doi: [https://doi.org/10.1016/0278-4343\(94\)00081-W](https://doi.org/10.1016/0278-4343(94)00081-W). URL <http://www.sciencedirect.com/science/article/pii/027843439400081W>.
- L. Tara, S. Ashton, and M. Joseph. The influence of land cover on shuttle radar topography mission (srtm) elevations in lowrelief areas. *Transactions in GIS*, 14(4):461–479, 2010. doi: 10.1111/j.1467-9671.2010.01217.x. URL <https://onlinelibrary.wiley.com/doi/abs/10.1111/j.1467-9671.2010.01217.x>.
- J. G. Titus and C. Richman. Maps of lands vulnerable to sea level rise: modeled elevations along the us atlantic and gulf coasts. *Climate Research*, 18(3):205–228, 2001. doi: 10.3354/cr018205. URL <https://www.int-res.com/abstracts/cr/v18/n3/p205-228/>.
- C. Tripp. *A History of Iraq*. Cambridge University Press, 3 edition, 2007. doi: 10.1017/CBO9780511804304.

- J. Tu. Spatially varying relationships between land use and water quality across an urbanization gradient explored by geographically weighted regression. *Applied Geography*, 31(1):376 – 392, 2011. ISSN 0143-6228. doi: <https://doi.org/10.1016/j.apgeog.2010.08.001>. URL <http://www.sciencedirect.com/science/article/pii/S0143622810000846>. Hazards.
- U. N. UN. Oil-for-food. Online, 2003. URL <http://www.un.org/Depts/oip/background/fact-sheet.html>.
- M. Vermeer and S. Rahmstorf. Global sea level linked to global temperature. *Proceedings of the National Academy of Sciences*, 106(51):21527–21532, 2009. ISSN 0027-8424. doi: 10.1073/pnas.0907765106. URL <http://www.pnas.org/content/106/51/21527>.
- A. Verruijt. A note on the ghyben-herzberg formula. *International Association of Scientific Hydrology. Bulletin*, 13(4):43–46, 1968. doi: 10.1080/02626666809493624. URL <https://doi.org/10.1080/02626666809493624>.
- J. M. Visser, C. E. Sasser, R. H. Chabreck, and R. G. Linscombe. Marsh vegetation types of the mississippi river deltaic plain. *Estuaries*, 21(4):818–828, Dec 1998. ISSN 0160-8347. doi: 10.2307/1353283. URL <https://doi.org/10.2307/1353283>.
- W. van de Lageweg, S. McLelland, and D. Parsons. Experimental investigations of natural diatomaceous biofilm behaviour and sediment stabilizing capacity. In *EGU General Assembly Conference Abstracts*, volume 19 of *EGU General Assembly Conference Abstracts*, page 1068, Apr. 2017.
- H. Wang, Y. P. Hsieh, M. A. Harwell, and W. Huang. Modeling soil salinity distribution along topographic gradients in tidal salt marshes in atlantic and gulf coastal regions. *Ecological Modelling*, 201(3):429 – 439, 2007. ISSN 0304-3800. doi: <https://doi.org/10.1016/j.ecolmodel.2006.10.013>. URL <http://www.sciencedirect.com/science/article/pii/S0304380006004959>.
- X. Wang, K. Jia, S. Liang, Q. Li, X. Wei, Y. Yao, X. Zhang, and Y. Tu. Estimating fractional vegetation cover from landsat-7 etm+ reflectance data based on a coupled radiative transfer and crop growth model. *IEEE Transactions on Geoscience and Remote Sensing*, 55(10):5539–5546, Oct 2017. ISSN 0196-2892. doi: 10.1109/TGRS.2017.2709803.
- A. D. Werner and C. T. Simmons. Impact of sealevel rise on sea water intrusion in coastal aquifers. *Groundwater*, 47(2):197–204, 2009. doi: 10.1111/j.1745-6584.2008.00535.x. URL <https://onlinelibrary.wiley.com/doi/abs/10.1111/j.1745-6584.2008.00535.x>.
- E. Williams. Aquatecture: Architectural adaptation to rising sea levels. Graduate Thesis and Dissertations., 2009. URL <http://scholarcommons.usf.edu/etd/85>.
- C. Wohlfart, B. Mack, G. Liu, and C. Kuenzer. Multi-faceted land cover and land use change analyses in the yellow river basin based on dense landsat time series: Exemplary analysis in mining, agriculture, forest, and urban areas. *Applied Geography*, 85:73 – 88, 2017. ISSN 0143-6228. doi: <https://doi.org/10.1016/j.apgeog.2017.06.004>. URL <http://www.sciencedirect.com/science/article/pii/S014362281630813X>.

- W. W. Wood, R. M. Bailey, B. A. Hampton, T. F. Kraemer, Z. Lu, D. W. Clark, R. H. James, and K. A. Ramadan. Rapid late pleistocene/holocene uplift and coastal evolution of the southern arabian (persian) gulf. *Quaternary Research*, 77(2):215 – 220, 2012. ISSN 0033-5894. doi: <https://doi.org/10.1016/j.yqres.2011.10.008>. URL <http://www.sciencedirect.com/science/article/pii/S0033589411001384>.
- B. Yassein, K. A Al Asaady, A. Alwaeli, and M. Chaichan. Environmental impacts of salt tide in shatt al-arab-basra/iraq. *IOSR Journal of Environmental Science, Toxicology and Food Technology*, 10:35–43, 01 2016. URL <http://un.uobasrah.edu.iq/papers/30.pdf>.
- A. P. Yunus, R. Avtar, S. Kraines, M. Yamamuro, F. Lindberg, and C. S. B. Grimmond. Uncertainties in tidally adjusted estimates of sea level rise flooding (bathtub model) for the greater london. *Remote Sensing*, 8(5), 2016. ISSN 2072-4292. doi: 10.3390/rs8050366. URL <http://www.mdpi.com/2072-4292/8/5/366>.
- S. Zellmer and C. Klein. Mississippi river stories: lessons from a century of unnatural disasters. *SMU Law Review*, 60:1471–1538, 06 2007. URL <https://digitalcommons.unl.edu/lawfacpub/12/>.
- X. Zhang, C. Liao, J. Li, and Q. Sun. Fractional vegetation cover estimation in arid and semi-arid environments using hj-1 satellite hyperspectral data. *International Journal of Applied Earth Observation and Geoinformation*, 21:506 – 512, 2013. ISSN 0303-2434. doi: <https://doi.org/10.1016/j.jag.2012.07.003>. URL <http://www.sciencedirect.com/science/article/pii/S0303243412001419>.